

Semiclassical analysis of the Loop Quantum Gravity volume operator: Area Coherent States

C. Flori¹ *

¹ MPI f. Gravitationsphysik, Albert-Einstein-Institut,
Am Mühlenberg 1, 14476 Potsdam, Germany

Preprint AEI-2009-026

Abstract

We continue the semiclassical analysis of the Loop Quantum Gravity (LQG) volume operator that was started in the companion paper [23]. In the first paper we prepared the technical tools, in particular the use of complexifier coherent states that use squares of flux operators as the complexifier. In this paper, the complexifier is chosen for the first time to involve squares of area operators.

Both cases use coherent states that depend on a graph. However, the basic difference between the two choices of complexifier is that in the first case the set of surfaces involved is discrete, while, in the second it is continuous. This raises the important question of whether the second set of states has improved invariance properties with respect to relative orientation of the chosen graph in the set of surfaces on which the complexifier depends. In this paper, we examine this question in detail, including a semiclassical analysis.

The main result is that we obtain the correct semiclassical properties of the volume operator for i) artificial rescaling of the coherent state label; and ii) particular orientations of the 4- and 6-valent graphs that have measure zero in the group $SO(3)$. Since such requirements are not present when analysing dual cell complex states, we conclude that coherent states whose complexifiers are squares of area operators are not an appropriate tool with which to analyse the semiclassical properties of the volume operator. Moreover, if one intends to go further and sample over graphs in order to obtain embedding independence, then the area complexifier coherent states should be ruled out altogether as semiclassical states.

I would like to dedicate this paper to my parents Elena Romani and Luciano Flori

*cecilia.flori@aei.mpg.de, ceciliaflori18@googlemail.com

Contents

1	Introduction	3
2	Volume Operator Expectation Values for Area Coherent States	6
2.1	General expectation value of the volume operator	7
2.2	Simplifying assumptions	9
2.3	Preliminary analysis of the graph geometry factor	12
2.4	Explicit calculation of the σ_e^I terms	13
2.4.1	Computation of the geometric factor for 4-, 6- and 8-valent graphs	19
3	The Higher, $\frac{1}{\delta}$-order Dependence of the Expectation Value of the Volume Operator	23
3.1	Initial preparations	23
3.2	Analysis of the expectation value of the volume operator for a 4-valent graph	29
3.2.1	Expectation value of the volume operator for a 4-valent graph	30
3.2.2	Expectation value of the volume operator for a rotated 4-valent graph	32
3.2.3	Expectation value of the volume operator for a translated 4-valent graph	36
3.3	Analysis of the expectation value of the volume operator for 6-valent graphs	38
3.3.1	Expectation value of the volume operator for a general 6-valent graph	38
3.3.2	Expectation value of the volume operator for a rotated 6-valent graph	40
3.3.3	Expectation value of the volume operator for a translated 6-valent graph	45
3.4	Analysis of the expectation value of the volume operator for 8-valent graphs	48
3.4.1	Expectation value of the volume operator for a general 8-valent graph	48
3.4.2	Expectation value of the volume operator for a rotated 8-valent graph	49
3.4.3	Expectation value of the volume operator for a translated 8-valent graph	50
4	Summary and Conclusions	52
A	Edge metric calculations	53
A.1	Edge metric components for the 4-valent graph	53
A.1.1	Rotated 4-valent graph	53
A.1.2	Translated 4-valent graph	54
A.2	Edge metric components for the 6-valent graph	55
A.2.1	Aligned 6-valent graph	55
A.2.2	Rotated 6-valent graph	58
A.2.3	Translated 6-valent graph	59
A.3	Edge-metric components for the 8-valent graph	64
A.3.1	Aligned 8-valent graph	64
A.3.2	Rotated 8-Valent graph	64
A.3.3	Translated 8-valent graph	65

1 Introduction

The volume operator in Loop Quantum Gravity¹ (LQG) plays a central role in the quantum dynamics of the theory. Without it, it is not possible to define the Hamiltonian constraint operators [4], the Master constraint operators [5], or the physical Hamiltonian operators [6]. The same applies to truncated models of LQG such as Loop Quantum Cosmology (LQC) [7] which is believed to describe well the homogeneous sector of the theory. In LQC the quantum evolution of operators that correspond to classically-singular Dirac observables typically remains finite. This can be traced back to the techniques used to quantize inverse powers of the local volume that enter into the expression for the triad, co-triad and other types of coupling between geometry and geometry, or geometry and matter [4]. Specifically, such derived operators arise as commutators between holonomy operators and powers of the volume operator.

In view of its importance, it is of considerable interest to verify whether the classical limit of the LQG volume operator coincides with the classical volume. By this we mean that (i) the expectation value of the volume operator with respect to suitable semiclassical states which are peaked at a given point in phase space, coincides with the value of the classical volume at that phase space point, up to small corrections; and (ii) its fluctuations are small.

It should be remarked that there are actually two versions of the volume operator that have been discussed in the literature [8, 9]. These come from inequivalent regularisations of the products of operator-valued distributions that appear at intermediate stages. However, only the operator in [9] survives the consistency test of [10], namely, writing the volume in terms of triads which then are quantised using the commutator mentioned above, gives the same operator up to \hbar -corrections as that obtained from direct quantisation. This consistency check is important as otherwise we could not trust the triad and co-triad quantisations that enter the quantum dynamics.

A semiclassical analysis of the volume operator has not yet been carried out, although, in principle, suitable semiclassical (even coherent) states for LQG are available [11]. This is because the spectral decomposition (projection-valued measure) of the volume operator cannot be computed exactly in closed form. However, this is needed for exact, practical calculations. More precisely, the volume operator is the fourth root of a positive operator, Q , whose matrix elements can be computed in closed form [12] but which cannot be diagonalised analytically.

In more detail, the volume operator has a discrete (that is, pure-point) spectrum and it attains a block-diagonal form where the blocks are labelled by the graphs and spin quantum numbers (labelling the edges of the graph) of spin-network functions (SNWF) [13]. SNWF form a convenient basis of the LQG Hilbert space [14] which carries a unitary representation of the spatial diffeomorphism group and the Poisson*-algebra of the elementary flux and holonomy variables [15]. The blocks turn out to be finite-dimensional matrices whose matrix elements can be expressed in terms of polynomials of 6j symbols. Fortunately, these complicated quantities can be avoided² by using a telescopic summation technique [16] related to the Elliot-Biedenharn identity [17], so that a manageable closed expression results. However, the size of these matrices grows exponentially with increasing spin quantum numbers and, since the expression for coherent states is a coherent superposition of SNWF's with arbitrarily large spin quantum numbers, a numerical computation of the expectation value using the numerical diagonalisation techniques, that are currently being developed [18], is still a long way off.³

One way forward is to use the semiclassical perturbation theory developed in [19], and applied already in [20, 21]. The basic idea is quite simple. In practical calculations one needs the expectation value of Q^q where q is a rational number in the range $0 < q \leq \frac{1}{4}$. In order to attain that, one has to introduce the

¹See [1, 2] for recent books and [3] for recent reviews.

²Notice that Racah's formula provides a closed expression for the 6j symbol but it also involves implicit sums and factorials that involve large integers. These quickly becomes unmanageable, even numerically.

³The coherent superposition contains a damping factor that suppresses large spins, and thereby large matrices, so that the complicated infinite series over spin quantum numbers can be truncated at finite values, making only negligible errors. However, the computational effort required is currently too high, even for supercomputers; for example, see the estimates of computation time reported in [18].

‘perturbation operator’, $X := \frac{Q}{\langle Q \rangle} - 1$, where the expectation value $\langle Q \rangle$ of the positive operator Q is exactly computable. Notice that X is bounded from below by -1 . Then trivially $\langle Q^q \rangle = \langle Q \rangle^q \langle [1+X]^q \rangle$. Now we exploit the existence of positive numbers p such that the classical estimates $1+qx-px^2 \leq (1+x)^q \leq 1+qx$ are valid for all $x \geq -1$. Finer estimates of this form involving arbitrary powers of x are also available [20]. By virtue of the spectral theorem, this classical estimate survives at the quantum level and we have $Y_- \leq Y \leq Y_+$ where $Y_+ = 1+qX$, $Y_- = Y_+ - pX^2$, $Y = (1+X)^q$. It follows that $\langle Y \rangle \in [\langle Y_- \rangle, \langle Y_+ \rangle]$. However, $\langle Y_+ \rangle = 1$ and $\langle X^2 \rangle = [\langle Q^2 \rangle - \langle Q \rangle^2] / \langle Q \rangle^2$ is proportional to the relative fluctuations of Q , which are of order of \hbar [11]. It follows that to zeroth-order in \hbar we may replace $\langle Q^q \rangle$ by $\langle Q \rangle^q$ which is computable, as are the error estimates in the way shown above.

The exact computation of $\langle Q \rangle$, $\langle Q^2 \rangle$, .. is feasible, but it is still quite involved. At this point it is convenient to use the fact that (see [11]), to zeroth-order in \hbar , the computation of these expectation values (more generally, the expectation values of low-order polynomials in the flux operators) for $SU(2)$ spin-network states coincides with the corresponding calculations for $U(1)^3$ spin networks. On the latter, the volume operator is even diagonal. Hence we conclude that, as long as we are only interested in the zeroth-order in \hbar contribution, we may evaluate the expectation value of the volume operator for a fictitious theory in which the non-Abelian group $SU(2)$ is replaced by the Abelian group $U(1)^3$. This dramatically simplifies all the calculations.

The coherent states developed so far for LQG have all been constructed using the complexifier method reviewed in [22]. This generalises the coherent-state construction for phase spaces that are cotangent bundles over a compact group; see [24]⁴. This construction involves computing the heat-kernel evolution of the delta distribution (which is the matrix element of the unit operator in the Schrödinger (position) representation) with respect to a generalized Laplace operator, called the ‘complexifier’, followed by a certain analytic continuation.

Now the unit operator in LQG can be written as a resolution of unity in terms of SNWF’s and, although the heat kernel is a damping operator, since the SNWF are not countable (the LQG Hilbert space is not separable), the resulting expression is not normalisable. However, it does give a well-defined distribution (in the algebraic dual of the finite linear span of SNWF’s) which can be conveniently written as a sum over cut-off states labelled by finite graphs. These states, called “shadows” in [24], are normalisable, and can be used to perform semiclassical calculations. Of course, one expects that the good semiclassical states will only be those cut-off states that are labelled by graphs which are sufficiently fine with respect to the classical three-metric to be approximated.

Thus the input in the semiclassical calculations consists in the choice of a complexifier and the choice of a graph. One may wonder why the complexifier has to be chosen *a priori* rather than being dictated by the dynamics of the theory: that is, why do the coherent states remain coherent under quantum time evolution? For example, for the harmonic oscillator, the complexifier is just the Laplacian on the real line.

The reason is two-fold. On the one hand, one could perform a constraint quantisation so that we are working at the level of the kinematical Hilbert space on which the quantum constraints have not yet been imposed. In this situation, all that is needed is to ensure that the volume operator, which is not gauge invariant (and thus does not preserve the physical Hilbert space), has a good classical limit on the kinematical Hilbert space. We would certainly not trust a constraint quantization for which even that was not true.

On the other hand, one could also work at the level of the physical Hilbert space, as outlined in [6]. Then, one would expect that the time evolution of any reasonable choice of complexifier coherent states with respect to the physical Hamiltonian should remain coherent (and peaked on the classical trajectory) for sufficiently short time intervals. Note that for interacting theories, even the simple example of the anharmonic oscillator, globally stable coherent states have yet to be found.

The choice of the complexifier will be guided by practical considerations: namely (i) it is diagonal on SNWF’s; and (ii) it is a damping operator that renders normalisable the heat-kernel evolution of the delta

⁴See also [25] for related ideas valid for Abelian gauge theories such as Maxwell theory or linearised gravity.

distribution restricted to a graph. Moreover, it should be gauge invariant under the $SU(2)$ gauge group. As for the choice of graph, for practical reasons one will use graphs that are topologically regular, that is, have a constant valence for each vertex. Indeed, the semiclassical calculations performed in [20, 21] were done using graphs of cubic topology, with good results.

The existing literature on such coherent states for LQG can be divided into two classes, depending on a certain structure that defines them. The first are *gauge-covariant flux* coherent states, which depend on collections of surfaces and path systems inside them [11]. The second are *area* coherent states, which also depend on collections of surfaces but involve area operators rather than flux operators [22]. In our companion paper [23] we have reviewed and generalised both constructions. In its most studied incarnations, the collection of surfaces involved in [11] is defined by a polyhedral partition of the spatial manifold, while the collection used in [22] uses a plaquette of foliations of the spatial manifold.

The main objective of this series of two papers is to analyse the semiclassical properties of the volume operator with respect to both classes of coherent state. In [23] we employed the states of [11]. In this paper we employ the states of [22]. This exhausts all known coherent states for LQG. The result of our analysis is that, if we use the states [11], *the correct semiclassical limit is attained with these states for $n = 6$ only*. If instead we use the states [22], the correct semiclassical limit is attained *only* for: 1) artificial rescaling of the coherent state label; and 2) particular embeddings of the 4-valent and 6-valent graphs with respect to the set of surfaces on which the complexifier depends. However, the combinations of Euler angles for which such embeddings are attained have measure zero in $SO(3)$, and are therefore negligible. Thus the *area complexifier coherent states are not the correct tools with which to analyse the semiclassical properties of the volume operator*.

If one wants to obtain embedding independence, a possible strategy is to sample over graphs (Dirichlet-Voronoi sampling [44]) as outlined in [11]. What this strategy amounts to is that, instead of singling out one particular coherent state $\psi_{\gamma,m}$ —as defined in terms of a single graph γ —one considers an ensemble of coherent states constructed by averaging the one-dimensional projections $\hat{P}_{\gamma,m}$ onto the states $\psi_{\gamma,m}$ over a subset Γ_m of the set of all allowed graphs. In other words, one considers a mixed state (with an associated density matrix) rather than a single coherent state. In such a way, if the subset Γ_m is big enough, it can be shown ([11]) that it is possible to eliminate the embedding dependence (the ‘staircase problem’⁵).

It is straightforward to deduce that the area complexifier coherent states cannot be used to construct embedding-independent, mixed coherent states because of condition 2) above. We thus claim that *area complexifier coherent states should be ruled out as semiclassical states altogether if one wants to attain embedding independence*. Instead one should use the flux coherent states, as was done in [11]. For such states we will show that *the correct semiclassical limit is attained only for $n = 6$* . In other words, *up to now, there are no semiclassical states known other than those with cubic-graph topology!*

Thus the implication of our result for LQG is that the semiclassical sector of the theory is spanned by SNWF that are based on cubic graphs. This has some bearing for spin-foam models [27] which are supposed to be—but, so far, have not been proved to be—the path-integral formulation of LQG. Spin foams are certain state-sum models that are based on simplicial triangulations of four manifolds whose dual graphs are therefore 5-valent. The intersection of this graph with a boundary three-manifold is 4-valent, and therefore we see that spin-foam models, based on simplicial triangulations, correspond to boundary Hilbert spaces spanned by spin-network states based on 4-valent graphs only⁶. However, we have proved that the

⁵Roughly the staircase problem can be stated as follows. Consider an area operator \hat{A}_S for a surface S . If we compute the expectation value for \hat{A}_S with respect to a coherent state $\psi_{\gamma,m}$, such that the surface S intersects transversely one and only one edge e of γ , then the expectation value of the area operator coincides with the classical value $A(m)$. However, if the surface S lies transversally to the edges, then we do not obtain the correct classical limit.

⁶As an aside, whether this boundary Hilbert space of spin foams really can be interpreted as the 4-valent sector of LQG is a subject of current debate, even with the recent improvements [28] in the Barrett–Crane model [29]. There are two problems: first, the boundary connection predicted by spin foams does not coincide with the LQG connection [30]. Secondly, the 4-valent sector of the LQG Hilbert space is not a superselection sector for the holonomy flux algebra of LQG. In fact, the LQG representation is known not only to be cyclic but even irreducible [31]. Therefore the 4-valent sector is not invariant under the LQG algebra.

correct semiclassical states for analysing the semiclassical properties of the volume operator are the *gauge covariant flux* states. For such states, only those of cubic topology give the correct semiclassical value of the volume operator.

Even if the mismatches between the 4-valent sector of LQG and the boundary Hilbert space of spin foams could be surmounted, the result of our analysis seems to be that *the boundary Hilbert space of current spin-foam models does not contain any semiclassical states!* This apparently contradicts recent findings that the graviton propagator derived from spin-foam models is correct [32]. However, it is notable that these latter results only show that the propagator has the correct fall-off behaviour: the correct tensorial structure has not yet been verified.

One straightforward way of possibly repairing this situation is to generalise spin-foam models to allow for arbitrary—in particular, cubic—triangulations, as suggested in [33, 34].

In the present paper we will perform detailed calculations of the expectation value of the volume operator for the 4-, 6-, and 8-valent graphs using the area coherent states reviewed in [23]. The main difference between the flux coherent states and the area coherent states is that the former depend on a discrete set of flux operators while the latter depend on a continuous family of area operators. In particular, the surfaces on which the area operators depend fill all of space. Hence the question arises whether the area coherent states depend less severely on the relative orientation of the chosen cut-off graph with respect to the system of surfaces. Specifically, it would be interesting to know if the calculations of the expectation values are insensitive to Euclidean motions of the graph (translations and rotations) when the spatial metric to be approximated is the Euclidean one.

The structure of the paper is as follows. In Section 2 we calculate the expectation value for a general graph. The expectation value depends on the edge metric, already encountered in [23], which is close to diagonal when the edge lengths, δ , are much larger than the lengths, l , of the boundaries of the surfaces. In order to compute the off-diagonal metric entries we stick to the graphs defined in our companion paper as otherwise we encounter severe ‘bookkeeping’ problems. These graphs are dual to tetrahedral, cubical and octahedral triangulations, all of which derive from a cubulation of the spatial manifold, as discussed in [23]. One can expand the expectation value into a convergent power series in l/δ . We establish that, contrary to the results in [23], to zeroth-order in both \hbar and l/δ the correct expectation value is obtained for $n = 6$ and $n = 4$, but *only* for specific embeddings of the graph with respect to the surfaces on which the area operators depend. However, we show that such embeddings have measure *zero* in $SO(3)$. Moreover, by using the coherent states in [11] we also find that the graphs (4-, 6, and 8-valent) are all Euclidean invariant, up to sets of measure zero in $SO(3)$ and up to linear order in l/δ . Nonetheless, the embeddings with non-zero measure all fail to give the correct semiclassical value for the volume operator.

This shows that coherent states [11] are not the correct tools for analysing the semiclassical properties of the volume operators.

In Section 3 we perform an explicit calculation of the expectation value of the volume operator for 4-, 6-, and 8-valent graphs, including the higher-order effects in l/δ . This contribution is only Euclidean-invariant up to linear order. For each of these valences we first consider a graph constructed in terms of regular simplicial, cubical and octahedron cell complexes, as done in [23]. After that, we study the effects of rotations and translations.

In Section 4 we summarise our results and draw appropriate conclusions.

The more technical calculations have been transferred to an appendix in order not to distract from the line of argument in the main text.

2 Volume Operator Expectation Values for Area Coherent States

In this Section we compute the expectation value of the operator $\hat{V}_{\gamma,v}$ for an arbitrary n -valent vertex, v , for the stack family coherent states using the replacement of $SU(2)$ by $U(1)^3$. This uses the calculational tools developed in [23], to which we refer for our notation. We may, therefore, replace the $SU(2)$ right-invariant vector fields by $U(1)^3$ right-invariant vector fields $X_{e_I(v)}^j = ih_I^j \partial / \partial h_I^j$ acting on $h_I^j := A^j(e_I(v))$.

The crucial simplification is that these vector fields mutually commute. Their common eigenfunctions are the spin-network functions which, for $U(1)^3$, take the explicit form

$$T_{\gamma,n}(A) = \prod_{e \in E(\gamma)} \prod_{j=1}^3 [A^j(e)]^{n_j^e} \quad (2.1)$$

We will refer to them as ‘charge network states’ because the $n_j^e \in \mathbb{Z}$ are integer valued. Using the spectral theorem we may immediately write down the eigenvalues of $\hat{V}_{\gamma,v}$ on $T_{\gamma,n}$ as

$$\lambda_{\gamma,n,v} = \ell_P^3 \sqrt{\left| \frac{1}{8} \sum_{\substack{v \in e_I \cap e_J \cap e_K \\ 1 \leq I \leq J \leq K \leq N}} \epsilon^{ijk} \epsilon(e_I, e_J, e_K) [n_i^{e_I} n_j^{e_J} n_k^{e_K}] \right|} \quad (2.2)$$

What follows is subdivided into four parts. We begin by performing the calculation for a general graph. This leads to the inverse of the edge metric which, for large graphs, is beyond analytical control. In the second part we restrict the class of graphs, which lets us perform perturbative computations of the inverse of the edge metric. This gives a good approximation of the actual expectation value. In the third and fourth parts we consider the dependence of our results on the relative orientation of the graph with respect to the family of stacks.

2.1 General expectation value of the volume operator

In this Section we drop the graph label and set $t_{ee'}^{jk} := \delta^{jk} t_{ee'}^\gamma$, $t := \ell_P^2/a^2$. This gives a positive, symmetric bilinear form on vectors $n := (n_j^e)_{e \in E(\gamma), j=1,2,3}$ that is defined by $t(n, n') := \sum_{e,e',j,k} n_j^e n_k^{e'} t_{ee'}^{jk} = n^T \cdot t \cdot n'$. We also set $Z^T \cdot n := \sum_{e,j} Z^j(e) n_j^e$.

The coherent state associated with an n -valent graph in which more than one edge intersects a given plaquette S , is as follows:

$$\psi_{Z,\gamma} = \sum_n e^{-\frac{1}{2} n^T \cdot t \cdot n} e^{Z^T \cdot n} T_{\gamma,n} \quad (2.3)$$

The norm of the coherent states is given by

$$\|\psi_{Z,\gamma}\|^2 = \sum_n e^{-n^T \cdot t \cdot n} e^{2P \cdot n} \quad (2.4)$$

where

$$P^j(e) = i \int_e (Z - A) =: \frac{1}{b^2} E_j^e \quad (2.5)$$

The length parameter, b , that appears here is generally different from the parameter, a , that enters the classicality parameter $t = \ell_P^2/a^2$, as explained in [23].

The expectation value for the volume operator is

$$\langle \hat{V}_v \rangle_{Z,\gamma} = \frac{\langle \psi_{Z,\gamma} \hat{V}_{\gamma,v} \psi_{Z,\gamma} \rangle}{\|\psi_{Z,\gamma}\|^2} = \frac{\sum_n e^{-n^T \cdot t \cdot n} e^{2P \cdot n} \lambda_{\gamma,v}(n)}{\|\psi_{Z,\gamma}\|^2} \quad (2.6)$$

where

$$\lambda_{\gamma,v}(n) = \ell_P^3 \sqrt{\left| \frac{1}{48} \sum_{e \cap e' \cap e'' = v} \epsilon(e, e', e'') \det_{ee'e''}(n) \right|} \quad (2.7)$$

are the eigenvalues of the volume operator $\hat{V}_{\gamma,v}$. We have introduced the notation

$$\det_{ee'e''}(n) := \epsilon^{jkl} n_j^e n_k^{e'} n_l^{e''} \quad (2.8)$$

The semiclassical limit of the volume operator is obtained from (2.6) in the limit of vanishing t . That is, it is the zeroth-order in t of the expansion of (2.6) in powers of t . Since (2.6) converges slowly for small values of t , we will perform a Poisson transform which replaces t by $\frac{1}{t}$ which converges quickly. To this end, analogous to [20], we introduce the following variables

$$t_e := t_{ee}, T_e := \sqrt{t_e}, x_j^e := T_e n_j^e, y_j^e(x) := x_j^e/T_e, C_j^e := P_j^e/T_e, w_j^e(n) := n_j^e/T_e, A_{ee'}^{jk} := A_{ee'} \delta^{jk} := \frac{t_{ee'}}{\sqrt{t_e t_{e'}}} \quad (2.9)$$

Notice that the diagonal entries of A equal unity. The off-diagonal ones, however, are bounded from above by unity by the Schwarz inequality applied to the scalar product defined by A and are restricted to the six-dimensional subspace restricted to vectors with non-zero entries for the e, e' components only.

Then (2.6) turns into

$$\langle \hat{V}_v \rangle_{Z, \gamma} = \frac{\sum_n e^{-x^T \cdot A \cdot x} e^{2C \cdot x} \lambda_{\gamma, v}(y(x))}{\sum_n e^{-x^T \cdot A \cdot x} e^{2C \cdot x}} \quad (2.10)$$

Applying the Poisson transform to (2.10) we obtain (recall $N := |E(\gamma)|$)

$$\langle \hat{V}_v \rangle_{Z, \gamma} = \frac{\sum_n \int_{\mathbb{R}^{3N}} d^{3N} x e^{-2\pi i w(n)^T \cdot x} e^{-x^T \cdot A \cdot x} e^{2C \cdot x} \lambda_{\gamma, v}(y(x))}{\sum_n \int_{\mathbb{R}^{3N}} d^{3N} x e^{-2\pi i w(n)^T \cdot x} e^{-x^T \cdot A \cdot x} e^{2C \cdot x}} \quad (2.11)$$

In order to perform the Gaussian integrals in (2.11) we notice that, by construction, A is a positive-definite, finite-dimensional matrix, so that its square root, \sqrt{A} , and its inverse are well defined via the spectral theorem. Hence we introduce as new integration variables

$$z_j^e := \sum_{e', k} (\sqrt{A})_{jk}^{ee'} x_k^{e'}, y_j^e(z) = \frac{1}{T_e} x_j^e = \frac{1}{T_e} \sum_{e', k} ([\sqrt{A}]^{-1})_{jk}^{e'e} z_k^{e'} \quad (2.12)$$

The Jacobian from the change of variables drops out in the fraction, and (2.11) becomes

$$\langle \hat{V}_v \rangle_{Z, \gamma} = \frac{\sum_n \int_{\mathbb{R}^{3N}} d^{3N} z e^{2(C - 2\pi i w(n))^T \cdot \sqrt{A}^{-1} \cdot z} e^{-z^T \cdot z} \lambda_{\gamma, v}(y(z))}{\sum_n \int_{\mathbb{R}^{3N}} d^{3N} z e^{2(C - 2\pi i w(n))^T \cdot \sqrt{A}^{-1} \cdot z} e^{-z^T \cdot z}} \quad (2.13)$$

Now one would like to shift z into the complex domain by $\sqrt{A}^{-1}(C - i\pi w)$ and then perform the ensuing Gaussian integral. This is unproblematic for the denominator of (2.11) which is analytic in z ; however, the numerator is not. The careful analysis in [20] shows the existence of branch cuts in \mathbb{C}^{3N} of the fourth-root function involved. In turn, this shows that, in the semiclassical limit, both numerator and denominator are dominated by the $n = 0$ term while the remaining terms in the series are of order \hbar^∞ (i.e they decay as $\exp(-k_n/t)$, $t = \ell_P^2/a^2$ for some $k_n > 0$, $\lim_{n \rightarrow \infty} k_n = \infty$). See [20] for the details.

The upshot is that to any polynomial order in \hbar we may replace (2.13) by

$$\langle \hat{V}_v \rangle_{Z, \gamma} = \frac{\int_{\mathbb{R}^{3N}} d^{3N} z e^{-z^T \cdot z} \lambda_{\gamma, v}(y(z + \sqrt{A}^{-1}C))}{\int_{\mathbb{R}^{3N}} d^{3N} z e^{-z^T \cdot z}} \quad (2.14)$$

which is now defined unambiguously because the argument of the fourth root is the square of a real number.

The denominator of (2.14) simply equals $\sqrt{\pi}^{3N}$. Therefore, the only \hbar -dependence of (2.14) lies in the numerator in the function $\lambda_{\gamma, v}$. We now note that the eigenvalues of the volume operator come with a factor of ℓ_P^3 , as displayed in (2.7). Pulling it under the square root into the modulus, and noticing that the modulus is a third-order polynomial in y , we see that

$$\lambda_{\gamma, v}(y(z + \sqrt{A}^{-1}C)) = \sqrt{\left| \frac{1}{48} \sum_{e \cap e' \cap e'' = v} \epsilon(e, e', e'') \det_{e, e', e''} (\ell_P^2 y(z + \sqrt{A}^{-1}C)) \right|} \quad (2.15)$$

where we have

$$\begin{aligned}
[\ell_P^2 y(z + \sqrt{A}^{-1})C]_j^e &= \frac{\ell_P^2}{T_e} \sum_{e',k} [\sqrt{A}^{-1}]_{jk}^{ee'} [z + \sqrt{A}^{-1}C]_k^{e'} \\
&= \frac{\sqrt{t}}{T_e} \sum_{e',k} \left(a^2 \sqrt{t} [\sqrt{A}^{-1}]_{jk}^{ee'} z_k^{e'} + \frac{\sqrt{t}}{T_{e'}} [A^{-1}]_{jk}^{ee'} \left(\frac{a}{b}\right)^2 E_k^{e'} \right)
\end{aligned} \tag{2.16}$$

where (2.5) has been used in the last line.

To extract the leading order in t of (2.14) is now easy. First note that the matrix elements of both A and T_e/\sqrt{t} are of order unity. Since a is some macroscopic length scale, the first term that is proportional to z in (2.16) is therefore of order \sqrt{t} , while the second is of zeroth-order in t . Therefore $F := \lambda_{\gamma,v}(y(z + \sqrt{A}^{-1}C))$ is of the form

$$F(z\sqrt{t}) = \sqrt[4]{Q + P(z\sqrt{t})} \tag{2.17}$$

where P is a certain sixth-order polynomial in $z\sqrt{t}$ with no zeroth-order term, while Q is independent of z . Moreover, $Q + P(z\sqrt{t})$ is non-negative for all z because it is the square of a third-order polynomial in z . In particular, this holds at $z = 0$, and therefore Q is also a non-negative number. Then, provided $Q > 0$, we can define

$$f(z\sqrt{t}) := \frac{F(z\sqrt{t})}{\sqrt[4]{Q}} =: \sqrt[4]{1 + R(z\sqrt{t})} \tag{2.18}$$

where R is a sixth-order polynomial with no zeroth-order term which is bounded from below by -1 . Now, as in [19], we exploit the existence of $r > 0$ such that

$$1 + \frac{1}{4}R - rR^2 \leq f \leq 1 + \frac{1}{4}R \tag{2.19}$$

for all $R \geq -1$. Inserting this estimate into (2.14) we can bound the integral from above and below because the Gaussian is positive. The integrals over R and R^2 are finite and are at least of order t because odd powers of z do not contribute to the Gaussian integral.

It follows that to zeroth-order in t we have

$$\langle \hat{V}_v \rangle_{Z,\gamma} = \sqrt{\left| \frac{1}{48} \sum_{e \cap e' \cap e'' = v} \epsilon(e, e', e'') \det_{e, e', e''} (Y) \right|} \tag{2.20}$$

where

$$Y_j^e := \left(\frac{a}{b}\right)^2 \sum_{e',k} \frac{t}{T_e T_{e'}} [A^{-1}]_{jk}^{ee'} E_k^{e'} \tag{2.21}$$

This is as far as we can go with the calculation for a general graph. Notice that the inverse of the edge metric appears in this expression and, for a general graph, this is beyond analytical control. Therefore we will now make restrictions on the graph so as to analyse (2.21) further.

2.2 Simplifying assumptions

The assumptions about the class of graphs to be considered are as follows:

1. Coordinate Chart

The graph, the region R and the families of stacks lie in a common coordinate chart $X : \mathbb{R}^3 \rightarrow \sigma$. This is not a serious restriction because the general situation may be reduced to this one by appropriately restricting attention to the various charts of an atlas that covers σ .

2. Tame Graphs

We assume that the graph is *tame* with respect to the stacks. By this we mean that for each direction I , and each stack α , a given edge, e , of the graph enters and leaves that stack at most once. This means that the graph does not ‘wiggle’ too much on the scale of the plaquettes. Analytically, it means that $l_N^{I\alpha\gamma}$ vanishes whenever $|N_e| \geq 2$ for any e , and that, for given e , the number $l_N^{I\alpha\gamma}$ is non-vanishing at most for either $N_e = +1$ or $N_e = -1$ but, not both, and independently of α . Finally, it means that the sets $S_N^{I\alpha\gamma}$ are connected.

3. Coarse Graphs

We assume that the graph is much coarser than the plaquettation in the sense that any edge intersects many different stacks in at least one direction I .

4. Non-Aligned Graphs

We exclude the possibility that distinct edges are ‘too aligned’ with each other in the sense that the number of stacks that they commonly traverse is much smaller than the number of stacks that they individually traverse .

Pictorially, the situation therefore typically looks as in figure 1. A consequence of the tameness, coarseness

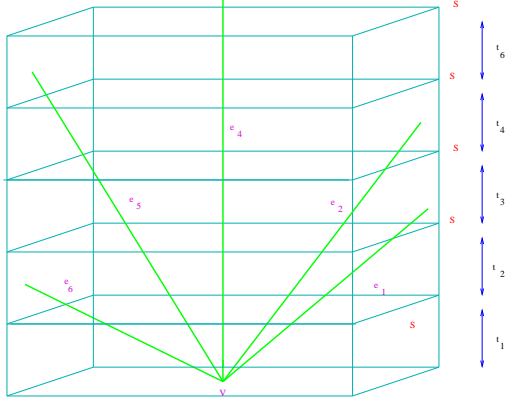


Figure 1: Example of a tame, coarse and non-aligned graph

and ‘alignedness’ assumption is that $|t_{e,e'}^\gamma| \ll t_e^\gamma = t_{ee}^\gamma$, $t_{e'}^\gamma = t_{e'e'}^\gamma$ for all e, e' , as is immediately obvious from the formulae displayed in our companion paper because the number of stacks with $|N_e| = |N_{e'}| = 1$ will be very much smaller than the number of stacks with $|N_e| = 1, N_{e'} = 0$ or $|N_{e'}| = 1, N_e = 0$. Hence the edge metric will be almost diagonal. This is important because we need its inverse, which can only be calculated with good approximation (that is, for large, semiclassically relevant graphs) if it is almost diagonal. The graphs that we will eventually consider are embeddings of subgraphs dual to tetrahedral, cubical or octahedral triangulations of \mathbb{R}^3 . These correspond to embeddings of regular 4-,6-,8-valent lattices, which ensures the non-alignedness property.

Thus, without loss of generality, we may choose the stacks and plaquettes as follows. Using the availability of the chart $X : \mathbb{R}^3 \rightarrow \sigma; s \rightarrow X(s)$ we consider the foliations F^I defined by the leaves $L_{It} := X_t^I(\mathbb{R}^2)$ where for $\epsilon_{IJK} = 1$ we set $X_t^I(u^1, u^2) := X(s^I := t, s^J := u^1, s^K := u^2)$. The stacks are labelled by $\alpha = (\alpha^1, \alpha^2) \in \mathbb{Z}^2$. The corresponding plaquettes are given by $p_{\alpha t}^I = \{X_t^I([\alpha + u]l); u \in [0, 1]^2\}$ where $l > 0$ is a positive number.

Likewise, using the availability of the chart, we take the edges of the graph to be embeddings of straight lines in \mathbb{R}^3 (with respect to the Euclidean background metric available there), that is, $e(t) = X(s_e + v_e \delta t)$ where v_e is a vector in \mathbb{R}^3 and $e(0) = X(s_e)$ defines the beginning point of the edge.

After these preparations, we can now analyse (2.20) and (2.21) further. Recall that

$$E_j^e = \sum_{\alpha, I} \int dt E_j(p_t^{\alpha I}) \sigma(p_t^{\alpha I}, e) \quad (2.22)$$

and

$$t_{ee'}^\gamma = \sum_{\alpha I} \int dt \sigma(p_t^{\alpha I}, e) \sigma(p_t^{\alpha I}, e') \quad (2.23)$$

By the assumption about the graphs made above, the signed intersection number takes at most the numbers ± 1 and independently of α , so that $\sigma(p_t^{\alpha I}, e)^2 = \sigma_e^I \sigma(p_t^{\alpha I}, e)$ for certain $\sigma_e^I = \pm 1$ which takes the value $+1$ if the orientation of e agrees with that of the leaves of the foliation, -1 if it disagrees, and 0 if it lies inside a leaf. If we assume that the electric field E_j^a is slowly varying at the scale of the graph (and hence at the scale of the plaquettes as well) then we may write

$$E_j^e \approx \sum_I t_{ee}^\gamma \sigma_e^I E_j(p_v^I) \quad (2.24)$$

where $p_v^I = p_{t_I(v)}^{\alpha I}$ and v is the vertex at which e is adjacent and which is under consideration in $V_{\gamma, v}$. It follows that (2.21) can be written as

$$Y_j^e = \left(\frac{a}{b}\right)^2 \sum_{e', k} \frac{t}{T_e T_{e'}} [A^{-1}]_{jk}^{ee'} \sum_I t_{e'e'}^\gamma \sigma_e^I E_k(p_v^I) = \left(\frac{a}{b}\right)^2 \sum_{e'} \sqrt{\frac{t_{e'e'}^\gamma}{t_{ee}^\gamma}} [A^{-1}]^{ee'} \sum_I \sigma_e^I E_j(p_v^I) \quad (2.25)$$

where we have used $T_e^2 = t t_{ee}^\gamma$.

Now, by construction, $A = 1 + B$ with B off-diagonal and with small entries

$$B_{ee'} = \frac{t_{ee'}^\gamma}{\sqrt{t_{ee}^\gamma t_{e'e'}^\gamma}} \quad (2.26)$$

which are of the order of l/δ since two distinct edges will typically only remain in the same stack for a parameter length l , while the parameter length of an edge is δ . Now notice that under the assumptions we have made, we have $l_{ee'}^\gamma = 0$ if e, e' are not adjacent. Define S_e to be the subset of edges which are adjacent to e . Then

$$\begin{aligned} \|Bx\|^2 &= \sum_e \sum_{e', e'' \in S_e} x_{e'} B_{e'e} B_{ee''} x_{e''} \\ &\leq [\sup_{e, e'} B_{ee'}^2] \sum_e \left[\sum_{e' \in S_e} x_{e'} \right]^2 \\ &\leq \left(\frac{l}{\delta}\right)^2 \sum_e \left[\left(\sum_{e' \in S_e} 1^2 \right)^{1/2} \left(\sum_{e' \in S_e} x_{e'}^2 \right)^{1/2} \right]^2 \\ &\leq \left(\frac{l}{\delta}\right)^2 M \sum_e \sum_{e' \in S_e} x_{e'}^2 \\ &= \left(\frac{l}{\delta}\right)^2 M \sum_{e'} x_{e'}^2 \sum_e \chi_{S_e}(e') \\ &\leq \left(\frac{l}{\delta}\right)^2 M^2 \|x\|^2 \end{aligned} \quad (2.27)$$

Here, in the second step we estimated the matrix elements of B from above; in the third step we applied the Schwarz inequality; in the fourth step we estimated $|S_e| \leq M$, where M is the maximal valence of a vertex in γ ; and in the sixth step we exploited the symmetry

$$\chi_{S_e}(e') = \begin{cases} 1 & : e' \cap e \neq \emptyset \\ 0 & : e' \cap e = \emptyset \end{cases} = \chi_{S_{e'}}(e) \quad (2.28)$$

as well as the definition of the norm of x .

It follows that for $l/\delta < M$, B is bounded from above by unity. Therefore, the geometric series $A^{-1} = 1 + \sum_{n=1}^{\infty} (-B)^n$ converges in norm. Hence we are able to consider the effects of a non-diagonal edge metric up to arbitrary order, n , in l/δ . Here we will consider $n = 1$ only and write $A^{-1} = 1 - (A - 1) = 2 \cdot 1 - A$. But before considering corrections from the off-diagonal nature of A notice that, to zeroth-order in l/δ , equation (2.25) becomes simply

$$Y_j^e = \left(\frac{a}{b}\right)^2 \sum_I \sigma_e^I E_j(p_v^I) \quad (2.29)$$

Inserting (2.29) into (2.20) we find

$$\langle \hat{V}_v \rangle_{Z,\gamma} \approx \left(\frac{a}{b}\right)^3 \sqrt{|\det(E)(v)|} \sqrt{\left| \frac{1}{48} \sum_{e \cap e' \cap e'' = v} \epsilon(e, e', e'') \det(\sigma) \det(p_v) \right|} \quad (2.30)$$

where

$$\det(p_v) = \frac{1}{3!} \epsilon_{IJK} \epsilon^{abc} \int_{[0,1]^2} d^2u n_{at}^{\alpha_I(v)I}(u) \int_{[0,1]^2} d^2u n_{bt}^{\alpha_J(v)I}(u) \int_{[0,1]^2} d^2u n_{ct}^{\alpha_K(v)I}(u) \quad (2.31)$$

On recalling that $n_{at}^{\alpha I} = \epsilon_{abc} X_{at,u^1}^{Ib} X_{at,u^2}^{Ic}$ with $X_{at}^{Ia}(u) = X^a(s^I = t, s^J = \alpha^1 + lu^1, s^K = \alpha^2 + lu^2)$ for $\epsilon_{IJK} = 1$, we find

$$\det(p_v) \approx l^6 \left[\det(\partial X(s)/\partial s) \right]_{X(s)=v} \quad (2.32)$$

Hence (2.30) becomes

$$\langle \hat{V}_v \rangle_{Z,\gamma} \approx \left(\frac{al}{b}\right)^3 \sqrt{|\det(E)(v)|} \left| \left[\det(\partial X(s)/\partial s) \right]_{X(s)=v} \right| \sqrt{\left| \frac{1}{48} \sum_{e \cap e' \cap e'' = v} \epsilon(e, e', e'') \det(s) \right|} \quad (2.33)$$

We can draw an important conclusion from expression (2.33). Namely, the first *three* factors approximate the classical volume $V_v(E)$ as determined by E of an embedded cube with parameter volume $(al/b)^3$. When we sum (2.33) over the vertices of γ , which have a parameter distance, δ , from each other where $l \ll \delta$ by assumption, then the volume expectation value only has a chance to approximate the classical volume when the graph is such that $\delta = al/b$, or $\delta/l = a/b$. This could never have been achieved for $b = a$ and explains why we had to rescale the labels of the coherent states by $(a/b)^2$ while keeping the classicality parameter at $t = \ell_P^2/a^2$. See our companion paper for a detailed discussion. There we also explained why one must have δ/l actually equal to a/b and not just of the same order: While one could use this in order to favour other valences of the volume operator, the expectation value of other geometrical operators such as area and flux would be incorrect.

Assuming $\delta/l = a/b$ we write (2.33) as

$$\langle \hat{V}_v \rangle_{Z,\gamma} =: V_v(E) G_{\gamma,v} \quad (2.34)$$

thereby introducing the graph geometry factor $G_{\gamma,v}$. It does not carry any information about the phase space, only about the embedding of the graph relative to the leaves of the three-foliations. From the fact that (2.34) reproduces the volume of a cube up to a factor, we may already anticipate that the geometry factor will be close to unity for, at most, a cubic graph. Whether this holds for an arbitrary orientation of the graph with respect to the stack family will occupy a large part of the analysis which follows.

2.3 Preliminary analysis of the graph geometry factor

We start by investigating the behaviour of the graph geometry factor $G_{\gamma,v}$ under diffeomorphisms, φ , of σ , that is, under $G_{\gamma,v} \mapsto G_{\varphi(\gamma),\varphi(v)}$ while the linearly-independent families of stacks are left untouched. This

will answer the question of how much the geometry factor depends on the relative orientation of the graph with respect to the stacks.

In fact, the orientation factor $\epsilon(e, e', e'')$ is invariant under diffeomorphisms of the spatial manifold σ . The signature factor

$$\det_{e, e', e''}(\sigma) = \epsilon_{IJK} \sigma_e^I \sigma_{e'}^J \sigma_{e''}^K \quad (2.35)$$

is obviously invariant under any diffeomorphism that preserves the foliations F^I , i.e. which map leaves onto leaves, because

$$\sigma_e^I = \frac{1}{2} \int_e dx^a \epsilon_{abc} \int_{L_{It}} dy^b \wedge dy^c \delta(x, y) \quad (2.36)$$

where L_{It} is any leaf in t which intersects e transversely. Since we consider graphs whose edges are embedded lines in \mathbb{R}^3 with the same embedding that defines the stacks, it follows that the geometry factor is invariant under any embedded global translations in \mathbb{R}^3 .

Next, since global rescaling in \mathbb{R}^3 preserves the foliations and the topological invariant (2.36), the geometry factor is also invariant under embedded global rescalings of \mathbb{R}^3 . Finally, any embedded global rotations of \mathbb{R}^3 that preserves all the orientation factors σ_e^I will leave the geometry factors invariant. Since the orientation factors only take the values $+1, -1, 0$ (depending on whether an edge agrees, disagrees with the orientation of the leaves, or lies within a leaf), there will be a vast range of Euler angles for which this condition is satisfied, if the graph is an embedded, regular lattice of constant valence⁷. Hence, in order to check whether the geometry factor is rotationally invariant under any rotation we need only worry about those rotations which lead to changes in the σ_e^I . Likewise, if we rotate a graph which is dual to a polyhedral complex, we expect that the expectation value remains invariant as long as the graph remains dual to the complex.

Fortunately, using the explicit formulae derived for the edges and vertices for $n = 4, 6, 8$ -valent graphs displayed in [23] we can calculate the σ_e^I for each edge e . Intuitively, it is clear, that whenever many of the σ_e^I change from $+1$ to -1 , we can expect a drastic change of the expectation value. However, one has to take into account the combined effect of these changes, and this is what makes rotational invariance possible. As a first step we determine the action of a rotation on the sign factors.

2.4 Explicit calculation of the σ_e^I terms

In what follows we discuss the cases that show a drastic change in the value of $\det_{e, e', e''}(\sigma) = \epsilon_{IJK} \sigma_e^I \sigma_{e'}^J \sigma_{e''}^K$ caused by a change in the values of σ_e^I . To carry out this calculation we will perform a rotation of each of the three different types of lattice analysed so far: namely, the 4-, 6- and 8-valent lattices. These rotations will be parameterised by Euler angles and will be centred at a particular vertex of the lattice, for example V_0 . The effects of a rotation will depend on the distance of the vertices from the centre of the rotation. In fact, the position of each vertex in the lattice after rotation will depend on both the distance from the centre of the rotation and the Euler angles used in the rotation. Fortunately, the values of the terms σ_e^I will not depend on the former but only on the latter.

This is easy to see since the value of σ_e^I can be either 1, -1 or 0 depending on whether the edge is outgoing, ingoing, or lies on the plaquette in the direction I . Thus it will only depend on the angle the edge makes with the perpendicular to the plaquette in any given direction, i.e. it will depend on the angles the edge makes with respect to a coordinate system centred at the vertex at which the edge is incident. Clearly, only the values of the Euler angles of the rotation will affect the angles each edge has with respect to the vertex at which it is incident. In particular, since the graph we are using is regular, following the rotation, all edges which were parallel to each other will remain such, and thus will have the same angles with respect to the vertex at which they are incident. This implies that in order to compute the values of the terms σ_e^I , we can consider each vertex separately and apply the same rotation to each vertex individually.

⁷In fact, for a random graph we may also have rotational invariance on large scales.

On the other hand, the distance from the centre of the rotation affects the position of each vertex with respect to the plaquette structure, and thereby affects both the values of the terms $t_{ee'}$ and the number of them that are different from zero. These effects can be easily understood with the aid of the two-dimensional diagram (Figure 2).

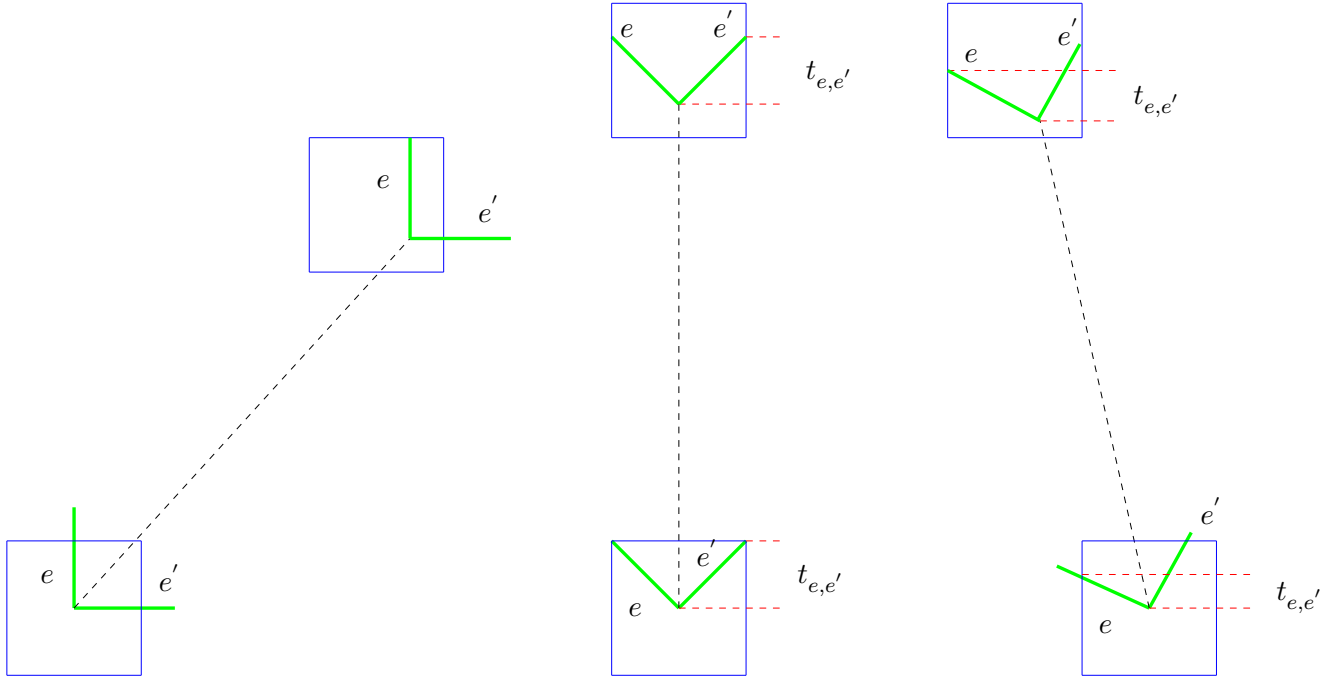


Figure 2: Example of translation and rotation

It is clear that, for any two parallel edges, the angle each of them has with respect to the vertex at which they are incident, is independent of the distance of the edge from the centre of rotation. On the other hand, the values of the $t_{ee'}$ will depend on both the rotation and the distance of the centre of rotation, since the position of the rotated vertex with respect to the plaquette depends on both these parameters. Therefore, we can tentatively assume that two different geometric factors will be involved in the computation of the volume operator:

- i) $G_{\gamma,V}$, which indicates how the terms σ^I are affected by rotation. This geometric factor affects all orders of approximation of the expectation value of the volume operator.
- ii) $C_{\gamma,V}$, which indicates the effect of rotation on the terms $t_{ee'}$. This term affects only the first- and higher-order approximations of the expectation value of the volume operator, not the zeroth-order.

In what follows we will analyse the geometric term $G_{\gamma,V}$: i.e., we will analyse the changes in the values of the σ_e^I due to a rotation applied at each vertex independently. We will do this for the 4-, 6- and 8-valent graphs separately. The geometric factor $C_{\gamma,V}$ will be analysed in subsequent Sections.

As we will not see, our calculations show that for all 4-, 6- and 8-valent graphs, the rotations that produce drastic change in the values of $\det_{e,e',e''}(\sigma) = \epsilon_{IJK}\sigma_e^I\sigma_{e'}^J\sigma_{e''}^K$ have measure zero in $SO(3)$ since they occur for specific Euler angles rather than for a range of them.

Let us start with the 6-valent graph (Figure 3). From the discussion above, we need only consider the effects of the rotation on one vertex, V_0 .

In order to compute the change in the values of the individual σ_e^I , we will divide into eight small sub-cubes the cube formed by the intersection of the plaquettes in the three directions and containing the vertex we are analysing (V_0). It is then easy to see that for each edge e , the corresponding value of σ_e^I depends on the sub-cube in which it lies. In particular, we have the following table for the values of σ_e^I .

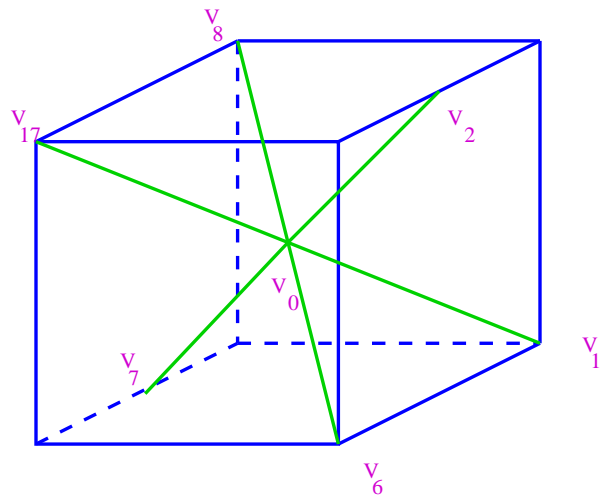


Figure 3: 6-valent vertex

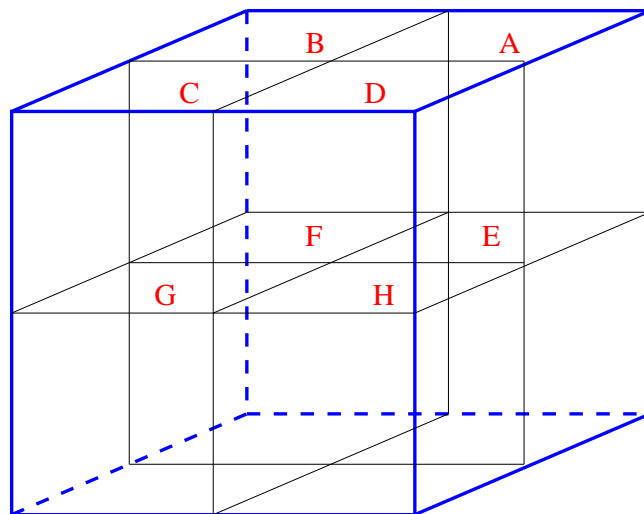


Figure 4: Division of the cube in 8 sub-cubes

	A	B	C	D	E	F	G	H
σ_e^x	+	-	-	+	+	-	-	+
σ_e^y	+	+	-	-	+	+	-	-
σ_e^z	+	+	+	+	-	-	-	-

From the above table it is clear that when an edge moves from one of the eight cubes to another, the values of each of the σ_e changes accordingly. Given any 6-valent vertex, each of the six edges incident at a vertex will be in one distinct cube. Moreover, since any two edges incident at a vertex can be either co-planar or perpendicular (in the abstract pull-back space with Euclidean metric), there are only certain combinations of allowed positions. For instance, for the edges $e_1, e_2, e_3, e_4, e_5, e_6$ only the combinations

$$C_1B_2D_3E_4F_5H_6, C_1D_2A_3F_4G_5E_6, A_1B_2C_3H_4E_5G_6, B_1A_2D_3H_4G_5F_6 \quad (2.37)$$

are allowed (here the notation A_i means that the edge i lies in the cube A); the combination $A_1B_2C_3D_4G_5F_6$ is not allowed.

Because of the highly symmetric structure of the 6-valent graph we do not have to analyse all possible combinations of all the six edges incident at a vertex, since different combinations are related by symmetry arguments. For example, the combination in which edges $e_1, e_2, e_3, e_4, e_5, e_6$ lie in the cubes $C_1D_2A_3F_4G_5E_6$, and the combination in which they lie in the cubes $F_1G_2H_3C_4D_5A_6$, lead to the same value of $|\det_{e,e',e''}(\sigma)| = |\epsilon_{IJK}\sigma_e^I\sigma_{e'}^J\sigma_{e''}^K|$, and an equal number of $\det_{e,e',e''}(\sigma) > 0$ and $\det_{e,e',e''}(\sigma) < 0$, but obtained from different triplets e, e', e'' . In particular, any consistent relabelling of the edges will produce the same overall result for the determinants of the triplets. These symmetries reduce considerably the number of cases that need to be analysed.

In what follows, we consider the cases for which the edges $e_1, e_2, e_3, e_4, e_5, e_6$ lie in the following combinations of cubes:

$$C_1B_2D_3E_4F_5H_6, C_1D_2A_3F_4G_5E_6, A_1B_2C_3H_4E_5G_6, B_1A_2D_3H_4G_5F_6 \quad (2.38)$$

For each of these cases there will be sub-cases according to whether one edge or more lie in a particular plaquette, or are parallel to a given direction I, J, K . These sub-cases are the following:

1. No edge lies in any plaquette, or is parallel to any of the directions.

In this case we obtain $|\det_{e,e',e''}(\sigma)| = 4$ for all triplets, but four of these triplets will have $\det_{e,e',e''}(\sigma) = -4$ while the remaining four will have $\det_{e,e',e''}(\sigma) = 4$.

2. Only one edge lies in a particular plaquette (say the J direction) (see Figure 3). This edge and its co-linear edge will have σ_e^J equal to zero (J being the direction of the plaquette in which the edge lies.)

In this case we obtain $\det_{e,e',e''}(\sigma) = -4$ for four triplets, and $\det_{e,e',e''}(\sigma) = 4$ for the remaining four triplets.⁸

3. Two edges lie in two different plaquettes such that each of these two edges and their respective co-linear edges will have σ_e^I equal to zero in the direction of the plaquette in which they lie. In this case, because of the geometry of the 6-valent lattice, the remaining edges will each be parallel to a given direction J such that all but the σ_e^J are zero.

In this case we obtain $\det_{e,e',e''}(\sigma) = 2$ for four triplets while the remaining four will have $\det_{e,e',e''}(\sigma) = -2$. (See Figure 5).

4. Each edge is parallel to a given direction such that all the σ_e^I (for any I, J, K) are equal to zero except for the one in the direction to which the edge is parallel. In this case we obtain $\det_{e,e',e''}(\sigma) = 1$ for four triplets and $\det_{e,e',e''}(\sigma) = -1$ for the remaining four. (See Figure 6)

⁸Note that the geometric factor associated to this edge orientation will coincide with the geometric factor as derived from case 1). In this sense, case 2) can be seen as a limiting case of 1)

Only sub-cases 3 and 4 might lead to a change of value for the geometric factor $G_{\gamma,V}$. However cases 2, 3 and 4 have measure zero in $SO(3)$.

As a demonstrative calculation on how this is derived we will choose case 3. In particular, we select the configuration depicted in Figure 5 which can be obtained by a rotation of the original configuration in Figure

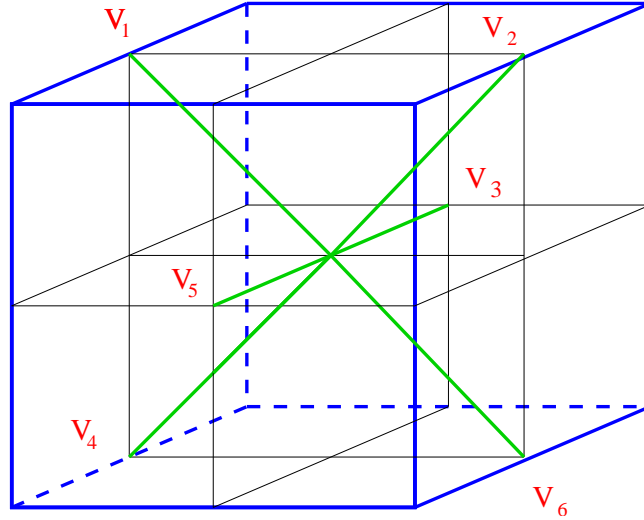


Figure 5: Example of configuration with zero measure in $SO(3)$

6. Let us consider the linearly-independent triples comprised of the edges that connect the barycenter of

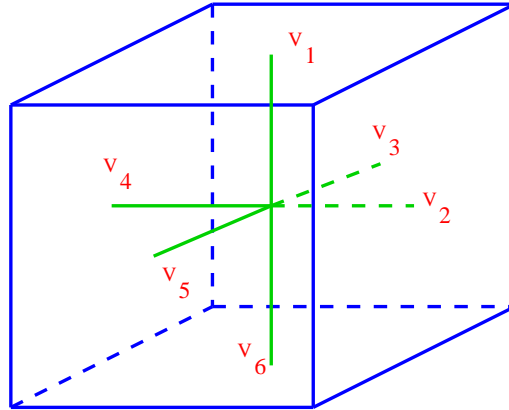


Figure 6: Regular 6-valent graph

the cube to the vertices V_1 , V_2 and V_3 . In the original configuration, the coordinates of these vertices are (in what follows we will denote the length of an edge, e , by $\delta_e = \delta$)

$$V_1 = (0, 0, \delta) , V_2 = (\delta, 0, 0) , V_3 = (0, \delta, 0) \tag{2.39}$$

By applying a general Euler rotation, whose matrix representation is given in (3.2.2), the coordinates of the rotated vertices become:

$$V_1 = (R_{13}\delta, R_{23}\delta, R_{33}\delta) , V_2 = (R_{11}\delta, R_{21}\delta, R_{31}\delta) , V_3 = (R_{12}\delta, R_{22}\delta, R_{32}\delta) \tag{2.40}$$

Our task now is to determine which Euler angles would give rise to the configuration in Figure 5. Since in such a configuration the edges e_{01} (the edge joining the barycenter of the cube to vertex V_1) and e_{03} lie

in the plane x - y , while the edge e_{01} is parallel to the z -direction, the coordinates of the rotated vertices are constrained by the following set of equations:

$$x_{V_1} = R_{13} = \sin \psi \sin \theta < 0 \quad y_{V_1} = R_{23} = \cos \psi \sin \theta = 0 \quad z_{V_1} = R_{33} = \cos \theta > 0 \quad (2.41)$$

$$x_{V_2} = R_{11} = \cos \psi \cos \phi - \cos \theta \sin \phi \sin \psi < 0 \quad y_{V_2} = R_{21} - \sin \psi \cos \phi - \cos \theta \sin \phi \cos \theta = 0 \quad (2.42)$$

$$z_{V_2} = R_{31} = \sin \theta \sin \phi > 0 \quad (2.43)$$

$$x_{V_3} = R_{12} \cos \psi \sin \phi + \cos \theta \cos \phi \sin \psi = 0 \quad y_{V_3} = R_{22} = -\sin \psi \sin \theta + \cos \theta \cos \phi \cos \psi > 0 \quad (2.44)$$

$$z_{V_3} = R_{32} = -\sin \theta \cos \phi = 0 \quad (2.45)$$

By solving this set of equations we find that the Euler angles ψ , ϕ and θ that give rise to the configuration in Figure 5 are

i) $\theta = (n + 1)\frac{\pi}{2}$ and $\psi = (p + 1)\frac{\pi}{2}$ for n =odd, p =even and $0 < \theta < \frac{\pi}{2}$

ii) $\theta = (n + 1)\frac{\pi}{2}$ and $\psi = (p + 1)\frac{\pi}{2}$ for n =even, p =odd and $\frac{3\pi}{2} < \theta < 2\pi$

It follows that the arrangement of edges under scrutiny has measure zero in $SO(3)$.

By a similar method it can be shown that whenever an edge lies in a plaquette, or is parallel to a plaquette, one of the Euler angles will have to be equal to $\frac{n}{\pi}$ for n odd or even. Therefore, that arrangement will have measure zero. This is not so for the general arrangement (number 1) delineated above. However, for any such arrangement, the values for the orientation factor and subsequently the geometric factor $G_{\gamma,V}$ will always be the same and, in zeroth-order, will not lead to any changes of the expectation value of the volume operator.

Hence, the only cases of interest—i.e. the cases with measure different from zero—will not lead to a rotational dependence of the expectation value of the volume operator in zeroth-order. This should not come as a surprise since the geometry of a regular 6-valent graph is such that to each edge there corresponds a co-linear one. Thus whenever the term σ_e^I for edge e changes from -1 to 1, the term $\sigma_{e'}^I$ of the co-linear edge undergoes the inverse transformation. As a consequence there will always be the same number of $\det_{e,e',e''}(\sigma) = -4$ and $\det_{e,e',e''}(\sigma) = 4$, although the triplets involved will be different in each case. It follows that the overall value of the geometric factor $G_{\gamma,V}$ remains constant.

A similar reasoning holds for the 8-valent graph since here too each edge has a corresponding co-linear edge. Therefore, there will always be an equal number of $\sigma_e^I = 1$ and $\sigma_e^I = -1$. This implies that, as in the case for 6-valent graph, when no edge lies on a plaquette, the value of the expectation value of the volume operator for each 8-valent vertex will be rotationally invariant. On the other hand, the orientation of edges in an 8-valent graph in which one or more edges lie in a plaquette, or an edge is parallel to a given direction, have measure zero in $SO(3)$, as was the case for the 6-valent graph. However, as previously stated, it is precisely such cases that lead to a change in the value of the geometric factor $G_{\gamma,V}$.

For the 4-valent case the situation is somewhat different since there are no co-planar edges. Those arrangements of edges with respect to the stacks of plaquettes that cause drastic changes in the values of the orientation factor are the following:

1. No edge lies in any plaquette. In this case we obtain $|\det_{e,e',e''}(\sigma)| = 4$ for all linearly-independent triplets.
2. Each edge lies in a given plaquette. This gives $|\det_{e,e',e''}(\sigma)| = 2$ for all linearly-independent triplets.
3. One edge is aligned with a given plaquette, one edge lies in a given plaquette, and the remaining edges do not lie in—and are not aligned to—any plaquette. In this case we obtain $|\det_{e,e',e''}(\sigma)| = 1$ for two triplets, $|\det_{e,e',e''}(\sigma)| = 2$ for one triplet, and $|\det_{e,e',e''}(\sigma)| = 4$ for the remaining triplet.

Similar calculations to those for the 6-valent graph then show that the cases 1 and 2 above have measure zero in $SO(3)$.

In summary, the discussion above shows that for all 4-, 6- and 8-valent graphs, those orientations of the edges with respect to the stacks that cause a drastic change in the orientation factor have measure zero in $SO(3)$. Therefore, up to measure zero in $SO(3)$, the geometric factor $G_{\gamma,V}$ for these graphs is rotationally invariant.

2.4.1 Computation of the geometric factor for 4-, 6- and 8-valent graphs

In this Section we will compute the geometric factor $G_{\gamma,v}$ for the 4-, 6- and 8-valent graphs. We recall from equation (2.33) that the expression for the geometric factor is

$$\begin{aligned} G_{\gamma,v} &:= \sqrt{\left| \frac{1}{48} \sum_{e \cap e' \cap e'' = v} \epsilon(e, e', e'') \det_{e, e', e''}(\sigma) \right|} \\ &= \sqrt{\left| \frac{1}{8} \sum_{1 \leq i < j < k \leq N} \epsilon(e_i, e_j, e_k) \det_{e_i, e_j, e_k}(\sigma) \right|} \end{aligned} \quad (2.46)$$

where N is the valence of the vertex and $\det_{e_i, e_j, e_k}(\sigma) = \epsilon_{IJK} \sigma_{e_i}^I \sigma_{e_j}^J \sigma_{e_k}^K$. In what follows we will calculate $G_{\gamma,v}$ for the 4-, 6- and 8-valent graphs respectively. In particular (for each valence) we will analyse each of the cases discussed in the previous Section which lead to different values of orientation factor. Any sub-case of these cases will lead to the same geometric factor.

4-valent graph: We now compute the geometric factor for the 4-valent vertex for different embeddings of the graph in the stack of surfaces.

1. The most general situation is one in which none of the edges is aligned to, or lies in, a given plaquette. Thus, for example, consider the situation in which the edges e_1, e_2, e_3 and e_4 are in the octants A, C, H and F respectively (see Figure 7). Such a combination has a non-zero measure in $SO(3)$.

The values for $\det_{e_i, e_j, e_k}(\sigma)$ relative to this case are given by

$$\begin{aligned} \det_{e_1, e_2, e_3}(\sigma) &= \det_{e_1, e_3, e_4}(\sigma) = -4 \\ \det_{e_1, e_2, e_4}(\sigma) &= \det_{e_2, e_3, e_4}(\sigma) = 4 \end{aligned} \quad (2.47)$$

Inserting these values in (2.46) gives

$$\begin{aligned} G_{\gamma,v} &= \sqrt{\left| \frac{1}{8} \sum_{1 \leq i < j < k \leq 4} \epsilon(e_i, e_j, e_k) \det_{e_i, e_j, e_k}(\sigma) \right|} \\ &= \sqrt{\left| \frac{1}{8} (-4\epsilon(e_1, e_2, e_3) - 4\epsilon(e_1, e_3, e_4) + 4\epsilon(e_1, e_2, e_4) + 4\epsilon(e_2, e_3, e_4)) \right|} \\ &= \sqrt{\frac{1}{8} 16} \end{aligned} \quad (2.48)$$

2. If instead we consider the case in which each of the edges lies in a plaquette as, for example, is depicted in Figure 8, then the value for the geometric factor is

$$\begin{aligned} G_{\gamma,v} &= \sqrt{\left| \frac{1}{8} \sum_{1 \leq i < j < k \leq 4} \epsilon(e_i, e_j, e_k) \det_{e_i, e_j, e_k}(\sigma) \right|} \\ &= \sqrt{\left| \frac{1}{8} (-2\epsilon(e_1, e_2, e_3) - 2\epsilon(e_1, e_3, e_4) + 2\epsilon(e_1, e_2, e_4) + 2\epsilon(e_2, e_3, e_4)) \right|} \\ &= \sqrt{\frac{1}{8} 8} \end{aligned} \quad (2.49)$$

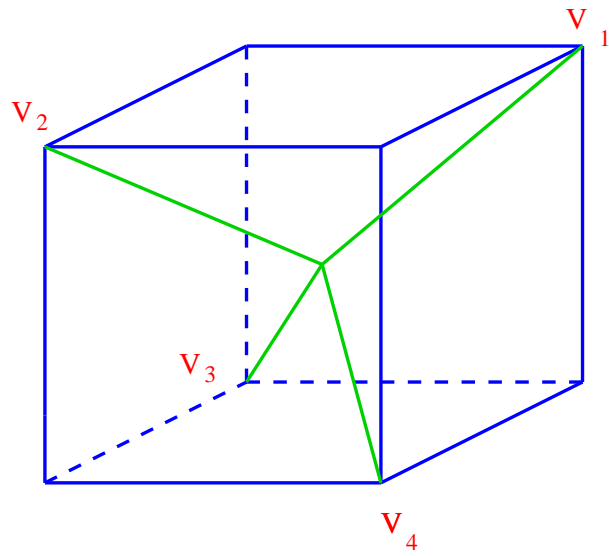


Figure 7: General 4-valent vertex

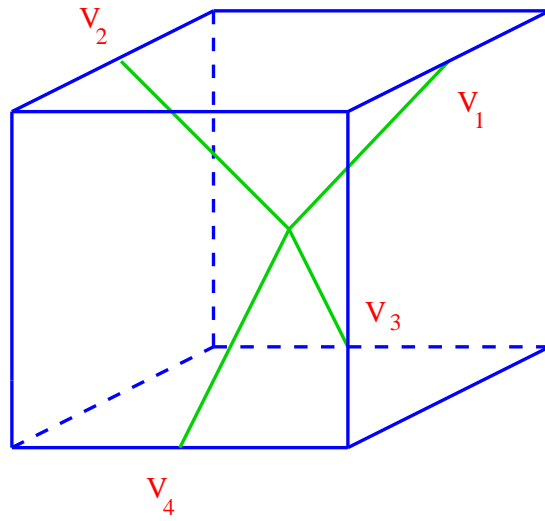


Figure 8: General 4-valent vertex

3. For the situation in which one edge lies in a plaquette and another edge is aligned with a plaquette in another direction (Figure 9), we obtain

$$\begin{aligned}
G_{\gamma,v} &= \sqrt{\left| \frac{1}{8} \sum_{1 \leq i < j < k \leq 4} \epsilon(e_i, e_j, e_k) \det_{e_i, e_j, e_k}(\sigma) \right|} & (2.50) \\
&= \sqrt{\left| \frac{1}{8} (-1\epsilon(e_1, e_2, e_3) - 4\epsilon(e_1, e_3, e_4) + 1\epsilon(e_1, e_2, e_4) + 2\epsilon(e_2, e_3, e_4)) \right|} \\
&= \sqrt{\frac{1}{8} 8}
\end{aligned}$$

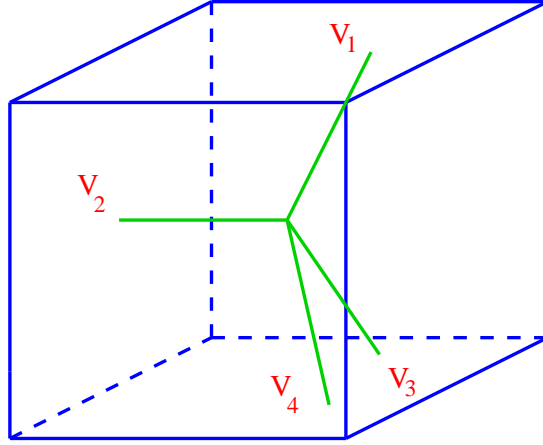


Figure 9: General 4-valent vertex

However, we proved above that the embeddings of the vertex with respect to the stack depicted in cases 2) and 3) have measure zero in $SO(3)$.

6-valent graph: We now compute the geometric factor for the 6-valent vertex in the cases 1 to 4 described in the previous Section and which lead to different values of the signature factor.

1. We start with the most general embedding of a 6-valent vertex with respect to the stacks. For example, consider the case in which the edges e_1, e_2, e_3, e_4, e_5 and e_6 are in the octants A H E B C and G respectively. We then obtain the following value for the geometric factor:

$$\begin{aligned}
G_{\gamma,v} &= \sqrt{\left| \frac{1}{8} \sum_{1 \leq i < j < k \leq 6} \epsilon(e_i, e_j, e_k) \det_{e_i, e_j, e_k}(\sigma) \right|} & (2.51) \\
&= \sqrt{\left| \frac{1}{8} (4\epsilon(e_1, e_2, e_3) + 4\epsilon(e_1, e_3, e_4) + 4\epsilon(e_1, e_4, e_5) - 4\epsilon(e_1, e_2, e_5) - 4\epsilon(e_2, e_3, e_4) + 4\epsilon(e_2, e_5, e_6) \right. \\
&\quad \left. - 4\epsilon(e_3, e_4, e_6) - 4\epsilon(e_4, e_5, e_6)) \right|} \\
&= \sqrt{\frac{1}{8} 4 \times 8}
\end{aligned}$$

2. For the geometric factor when only *one* edge and its co-planar edge lie in a plaquette (Figure 3) we obtain: $G_{\gamma,v} = 2$.

3. For the case in which *two* edges and their co-planar edge lie in two different plaquettes in two different directions, while the remaining edge and its co-planar edge are aligned with the plaquette in the third direction (Figure 5), we obtain $G_{\gamma,v} = \sqrt{2}$.
4. For the case in which all the edges are aligned with the stacks (Figure 6) we obtain $G_{\gamma,v} = 1$, since in that case $|\det_{e_i,e_j,e_k}| = 1$ for all linearly independent triplets e_i, e_j, e_k .

However, we have proved above that cases 2), 3) and 4) have measure zero in $SO(3)$.

8-valent graph: We now compute the geometric factor for the 8-valent vertex for different embeddings of the graph with respect to the stack of surfaces.

1. In the most general case, none of the edges lie in, or are aligned to, a given plaquette: for example, when the edges $e_1, e_2, e_3, e_4, e_5, e_6, e_7$ and e_8 are in the octants B, C, A, D, H, E, G and F respectively. This leads to the following result

$$\begin{aligned}
G_{\gamma,v} &= \sqrt{\left| \frac{1}{8} \sum_{1 \leq i \leq j \leq k \leq 4} \epsilon(e_i, e_j, e_k) \det_{e_i, e_j, e_k}(\sigma) \right|} & (2.52) \\
&= \sqrt{\left| \frac{1}{8} (4\epsilon(e_1, e_2, e_3) + 4\epsilon(e_1, e_2, e_4) - 4\epsilon(e_1, e_2, e_8) - 4\epsilon(e_1, e_2, e_7) - 4\epsilon(e_1, e_3, e_4) + 4\epsilon(e_1, e_3, e_6) \right. \\
&\quad \left. + 4\epsilon(e_1, e_3, e_8) + 4\epsilon(e_1, e_4, e_6) - 4\epsilon(e_1, e_4, e_7) + 4\epsilon(e_1, e_6, e_7) + 4\epsilon(e_1, e_6, e_8) - 4\epsilon(e_1, e_7, e_8) \right. \\
&\quad \left. - 4\epsilon(e_2, e_3, e_4) - 4\epsilon(e_2, e_3, e_5) \dots) \right|} \\
&= \sqrt{\frac{1}{8} 4 \times 32} & (2.53)
\end{aligned}$$

2. A more restricted case is when one edge and its co-planar edge are aligned with a plaquette in a given, different direction, while the remaining three edges and their co-planar edge lie in a given plaquette. Here we obtain $G_{\gamma,v} = \sqrt{5}$.
3. A special case is when each edge lies in a given plaquette: this gives $G_{\gamma,v} = 2\sqrt{2}$.

Similarly to the 4- and 6-valent vertex above, arrangement 2) and 3) have measure zero in $SO(3)$.

From the discussion above of the geometric factor we can already deduce that, ignoring off-diagonal entries of the edge metric A , the expectation value of the volume operator gives the correct semiclassical value only for combinations of edges that have measure zero in $SO(3)$.

In fact, in zeroth-order in $\frac{l}{b}$ the expectation value of the volume operator is given by

$$\langle \hat{V}_v \rangle_{Z,\gamma} \approx \left(\frac{al}{b}\right)^3 \sqrt{|\det(E)(v)|} \left| [\det(\partial X(s)/\partial s)]_{X(s)=v} \right| \sqrt{\left| \frac{1}{48} \sum_{e \cap e' \cap e'' = v} \epsilon(e, e', e'') \det_{e, e', e''}(\sigma) \right|} \quad (2.54)$$

where $\left(\frac{al}{b}\right)^3 \sqrt{|\det(E)(v)|} \left| [\det(\partial X(s)/\partial s)]_{X(s)=v} \right|$ approximates the classical volume $V_v(E)$ as determined by E of an embedded cube with parameter volume $(al/b)^3$. It is straightforward to see that the correct semiclassical behaviour is attained for $G_{\gamma,v} = 1$.

The fact that the correct semiclassical behaviour of the volume operator is attained *only* for cases in which the graph is aligned to the plaquettation (6-valent case), or each edge lies in a given plaquette (the 4-valent case), seems rather puzzling since, both cases, have measure zero in $SO(3)$. This makes one question the *prima facie* validity of utilizing the area coherent states to compute the expectation value of the volume operator. However, it is interesting to note that case 4) of the 6-valent graph is precisely what one gets when constructing such a graph as the dual of a cubical cell complex.

We will now proceed to compute the higher, $\frac{l}{b}$ -order dependence of the expectation value of the volume operator for 4-, 6- and 8-valent graphs respectively.

3 The Higher, $\frac{l}{\delta}$ -order Dependence of the Expectation Value of the Volume Operator

In this Section we compute the expectation value of the volume operator for the 4-, 6-, and 8-valent graphs. The construction of these graphs was discussed in [23] in terms of regular simplicial, cubical and octahedral cell complexes respectively.

The following Section is subdivided into four parts. In the first we explain the general method to be applied in the subsequent Sections. In the second, third and fourth parts we apply this method to our 4-, 6- and 8-valent graphs respectively. Each of these subsections is itself subdivided into three parts: in the first, the stack family and the cubulation that defines the platonic-body cell complex dual to the graph are aligned (see [23]); in the second we study the effect of a rotation; and in the third we study the effect of a translation.

3.1 Initial preparations

As a first step towards computing the expectation value of the volume operator, we must calculate the values of the quantities t_e^γ and $t_{ee'}^\gamma$, defined in [23], which indicate the number of surfaces, $s_{\alpha t}^I$, that the edge e intersects, and the number of surfaces, $s_{\alpha t}^I$, which are intersected by both edges e and e' . Both these quantities depend explicitly on how the graph is embedded in the stack family S^I (see [23]). In fact, the conditions for two or more edges to intersect a common surface are the following:

- 1) Two edges e_i and e_j intersect the same plaquette, $s_{\alpha t}^z$, iff $0 < \phi_i, \phi_j < \frac{\pi}{2}$ or $\frac{\pi}{2} < \phi_i, \phi_j < \pi$
- 2) Two edges e_i and e_j intersect the same plaquette, $s_{\alpha t}^x$, iff $-\frac{\pi}{2} < \theta_i, \theta_j < \frac{\pi}{2}$ or $\frac{\pi}{2} < \theta_i, \theta_j < \frac{3\pi}{2}$
- 3) Two edges e_i and e_j intersect the same plaquette, $s_{\alpha t}^y$, iff $0 < \theta_i, \theta_j < \pi$ or $\pi < \theta_i, \theta_j < 2\pi$
- 4) If we have equalities in any of the above conditions, such that the angles of each of the two edges correspond to a different limiting case, we obtain $t_{e_i e_j}^I = \{t_i \in \mathbb{R} | S_t^I \cap e_k \neq \emptyset, k = i, j\} = \emptyset$.

We can also have situations in which two or more edges intersect a common plaquette in more than one stack. The conditions for such occurrences are the following:

- a) Given condition (1), two edges e_i and e_j will intersect more than one z -stack iff $|\theta_i| + |\theta_j| < \pi/2$ and such that $n\frac{\pi}{4} < \theta_i, \theta_j < (n+1)\frac{\pi}{4}$, where $n = \{1, 2, 3, 4, 5, 6, 7, 8\}$.
- b) Given condition (2), two edges e_i and e_j will intersect more than one x -stack iff condition (1) above is satisfied and $n\frac{\pi}{4} < \theta_i, \theta_j < (n+1)\frac{\pi}{4}$, where $n = \{1, 2, 3, 4, 5, 6, 7, 8\}$.
- c) Given condition (3), two edges e_i and e_j will intersect more than one y -stack iff condition (1) above is satisfied and $n\frac{\pi}{4} < \theta_i, \theta_j < (n+1)\frac{\pi}{4}$, where $n = \{1, 2, 3, 4, 5, 6, 7, 8\}$.

The conditions above imply that rotating the graph will change the values of the $t_{e_i e_j}^I$ and also the number of the $t_{e_i e_j}^I$ that are non-zero.

We will now briefly explain, with the aid of an easy example, the strategy we use to compute the terms $\frac{t_{e_i e_j}^I}{\sqrt{t_{e_i}^I t_{e_j}^I}}$ that are used in the calculations of the expectation value of the volume operator for the 4-, 6- and 8-valent graphs. To this end, consider an edge, $e \in \gamma$, of a generic graph whose length is given by δ . This edge will intersect the stacks of plaquettes in each direction a certain number of times. In particular, given

a length l of a plaquette, each edge will have n intersections with the stacks of any given direction, where n is identified with the Gauss bracket $[\frac{c_i}{l}]$ and c_i is proportional to δ , where c_i for $i \in \{x, y, z\}$ are the coordinates of the edge.

For example, in the two-dimensional case of Figure 10, the values of n in any given direction for vertex V_1 (or equivalently the edge $e_{0,1}$ of length δ), whose coordinates are $V_1 = (\delta \cos(a), \delta \sin(a))$, would be

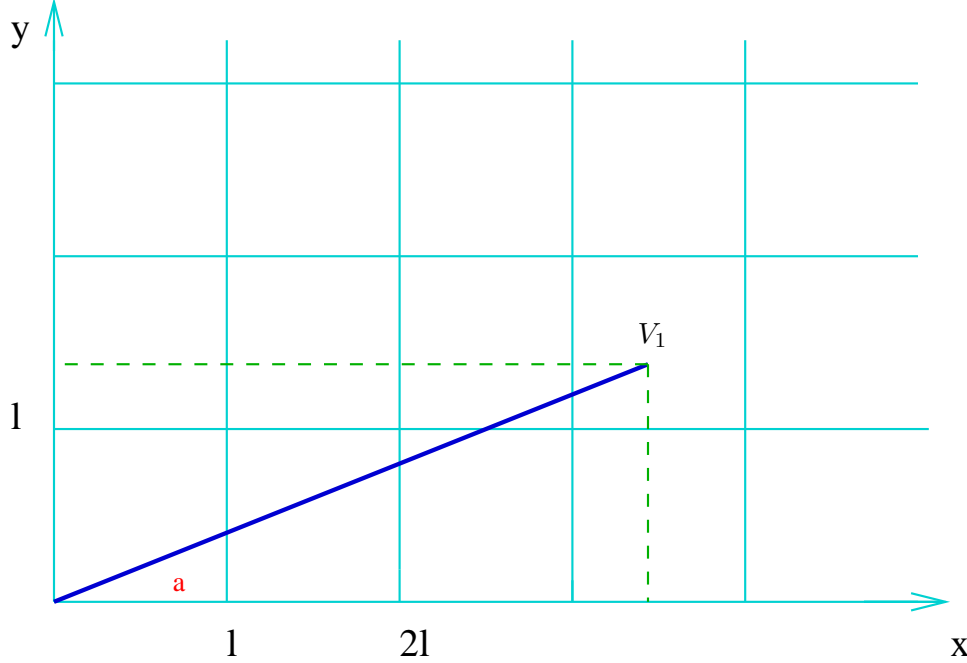


Figure 10: Intersections of an edge with the plaquettes in 2-dimensions

$$n_x = [\frac{\delta \cos(a)}{l}] \text{ and } n_y = [\frac{\delta \sin(a)}{l}].$$

The values n_i , $i \in \{x, y, z\}$, depend on both the angle a and the ratio $\frac{l}{\delta}$. Concomitantly, the expectation value of the volume operator will also depend on such parameters.

The rotational dependence will be dealt with later. In the present Section we will focus on the $\frac{l}{\delta}$ dependence. We need to consider three different sub-cases:

1. $\frac{\delta}{l} > 1$
2. $\frac{\delta}{l} = 1$
3. $\frac{\delta}{l} < 1$

and determine which of the them leads to consistent solutions.

However, to obtain an expansion of \sqrt{A}^{-1} we need to perform a Taylor series. The condition for applying such an expansion is that $\|A - 1\| < 1$. From the expression for the (square) matrix A (see (2.26)) it is clear that the condition above is satisfied iff $m(m-1) \frac{t_{ee'}}{\sqrt{t_e t'_e}} < 1$ where m is the dimension of the matrix. As we will show, $\frac{t_{ee'}}{\sqrt{t_e t'_e}} = C \times \frac{l'}{\delta_e}$ where C =constant and $l' < l$; thus the condition $m(m-1) \frac{t_{ee'}}{\sqrt{t_e t'_e}} < 1$ becomes $l \ll \delta_e$, i.e. we need to choose the parquet to be much finer than the edge length (see Section 2.2). If this requirement is satisfied, then we can perform a Taylor expansion of \sqrt{A} obtaining $\sqrt{A} = 1 + \frac{1}{2}(A-1) + \frac{1}{8}(A-1)^2 + \mathcal{O}(A-1)^3$. Actually, we are only interested in first-order terms, and so we shall only consider the approximation $\sqrt{A} \simeq 1 + \frac{1}{2}(A-1)$ whose inverse, in first-order, is simply $(\sqrt{A})^{-1} \simeq 1 - \frac{1}{2}(A-1)$. Since the parquet length must be much finer than the edge length, in the remainder of the paper we will consider only case (1) and analyse whether it gives the correct semiclassical limit.

The first step in the calculation is to determine the range of allowed positions for each vertex, V_i , of the graph with respect to the plaquette. Since the graphs we consider are regular, determining the position of one vertex suffices to derive the positions of the remaining vertices in the graph.

As an explanatory example let us consider a regular 4-valent graph γ whose vertex V_0 coincides with the point $(0, 0, 0)$ of the plaquettation and whose vertex V_2 (equivalently the edge $e_{0,2}$) has coordinates $(\frac{-\delta}{\sqrt{3}}, \frac{\delta}{\sqrt{3}}, \frac{\delta}{\sqrt{3}})$. It follows that the range of allowed positions of V_2 is from (nl, nl, nl) to $(nl+1, nl+1, nl+1)$ where $n_x = n_y = n_z = n = \lfloor \frac{\delta}{\sqrt{3}l} \rfloor$, as depicted in Figure 11.

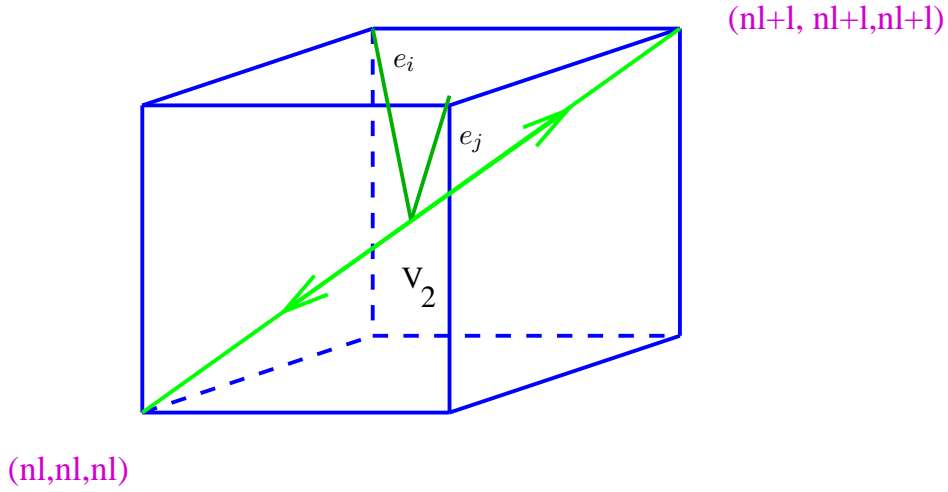


Figure 11: Allowed positions of a vertex

It is straight-forward to understand that different positions of V_2 will determine different values of $t_{e_i e_j}$ for any two edges e_i and e_j incident at V_2 . A detailed analysis shows that the terms $t_{e_i e_j}$ differ according to which of the following conditions is satisfied:

- I) $|x_{V_2}| > |nl + \frac{l}{2}|$
- II) $|x_{V_2}| < |nl + \frac{l}{2}|$
- III) $|x_{V_2}| = |nl + \frac{l}{2}|$

Similar conditions apply for all vertices in γ .

Since the position of V_2 will determine the positions of all other vertices, it is possible to establish which positions of V_2 will lead to different values of the terms $\frac{t_{e_i e_j}}{\sqrt{t_{e_i} t_{e_j}}}$ for all edges of all vertices of the graph γ . Such positions of V_2 for a regular 4-valent graph are:

- a) $|nl| \leq |x_{V_2}| \leq |nl + \frac{l}{6}|$
- b) $|nl + \frac{l}{6}| \leq |x_{V_2}| \leq |nl + \frac{l}{4}|$
- c) $|nl + \frac{l}{4}| \leq |x_{V_2}| \leq |nl + \frac{l}{2}|$
- d) $|nl + \frac{l}{2}| \leq |x_{V_2}| \leq |nl + \frac{l}{3}|$
- e) $|nl + \frac{l}{3}| \leq |x_{V_2}| \leq |nl + \frac{3l}{4}|$
- f) $|nl + \frac{3l}{4}| \leq |x_{V_2}| \leq |nl + 2l|$

For each such condition it is possible to derive the respective conditions for both the y - and the z -coordinates in the three-dimensional case. It turns out that similar relations hold for the 6- and 8-valent graphs as well.

To explicitly compute the terms $t_{e_i e_j}$ we must choose one of the above conditions ($a \rightarrow f$), each of which will lead to different values for each $t_{e_i e_j}$. However, the computation procedures are the same. In the calculations of Sections 3.2 we will choose case (a).

To describe the method for computing the values of $t_{e_i e_j}$, we go back to a very simple example in two dimensions. We will then give the general outline of how this calculation can be generalised to the 3-dimensional case.

Let us consider Figure 12, where we chose $x_{v_1} > nl + \frac{l}{2}$. For simplicity we are assuming that the vertex

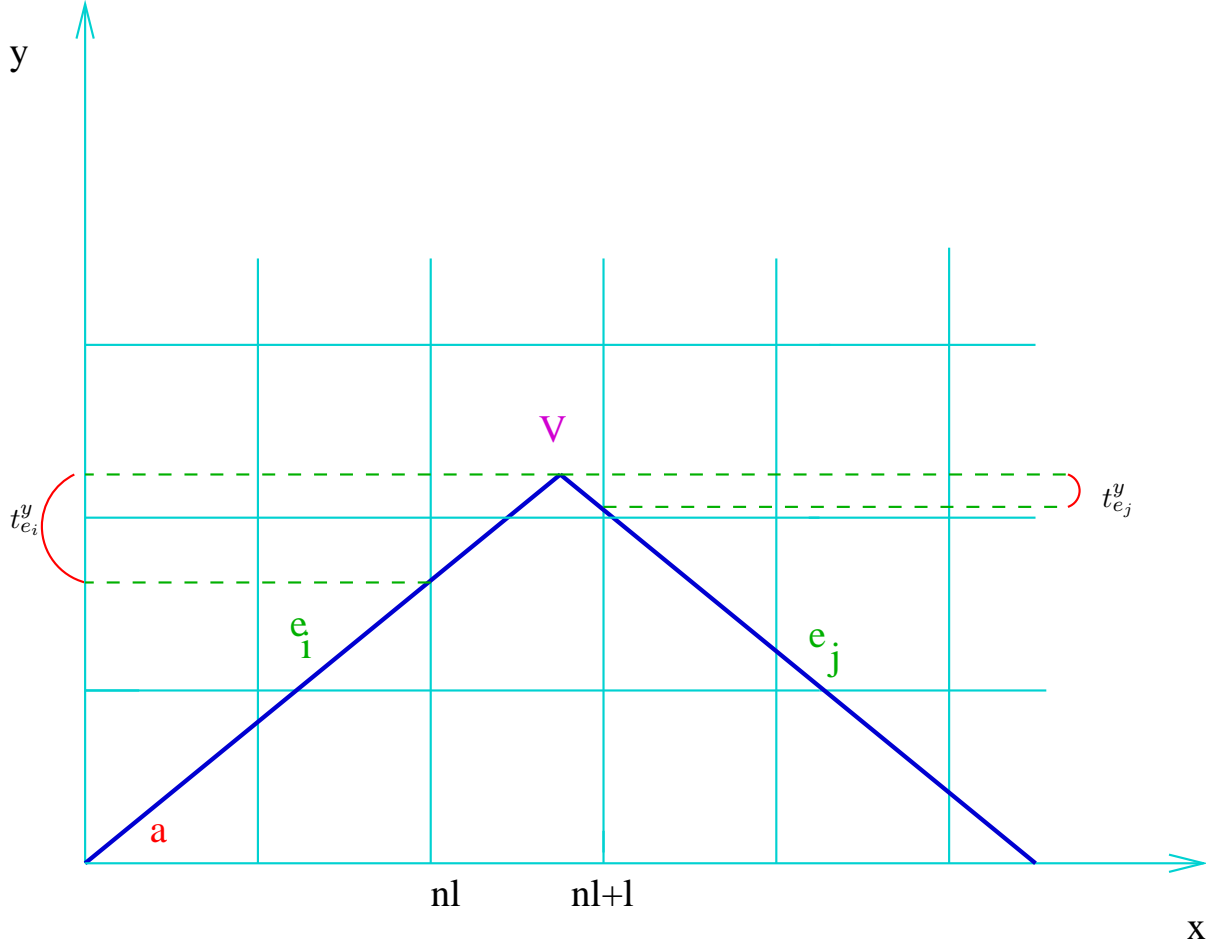


Figure 12: Example in two dimensions

is symmetric with respect to the axis, i.e., the angles, ϕ , made by the two edges with respect to the y -axis are the same.

We now want to compute the values of $t_{e_i e_j} = t_{e_i e_j}^y + t_{e_i e_j}^x + t_{e_i e_j}^z$ where for each $t_{e_i e_j}^k$, $k = \{x, y, z\}$ we have $t_{e_i e_j}^k = t_{e_i}^k \cap t_{e_j}^k$.

As a first step we compute for each edge, e_i , the value of $t_{e_i}^y$ in the y -direction, obtaining

$$t_{e_i}^y = (nl + l - x_{v_1}) \cot a \quad \text{and} \quad t_{e_j}^y = (x_{v_1} - nl) \cot a \quad (3.1)$$

Since the two edges commonly intersect only one y stack, in order to define the value of $t_{e_i e_j}^y = t_{e_i}^y \cap t_{e_j}^y$ we need to establish which of the two terms $t_{e_i}^y$ or $t_{e_j}^y$ is the smallest. Thus, for example,

$$x_{v_1} - nl > nl + l - x_{v_1} \quad \text{iff} \quad x > nl + \frac{l}{2} \quad (3.2)$$

Since we have chosen $x_{v_1} > nl + \frac{l}{2}$ it follows that $t_{e_i}^y < t_{e_j}^y$ which implies that $t_{e_i e_j}^y = t_{e_j}^y = (nl + l - x_{v_1}) \cot a$. As can be seen from Figure 12, there are no intersections in the x stacks, therefore we obtain

$$t_{e_i e_j} = t_{e_i e_j}^y + t_{e_i e_j}^x = t_{e_i e_j}^y \quad (3.3)$$

We now want to determine the values for $\frac{t_{e_i e_j}}{\sqrt{t_{e_i} t_{e_j}}}$ where, in this situation, $t_{e_i} = \tau_{e_i}^x + \tau_{e_i}^y = \delta \sin a + \delta \cos a = t_{e_j}$; therefore, $\frac{t_{e_i e_j}}{\sqrt{t_{e_i} t_{e_j}}} = \frac{(nl + l - x_{v_1}) \cot a}{\sqrt{(\delta \sin a + \delta \cos a)^2}}$.

This calculation is very simple since the intersection of the two edges occurs only in one y stack. But it could well be the case that the angle between two edges is such that they intersect more than one stack in a given direction. For example, consider Figure 13, always in two dimensions. In this case we would have

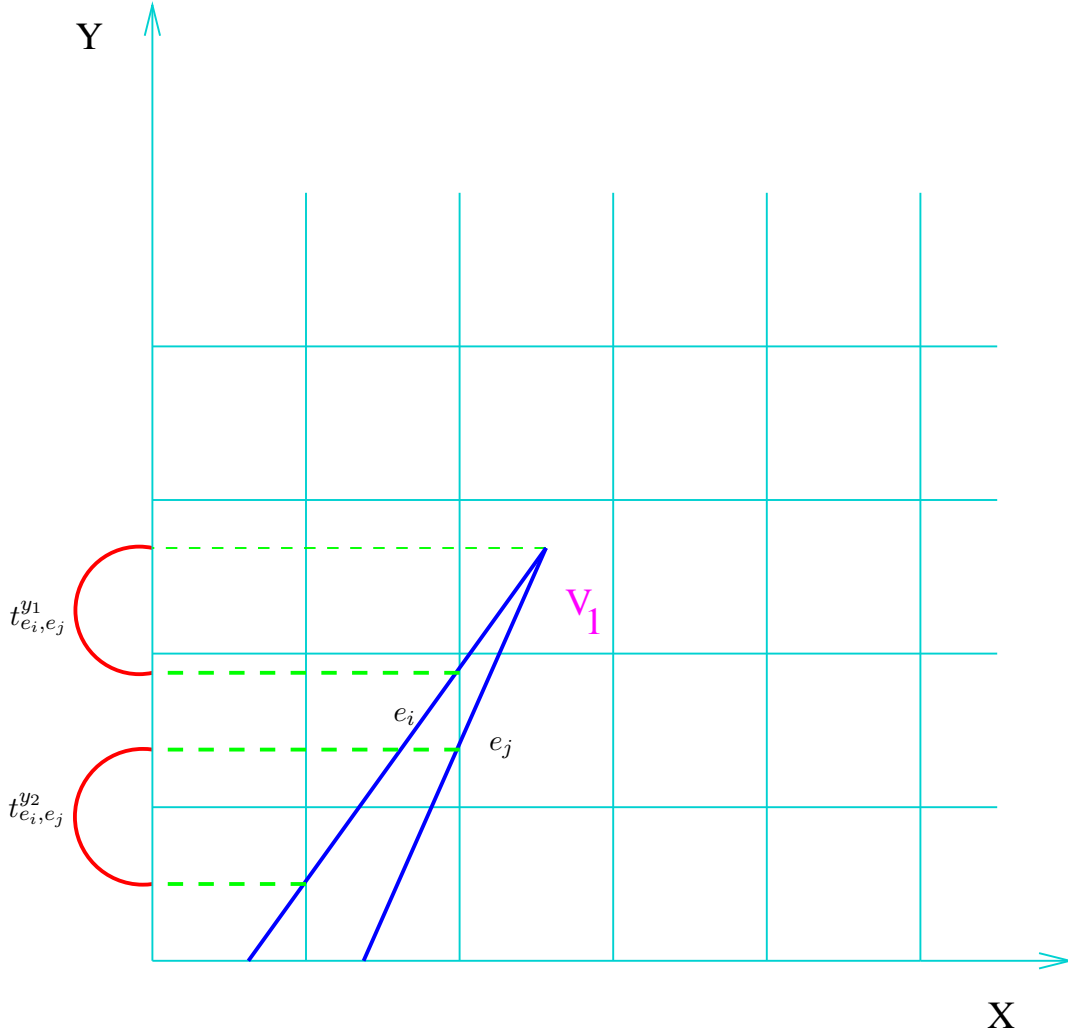


Figure 13: The second example in two dimensions

$$t_{e_i e_j}^y = t_{e_i e_j}^{y1} + t_{e_i e_j}^{y2}.$$

Since in analysing the expectation value for the volume operator we will be considering graphs formed by regular 4-, 6- and 8-valent lattice, it turns out that the angles θ_i —the angle formed by the projection on the edge on the x - y -plane and the x -axis—and the angle, ϕ_i , with respect to the z -axis for any edge, are such that two or more edges can only commonly intersect at most one plaquette in a given direction.

When generalising the procedure described above for calculating the values of $\frac{t_{e_i e_j}}{\sqrt{t_{e_i} t_{e_j}}}$ to the 3-dimensional case, some extra care is needed. In fact, consider Figure 14. It is clear that the values for $t_{e_i}^z$ can be computed

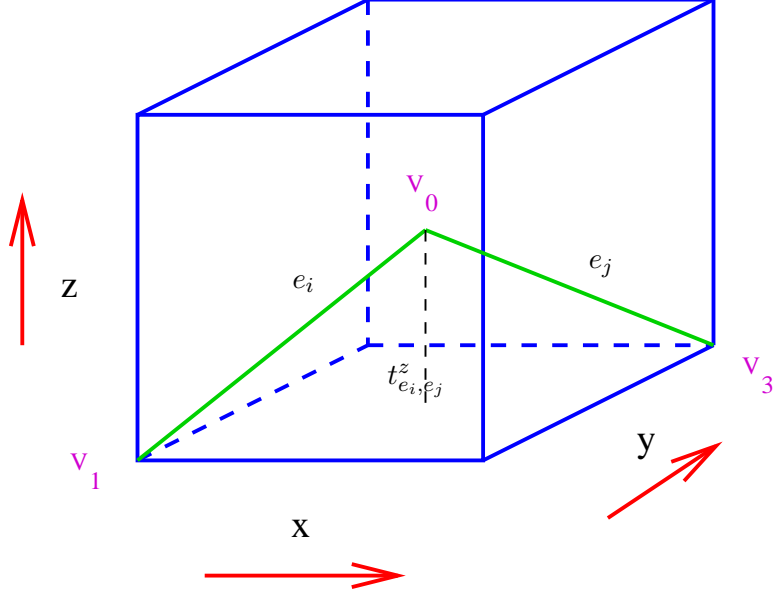


Figure 14: Example in three dimensions

with respect to both the x - and the y -coordinates as follows

$${}^x t_{e_i}^z = a \times \cot \phi \frac{1}{\cos \theta} = a \times Z_{e_i}^x \quad {}^y t_{e_i}^z = c \times \cot \phi \frac{1}{\sin \theta} = c \times Z_{e_i}^y \quad (3.4)$$

where

$$a = \begin{cases} x_{V_j} - n_{x_{V_j}} l & \text{iff the edge points in the negative } x \text{ direction} \\ n_{x_{V_j}} l + l - x_{V_j} & \text{iff the edge points in the positive } x \text{ direction} \end{cases}$$

and

$$c = \begin{cases} y_{V_j} - n_{y_{V_j}} l & \text{iff the edge points in the negative } y \text{ direction} \\ n_{y_{V_j}} l + l - y_{V_j} & \text{iff the edge points in the positive } y \text{ direction} \end{cases}$$

The term ${}^x t_{e_i}^z$ in these equations represents the value of $t_{e_i}^z$ as computed with respect to the x -coordinate, while ${}^y t_{e_i}^z$ is the value of $t_{e_i}^z$ as computed with respect to the y -coordinate. The non-uniqueness of the computation of the values $t_{e_i}^z$ implies that there is an extra difficulty in the three-dimensional case. We will illustrate this with the aid of an example.

Consider the edge e_i in figure 15. The value of $t_{e_i}^z$ can be computed with respect to both the x and the y coordinate, thus obtaining ${}^x t_{e_i}^z$ or ${}^y t_{e_i}^z$ respectively. However, it is clear from the diagram that the intersection of the edge e_i with the stack of plaquettes in the z direction containing the vertex V_j is given by ${}^x t_{e_i}^z$. On the other hand ${}^y t_{e_i}^z$ defines the intersection of the edge e_i with the stacks of plaquettes in the z direction containing the vertex *plus* the stack in the z direction delimited, in the x direction, by the values $nl + l$ and $nl + al$.

This example shows that, given the values ${}^x t_{e_i}^z$ and ${}^y t_{e_i}^z$, the intersection of the edge e_i with the stacks of plaquettes in the z direction which contain the vertex V_j is given by the smallest term, i.e., $t_{e_i}^z = {}^x t_{e_i}^z \cap {}^y t_{e_i}^z$. It follows that, given two edges e_i and e_j , in order to find $t_{e_i, e_j}^z := t_{e_i}^z \cap t_{e_j}^z$ we first need to establish whether $t_{e_i}^z = {}^x t_{e_i}^z$ or $t_{e_i}^z = {}^y t_{e_i}^z$ and similarly for the edge e_j . Once the value of the terms $t_{e_i}^z$ and $t_{e_j}^z$ is determined, we can proceed as for the two-dimensional case and identify t_{e_i, e_j}^z with the smallest t^z , i.e. $t_{e_i, e_j}^z := t_{e_i}^z \cap t_{e_j}^z$.

For intersections in the x and y stacks the procedure for computing the values of t_{e_i, e_j} is essentially the same. However, the formulae for the values of the individual terms, ${}^j t_{e_i}^k$, are different. Specifically, for the

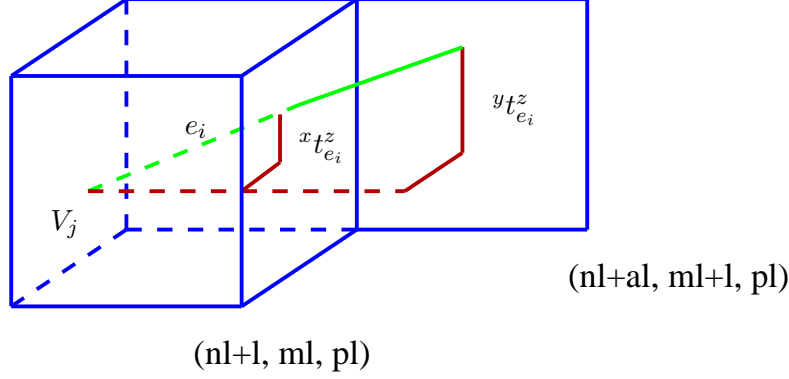


Figure 15: Computation for the terms $t_{e_i}^z$ in 3-dimensions

x -direction we have:

$${}^z t_{e_i}^x = d \times \tan \phi \cos \theta = d \times F_{e_i}^x \quad {}^y t_{e_i}^x = c \times \cot \theta = c \times T_{e_i}^x \quad (3.5)$$

where

$$d = \begin{cases} z_{V_j} - n_{z_{V_j}} l & \text{iff the edge points upwards} \\ n_{z_{V_j}} l + l - z_{V_j} & \text{iff the edge points downwards} \end{cases}$$

and c is defined as above. For the y -direction we have

$${}^z t_{e_i}^y = d \times \tan \phi \sin \theta = d \times F_{e_i}^y \quad {}^x t_{e_i}^y = a \times \tan \theta = a \times T_{e_i}^y \quad (3.6)$$

where a and d are defined as above.

When computing the values of $\frac{t_{e_i e_j}}{\sqrt{t_{e_i} t_{e_j}}}$ in three dimensions, as for the two-dimensional case we need to compute the values for t_{e_i} , which in this case are simply $t_{e_i} = t_{e_i}^x + t_{e_i}^y + t_{e_i}^z = \delta_{e_i} \cos(90 - \phi_{e_i}) \cos \theta_{e_i} + \delta_{e_i} \cos(90 - \phi_{e_i}) \sin \theta_{e_i} + \delta_{e_i} \cos \phi_i$. The explicit values of the terms $\frac{t_{e_i e_j}}{\sqrt{t_{e_i} t_{e_j}}}$ obtained for the 4-, 6-, and 8-valent graph which satisfies condition (a) above, namely $|nl| \leq |x_{V_2}| \leq |nl + \frac{l}{6}|$, for the 4-valent graph and an equivalent condition for the 6- and 8-valent graphs are given in the Appendix.

Since for all 4-, 6- and 8-valent graphs we are dealing with symmetric lattices, after a certain number of vertices the values for the terms $\frac{t_{e_i e_j}}{\sqrt{t_{e_i} t_{e_j}}}$ will repeat, i.e., there will be a periodicity in the values of the terms $\frac{t_{e_i e_j}}{\sqrt{t_{e_i} t_{e_j}}}$. Therefore, in computing these values we need only consider those vertices which comprise the periodicity cell, i.e., those vertices for which the values of the term $\frac{t_{e_i e_j}}{\sqrt{t_{e_i} t_{e_j}}}$ cannot be obtained through symmetry arguments. As we will see later, this periodicity is different for graphs of different valency.

We now proceed to compute the expectation value of the volume operator for the 4-, 6- and 8-valent cases, utilising the values of the terms $\frac{t_{e_i e_j}}{\sqrt{t_{e_i} t_{e_j}}}$ given in the Appendix.

3.2 Analysis of the expectation value of the volume operator for a 4-valent graph

In this Section we will compute the expectation value of the volume operator as applied to a 4-valent graph. We will first take into consideration the non-rotated graph. In establishing rotational and translational dependence of the expectation value we will perform both a rotation by arbitrary Euler angles and a translation and, then, recalculate the expectation value. We will see that the contributions that come from the terms $\frac{t_{e_i e_j}}{\sqrt{t_{e_i} t_{e_j}}}$, which comprise the off-diagonal elements of the matrix \sqrt{A}^{-1} , are not trivial, thereby producing a strong rotational and translational dependence in the expectation value of the volume operator in higher order in $\frac{l}{\delta}$.

3.2.1 Expectation value of the volume operator for a 4-valent graph

To calculate the expectation value of the volume operator we will consider a 4-valent graph constructed from the simplicial cell complex as discussed in [23]. We choose the vertex V_0 to be $V_0 = (0, 0, 0)$, and the angles $\phi_e = \cos^{-1}(\frac{1}{\sqrt{3}})$ and $\theta_e = 45^\circ$ for all $e \in \gamma$ such that we obtain the configuration depicted in picture 16. The periodicity cell for a 4-valent graph contains four vertices, including V_0 . The coordinates of the

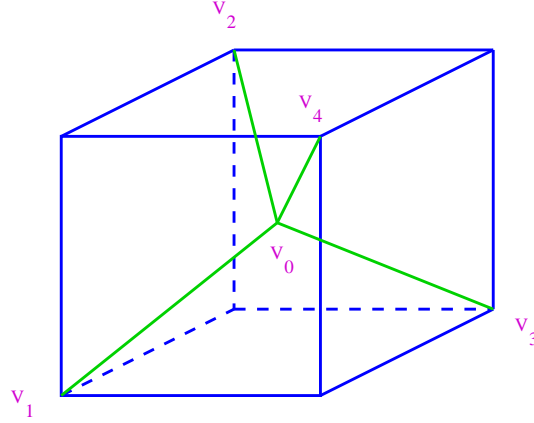


Figure 16: General vertex of a 4-valent graph

remaining three vertices are $V_2 = (\frac{\delta}{\sqrt{3}}, \frac{\delta}{\sqrt{3}}, \frac{\delta}{\sqrt{3}})$; $V_8 = (\frac{\delta}{\sqrt{3}}, 3\frac{\delta}{\sqrt{3}}, \frac{\delta}{\sqrt{3}})$; $V_{13} = (0, 2\frac{\delta}{\sqrt{3}}, 2\frac{\delta}{\sqrt{3}})$.

It follows that the edges $e_{0,1}$, $e_{0,2}$, $e_{0,3}$ and $e_{0,4}$ lie in the octants G , B , E and D respectively. This implies that the geometric factor for the vertex V_0 will be $G_{\gamma,V} = \sqrt{2}$. Because of the geometry of a regular 4-valent graph, it turns out that all the vertices comprising the periodicity cell, V_2 , V_8 and V_{13} will have $G_{\gamma,V_i} = \sqrt{2}$.

The following table gives the values obtained for the terms $\frac{t_{e_i e_j}}{\sqrt{t_{e_i} t_{e_j}}}$ for the 4-valent graph that satisfies condition (a) as defined in the previous Section, namely $|nl| \leq |x_{V_2}| \leq |nl + \frac{1}{6}|$.

It should be noted that, because of the geometry of the 4-valent graph, the terms $T_{e_i}^{\{x,y\}}$, $F_{e_i}^{\{x,y\}}$, $Z_{e_i}^{\{x,y\}}$ in equations 3.4, 3.5 and 3.6 are all equal to 1 for each edge e_i :

V_0	six terms $\frac{t_{e_i e_j}}{\sqrt{t_{e_i} t_{e_j}}} = 0$
V_2	six terms $\frac{t_{e_i e_j}}{\sqrt{t_{e_i} t_{e_j}}} = (\frac{\delta}{\sqrt{3}} - nl) \frac{1}{\delta\sqrt{3}}$
V_8	six terms $\frac{t_{e_i e_j}}{\sqrt{t_{e_i} t_{e_j}}} = (\frac{\delta}{\sqrt{3}} - nl) \frac{1}{\delta\sqrt{3}}$
V_{13}	two terms $\frac{t_{e_i e_j}}{\sqrt{t_{e_i} t_{e_j}}} = (\frac{2\delta}{\sqrt{3}} - 2nl) \frac{1}{\delta\sqrt{3}}$

Here, δ is the length of the edge e . In order to apply equation (2.20), we first need to determine the values of the term $\det_{e,e',e''}(\sqrt{A}^{-1})$ for each triplet of linearly-independent edges e, e', e'' . Using the fact that, in first-order approximation, $(\sqrt{A})^{-1} = 1 - \frac{1}{2}(A - 1)$, the explicit expression for $(\sqrt{A})^{-1}$ for the 4-valent graph

under consideration is

	$e_{0,1}$	$e_{0,2}$	$e_{0,11}$	$e_{0,12}$	$e_{2,7}$	$e_{2,5}$	$e_{2,6}$	$e_{13,9}$	$e_{13,8}$	$e_{13,10}$	$e_{13,11}$	$e_{8,13}$	$e_{8,14}$	$e_{8,15}$	$e_{8,5}$
$e_{0,1}$	1	0	0	0	0	0	0	0	0	0	0	0	0	0	0
$e_{0,2}$	0	1	0	0	$\frac{1}{2}\alpha$	$-\frac{1}{2}\alpha$	$-\frac{1}{2}\alpha$	0	0	0	0	0	0	0	0
$e_{0,11}$	0	0	1	0	0	0	0	0	0	0	0	0	0	0	0
$e_{0,12}$	0	0	0	1	0	0	0	0	0	0	0	0	0	0	0
$e_{2,7}$	0	$-\frac{1}{2}\alpha$	0	0	1	$-\frac{1}{2}\alpha$	$-\frac{1}{2}\alpha$	0	0	0	0	0	0	0	0
$e_{2,5}$	0	$-\frac{1}{2}\alpha$	0	0	$-\frac{1}{2}\alpha$	1	$-\frac{1}{2}\alpha$	0	0	0	0	0	0	0	0
$e_{2,6}$	0	$-\frac{1}{2}\alpha$	0	0	$-\frac{1}{2}\alpha$	$-\frac{1}{2}\alpha$	1	0	0	0	0	0	0	0	0
$e_{13,9}$	0	0	0	0	0	0	0	1	$-\frac{1}{2}\alpha$	$-\frac{1}{2}\alpha$	$-\frac{1}{2}\alpha$	0	0	0	0
$e_{13,8}$	0	0	0	0	0	0	0	$-\frac{1}{2}\alpha$	1	$-\frac{1}{2}\alpha$	$-\frac{1}{2}\alpha$	0	0	0	0
$e_{13,10}$	0	0	0	0	0	0	0	$-\frac{1}{2}\alpha$	$-\frac{1}{2}\alpha$	1	$-\frac{1}{2}\alpha$	0	0	0	0
$e_{13,11}$	0	0	0	0	0	0	0	$-\frac{1}{2}\alpha$	$-\frac{1}{2}\alpha$	$-\frac{1}{2}\alpha$	1	0	0	0	0
$e_{8,13}$	0	0	0	0	0	0	0	0	0	0	0	1	0	$-\alpha$	0
$e_{8,14}$	0	0	0	0	0	0	0	0	0	0	0	0	1	0	$-\alpha$
$e_{8,15}$	0	0	0	0	0	0	0	0	0	0	0	$-\alpha$	0	1	0
$e_{8,5}$	0	0	0	0	0	0	0	0	0	0	0	0	$-\alpha$	0	1

where $\alpha = \frac{t_{e_i e_j}}{\sqrt{t_{e_i} t_{e_j}}} = \left(\frac{\delta}{\sqrt{3}} - nl\right) \frac{1}{\delta\sqrt{3}}$ and the terms $t_{e_i e_j}$, t_{e_i} and t_{e_j} are computed using the techniques defined in the previous Section.

Now that we have an expression for the inverse of the matrix \sqrt{A} we can compute the expectation value of the volume operator for each of the four vertices in the periodicity cell and, then, sum their contributions.

We start with the vertex V_0 . First consider the sub-matrix of the matrix $(\sqrt{A})^{-1}$ formed by all the edges incident at V_0 . This is

$$\left(\begin{array}{c|cccc} & e_{0,1} & e_{0,2} & e_{0,11} & e_{0,12} \\ \hline e_{0,1} & 1 & 0 & 0 & 0 \\ e_{0,2} & 0 & 1 & 0 & 0 \\ e_{0,11} & 0 & 0 & 1 & 0 \\ e_{0,12} & 0 & 0 & 0 & 1 \end{array} \right)$$

Because of the geometry of the 4-valent graph, at each vertex there are four triplets of linearly-independent edges. Keeping this in mind and computing the determinant of the matrices formed by each such set of triplets, we obtain the following expression for the expectation value of the volume operator at V_0 :

$$\delta^3 \sqrt{\frac{1}{8}} \sqrt{\det(E_j^a(u))} \left| 16 \left| \det \left(\frac{\partial X_S^a}{\partial(s, u^1, u^2)} \right) \right|^2 \right|^{\frac{1}{2}} \quad (3.7)$$

By a similar procedure for vertices V_2 and V_3 we obtain

$$\delta^3 \sqrt{\frac{1}{8}} \sqrt{\det(E_j^a(u))} \left| 16 \left(1 - \frac{3\alpha^2}{4} - \frac{\alpha^3}{4} \right) \left| \det \left(\frac{\partial X_S^a}{\partial(s, u^1, u^2)} \right) \right|^2 \right|^{\frac{1}{2}} \quad (3.8)$$

In both cases, the sub-matrix of \sqrt{A}^{-1} we consider is

$$\left(\begin{array}{cccc} 1 & -\frac{1}{2}\alpha & -\frac{1}{2}\alpha & -\frac{1}{2}\alpha \\ -\frac{1}{2}\alpha & 1 & -\frac{1}{2}\alpha & -\frac{1}{2}\alpha \\ -\frac{1}{2}\alpha & -\frac{1}{2}\alpha & 1 & -\frac{1}{2}\alpha \\ -\frac{1}{2}\alpha & -\frac{1}{2}\alpha & -\frac{1}{2}\alpha & 1 \end{array} \right)$$

and then we compute the determinant of all the sub-matrices formed by linearly-independent triplets of edges.

For the vertex V_4 we obtain

$$\delta^3 \sqrt{\frac{1}{8}} \sqrt{\det(E_j^a(u))} \left| 16(1 - \alpha^2) \left| \det \left(\frac{\partial X_S^a}{\partial(s, u^1, u^2)} \right) \right|^2 \right|^{\frac{1}{2}} \quad (3.9)$$

where we have used the sub-matrix

$$\begin{pmatrix} 1 & 0 & -\alpha & 0 \\ 0 & 1 & 0 & -\alpha \\ -\alpha & 0 & 1 & 0 \\ 0 & -\alpha & 0 & 1 \end{pmatrix}$$

Summing up these contributions gives

$$\begin{aligned} V_R = & \delta^3 \sqrt{\frac{1}{8}} 4 \left| \det \left(\frac{\partial X_S^a}{\partial(s, u^1, u^2)} \right) \right| \left| \left(1 \sqrt{|\det(E_j^a(u))|} + \sqrt{|\det(E_j^a(u))|} \left(\left| 1 - \frac{3\alpha^2}{4} - \frac{\alpha^3}{4} \right| \right)^{\frac{1}{2}} \right. \right. \\ & \left. \left. + \sqrt{|\det(E_j^a(u))|} \left(\left| 1 - \frac{3\alpha^2}{4} - \frac{\alpha^3}{4} \right| \right)^{\frac{1}{2}} + \sqrt{|\det(E_j^a(u))|} \left(|1 - \alpha^2| \right)^{\frac{1}{2}} \right) \right|^{\frac{1}{2}} \end{aligned} \quad (3.10)$$

To first-order approximation we obtain

$$V_R = \delta^3 2\sqrt{2} \sqrt{|\det(E_j^a(u))|} \left| \det \left(\frac{\partial X_S^a}{\partial(s, u^1, u^2)} \right) \right| \left| 1 - \frac{1}{2} \left(\frac{3\alpha^2}{16} - \frac{\alpha^2}{4} \right) \right| + \mathcal{O}(3) \quad (3.11)$$

It should be noted that, although the term $\det(E_j^a(u))$ is vertex dependent, we can safely assume that, to first-order in l/δ , the values will be the same for each vertex within each periodicity cell that involves only an order of four vertices. Thus this term can be factored out from the equation. This first-order approximation will be used throughout the rest of this paper. As mentioned previously this is justified since we choose $\frac{l}{\delta} \ll 1$. It follows that the terms $\alpha^2 \propto \frac{l-x}{\delta}$, which are much smaller than *one* (see Section 2.2).

The term proportional to α^2 in the equation above represents the l/δ -correction for the expectation value of the volume operator for a given region R . As in [23], for a general 4-valent graph, even in the zeroth-order approximation the expectation value for the volume of a given region R does not coincide with the classical value for the volume of that region. Notably, there is no linear correction in l/δ !

3.2.2 Expectation value of the volume operator for a rotated 4-valent graph

We now analyse how the results of the calculations above depend on how the graph is embedded in \mathbb{R}^3 . Here we will consider rotational invariance; translational invariance is discussed in the following subsection.

To analyse the rotational dependence of the expectation value of the volume operator, we will perform an Euler rotation of the graph with respect to some arbitrary Euler angles β , ψ , α and then repeat the calculation. The transformation matrix is

$$R = \begin{pmatrix} \cos \phi \cos \psi - \sin \phi \cos \theta \sin \psi & \cos \psi \sin \phi + \cos \theta \cos \phi \sin \psi & \sin \psi \sin \theta \\ -\sin \psi \cos \phi - \cos \theta \sin \phi \cos \psi & -\sin \psi \sin \phi + \cos \theta \cos \phi \sin \psi & \cos \psi \sin \theta \\ \sin \theta \sin \phi & -\sin \theta \cos \phi & \cos \theta \end{pmatrix}$$

The coordinates of the rotated vertices are then given by $V'_i = R \cdot \vec{V}_i$

$$\begin{pmatrix} x_{V'_i} \\ y_{V'_i} \\ z_{V'_i} \end{pmatrix} = \begin{pmatrix} R_{11}x_{v_i} + R_{12}y_{v_i} + R_{13}z_{v_i} \\ R_{21}x_{v_i} + R_{22}y_{v_i} + R_{23}z_{v_i} \\ R_{31}x_{v_i} + R_{32}y_{v_i} + R_{33}z_{v_i} \end{pmatrix}$$

Applying this transformation matrix to the 4-valent graph we obtain the following new coordinates for the vertices:

$$V'_2 = \left((-R_{11} + R_{12} + R_{13})\frac{\delta}{\sqrt{3}}, (-R_{21} + R_{22} + R_{23})\frac{\delta}{\sqrt{3}}, (-R_{31} + R_{32} + R_{33})\frac{\delta}{\sqrt{3}} \right) \quad (3.12)$$

$$V'_8 = \left((R_{11} + 3R_{12} + R_{13})\frac{\delta}{\sqrt{3}}, (R_{21} + 3R_{22} + R_{23})\frac{\delta}{\sqrt{3}}, (R_{31} + 3R_{32} + R_{33})\frac{\delta}{\sqrt{3}} \right) \quad (3.13)$$

$$V'_{13} = \left(2(R_{12} - R_{13})\frac{\delta}{\sqrt{3}}, 2(R_{22} - R_{23})\frac{\delta}{\sqrt{3}}, 2(R_{32} - R_{33})\frac{\delta}{\sqrt{3}} \right) \quad (3.14)$$

The new angles between the rotated edges and the x, y, z -axes can now easily be computed using elementary trigonometry.

As an explanatory example let us consider the edge $e_{0,2}$. To find the angles this edge has with respect to the axes we need first to compute the coordinates of the vector $e_{0,2}$ starting at vertex V_0 and ending at vertex V_2 . In this case, the coordinates of $e_{0,2}$ coincide with the coordinates of the vertex V_2 :

$$e_{0,2} = \left((R_{11} + R_{12} + R_{13})\frac{\delta}{\sqrt{3}}, (R_{21} + R_{22} + R_{23})\frac{\delta}{\sqrt{3}}, (R_{31} + R_{32} + R_{33})\frac{\delta}{\sqrt{3}} \right) \quad (3.15)$$

If instead we considered the edge e_{25} we would get

$$e_{25} = e_{02} - e_{05} = \left(-(R_{11} + R_{12} + R_{13})\frac{\delta}{\sqrt{3}}, -(R_{21} + R_{22} + R_{23})\frac{\delta}{\sqrt{3}}, -(R_{31} + R_{32} + R_{33})\frac{\delta}{\sqrt{3}} \right) \quad (3.16)$$

Once we have the coordinates for $e_{2,0}$, the angle, $\phi_{e_{2,0}}$, it forms with respect to the z -coordinate is

$$\phi_{e_{2,0}} = \tan^{-1} \left(\frac{\sqrt{x^2 + y^2}}{z} \right) = \tan^{-1} \left(\frac{\sqrt{(-R_{11} + R_{12} + R_{13})^2 + (-R_{21} + R_{22} + R_{23})^2}}{(-R_{31} + R_{32} + R_{33})} \right) \quad (3.17)$$

The angle, $\theta_{e_{2,0}}$, between the projection of the vector on the x - y plane and the x -axis is given by

$$\theta_{e_{2,0}} = \tan^{-1} \left(\frac{y}{x} \right) = \tan^{-1} \left(\frac{-R_{21} + R_{22} + R_{23}}{-R_{11} + R_{12} + R_{13}} \right) \quad (3.18)$$

In the same way we can obtain the angles for all the edges in our graph in terms of the elements of the transformation matrix. Thus the orientation of each of the edges of the graph will depend on the matrix elements of the transformation matrix, i.e., on the Euler angles that parameterise the rotation.

In order to determine the rotational dependence of the expectation value of the volume operator, we have performed a case study in which the expectation values were computed for all possible orientations of the graphs that have non-zero measure in $SO(3)$. Such possible orientations were described in Section 2.4. To aid calculational simplicity, these sub-cases are defined in terms of possible ranges of values for the angles θ and ϕ for each edge in the graph, rather than on possible values for the Euler angles.

In order to keep our results as general as possible, we performed our subdivisions so as to cover all possible situations. This is less tedious than it might seem since we are dealing with regular lattices and, therefore, once the angles for the edges of one vertex are fixed, we immediately know the orientation of the edges of all other vertices.

Let us choose V'_0 as our reference vertex with respect to which the possible orientations of the edges are defined. The edges incident at V'_0 are $e_{0,1}$, $e_{0,2}$, $e_{0,3}$, $e_{0,4}$. In defining the orientation we use the convention that both $0 < \phi < 2\pi$ and $0 < \theta < 2\pi$ increases anti-clockwise.

Once the rotational matrix has been applied, whatever the values of the Euler angles might be, we will end up in a situation in which two edges e_i, e_j point upwards, i.e., $-\frac{\pi}{2} < \phi_{e_i}, \phi_{e_j} < \frac{\pi}{2}$, and the remaining two edges point downwards, i.e. $\frac{\pi}{2} < \phi_{e_k}, \phi_{e_l} < \frac{3\pi}{2}$. This is a consequence of the geometry of the 4-valent graph. We will call two edges pointing in the same up, or down, direction an 'up', or 'down', couple respectively.

Since we are considering only those edge orientation with measure *non-zero* in $SO(3)$, the angles of the edges e_i, e_j of each up/down couple will satisfy the following conditions: $|\theta_{e_i}| = |90 + \theta_{e_j}|$ and $|\phi_{e_i}| = |\phi_{e_j} - 54.75|$

Given a particular choice of up and down couple we have to specify in which octant (see Figure 4) each edge lies. This is required since different octants induce different values for the geometric factor $G_{\gamma,V}$. The angles θ_{e_i} and ϕ_{e_i} required for an edge e_i to lie in each of the octants are listed in Table 1 where, again, we use the convention that $0 < \phi_{e_i} < 2\pi$ and $0 < \theta_{e_i} < 2\pi$, with both angles increasing in an anticlockwise direction. However, because of the geometry of a 4-valent graph, the allowed angle-ranges

	A	B	C	D
ϕ_{e_i}	$\frac{3\pi}{2} < \phi_{e_i} < 2\pi$	$0 < \phi_{e_i} < \frac{\pi}{2}$	$0 < \phi_{e_i} < \frac{\pi}{2}$	$\frac{3\pi}{2} < \phi_{e_i} < 2\pi$
θ_{e_i}	$0 < \theta_{e_i} < \frac{\pi}{2}$	$\frac{\pi}{2} < \theta_{e_i} < \pi$	$\pi < \theta_{e_i} < \frac{3\pi}{2}$	$\frac{3\pi}{2} < \theta_{e_i} < 2\pi$

	E	F	G	H
ϕ_{e_i}	$\pi < \phi_{e_i} < \frac{3\pi}{2}$	$\frac{\pi}{2} < \phi_{e_i} < \pi$	$\frac{\pi}{2} < \phi_{e_i} < \pi$	$\pi < \phi_{e_i} < \frac{3\pi}{2}$
θ_{e_i}	$0 < \theta_{e_i} < \frac{\pi}{2}$	$\frac{\pi}{2} < \theta_{e_i} < \pi$	$\pi < \theta_{e_i} < \frac{3\pi}{2}$	$\frac{3\pi}{2} < \theta_{e_i} < 2\pi$

Table 1: Angle-ranges for each octant

have to be restricted to those listed in Table 2.

	A	B	C	D
ϕ_{e_i}	$\frac{3\pi}{2} < \phi_{e_i} < 2\pi - \sin^{-1}(\frac{1}{3})$	$\sin^{-1}(\frac{1}{3}) < \phi_{e_i} < \frac{\pi}{2}$	$\sin^{-1}(\frac{1}{3}) < \phi_{e_i} < \frac{\pi}{2}$	$\frac{3\pi}{2} < \phi_{e_i} < 2\pi - \sin^{-1}(\frac{1}{3})$
θ_{e_i}	$0 < \theta_{e_i} < \frac{\pi}{2}$	$\frac{\pi}{2} < \theta_{e_i} < \pi$	$\pi < \theta_{e_i} < \frac{3\pi}{2}$	$\frac{3\pi}{2} < \theta_{e_i} < 2\pi$

	E	F	G	H
ϕ_{e_i}	$\pi + \sin^{-1}(\frac{1}{3}) < \phi_{e_i} < \frac{3\pi}{2}$	$\frac{\pi}{2} < \phi_{e_i} < \pi - \sin^{-1}(\frac{1}{3})$	$\frac{\pi}{2} < \phi_{e_i} < \pi - \sin^{-1}(\frac{1}{3})$	$\pi + \sin^{-1}(\frac{1}{3}) < \phi_{e_i} < \frac{3\pi}{2}$
θ_{e_i}	$0 < \theta_{e_i} < \frac{\pi}{2}$	$\frac{\pi}{2} < \theta_{e_i} < \pi$	$\pi < \theta_{e_i} < \frac{3\pi}{2}$	$\frac{3\pi}{2} < \theta_{e_i} < 2\pi$

Table 2: 4-valent graph angle-ranges for each octant

Our calculations show that for all possible sub-cases of angle arrangements defined in Table 2, the expectation value for the volume operator is rotational invariant *only* at the zeroth-order⁹, while higher-order terms *are* rotationally dependent. Therefore, in what follows, we will not compute the expectation value for the volume operator as computed for each possible orientation of the graph. Instead we will choose a particular sub-case of Table 2 and compute the expectation value for such a sub-case. Specifically we will choose the case in which the arrangement of edges, incident at the vertex V_0 , after a rotation, is given by the following ranges:

$$\begin{aligned}
0 < \theta_{e_{0,2}} < \frac{\pi}{2} & & \frac{3\pi}{2} < \phi_{e_{0,2}} < 2\pi - \sin^{-1}\frac{1}{3} \\
\pi < \theta_{e_{0,4}} < \frac{3\pi}{2} & & \sin^{-1}(\frac{1}{3}) < \phi_{e_{0,4}} < \frac{\pi}{2} \\
\frac{\pi}{2} < \theta_{e_{0,1}} < \pi & & \frac{3\pi}{2} < \phi_{e_{0,1}} < \pi - \sin^{-1}(\frac{1}{3}) \\
\frac{3\pi}{2} < \theta_{e_{0,3}} < 2\pi & & \pi + \sin^{-1}(\frac{1}{3}) < \phi_{e_{0,3}} < \frac{3\pi}{2}
\end{aligned} \tag{3.19}$$

This implies that the edges $e_{0,2}, e_{0,3}, e_{0,4}$ and $e_{0,1}$ lie in the octants A, H, C and F . From the geometry of the 4-valent lattice, the angles of the edges incident at all the other vertices follow.

There is a vast range of Euler angles for which the case above is obtained but, for the sake of brevity, we will not list them here. What is important, though, is that such case has a non-zero measure in $SO(3)$.

⁹This is a consequence of the fact that the geometric factors G_{γ,V_i} for each of the sub-cases in Table 2 will be the same (see Section 2.4.1)

It should be noted that different combinations of angles within the angle ranges in (3.19) lead to different outcomes for the expectation value of the volume operator, since they lead to different values of the terms $\frac{t_{e_i e_j}}{\sqrt{t_{e_i} t_{e_j}}}$. However, in zeroth-order, the expectation value of the volume operator will be the same irrespectively of which angles satisfying (3.19) we decide to utilise. In fact, the rotational dependence of the expectation value of the volume operator, in the zeroth-order in $\frac{l}{\delta}$, is determined *solely* by the geometric factors G_{γ, V_i} . For the case which we are analysing (3.19), the values of G_{γ, V_i} will be the same irrespectively of which sub-case of (3.19) we analyse. On the other hand, the dependence of the expectation value of the volume operator on higher orders of $\frac{l}{\delta}$ is determined by the terms $\frac{t_{e_i e_j}}{\sqrt{t_{e_i} t_{e_j}}}$ and, therefore, will depend on the sub-cases we analyse.

This discussion shows that for higher orders in $\frac{l}{\delta}$ the expectation value of the volume operator is rotational dependent since, as stated above, for differing angle-ranges that lead to the same geometric factors, the values of the terms $\frac{t_{e_i e_j}}{\sqrt{t_{e_i} t_{e_j}}}$ will differ.

We will now compute the expectation value of the volume operator for the periodicity cell in the 4-valent graph for the case in which the angles of the edges incident at vertex V_0 satisfy condition (3.19). The first step in order to compute the expectation value of the volume operator is to define the matrix \sqrt{A}^{-1} , whose off-diagonal entries are the terms $\frac{t_{e_i e_j}}{\sqrt{t_{e_i} t_{e_j}}}$. This matrix is given in Table A.1.1 in the Appendix. Although different combinations of angles satisfying condition (3.19) will lead to different values of the terms $\frac{t_{e_i e_j}}{\sqrt{t_{e_i} t_{e_j}}}$, however, any such combination will lead to the same non-zero entries of the matrix \sqrt{A}^{-1} . This means that the pairs of edges commonly intersecting a plaquette in a given direction will coincide for *any* combination of angles satisfying conditions (3.19), even though the number t_{e_i, e_j} of plaquettes they commonly intersect will differ in each case. Therefore in computing the matrix \sqrt{A}^{-1} we will not determine the precise value of the individual entries, but we will leave them as general as possible. Their precise values can be computed once a specific combination of angles satisfying (3.19) is chosen.

Given the matrix \sqrt{A}^{-1} we are then able to apply formula (2.33) for computing the expectation value of the volume operator. As in the aligned case, we first compute the expectation value of the volume operator for each of the four vertices, and then sum their contributions. In what follows, the term $\frac{t_{e_i, e_j}}{\sqrt{t_{e_i} t_{e_j}}}$ is denoted by $\alpha_{e_i, e_j} = \frac{t_{e_i, e_j}}{\sqrt{t_{e_i} t_{e_j}}}$. An explicit form for these terms can be found in Section 11.1 of the Appendix.

The expectation value for the volume operator for the entire periodicity cell, up to first-order in $\frac{l}{\delta}$ is:

$$\begin{aligned}
V_R = & \delta^3 \sqrt{\frac{1}{8}} \left| \det \left(\frac{\partial X_S^a}{\partial (s, u^1, u^2)} \right) \right| \left(4 \sqrt{|\det(E_j^a(u))|} \right. \\
& + 4 \sqrt{\left| 1 + \frac{1}{2} (-\alpha_{e_8, 10, e_8, 11}^2 - \alpha_{e_8, 10, e_8, 12}^2 - \alpha_{e_8, 10, e_8, 5}^2 - \alpha_{e_8, 11, e_8, 12}^2 - \alpha_{e_8, 11, e_8, 5}^2 - \alpha_{e_8, 12, e_8, 5}^2) \right| \sqrt{|\det(E_j^a(u))|} } \\
& + 4 \sqrt{\left| 1 + \frac{1}{2} (-\alpha_{e_{13}, 18, e_{13}, 15}^2 - \alpha_{e_{13}, 19, e_{13}, 15}^2 - \alpha_{e_{13}, 19, e_{13}, 18}^2 - \alpha_{e_{13}, 3, e_{13}, 15}^2 - \alpha_{e_{13}, 3, e_{13}, 18}^2 - \alpha_{e_{13}, 3, e_{13}, 19}^2) \right| \sqrt{|\det(E_j^a(u))|} } \\
& \left. + 4 \sqrt{\left| 1 + \frac{1}{2} (-\alpha_{e_{2, 0}, e_{2, 5}}^2 - \alpha_{e_{2, 0}, e_{2, 6}}^2 - \alpha_{e_{2, 0}, e_{2, 7}}^2 - \alpha_{e_{2, 5}, e_{2, 6}}^2 - \alpha_{e_{2, 5}, e_{2, 7}}^2 - \alpha_{e_{2, 6}, e_{2, 7}}^2) \right| \sqrt{|\det(E_j^a(u))|} } \right) + \mathcal{O}(3)
\end{aligned} \tag{3.20}$$

By performing a Taylor expansion for each of the roots present in the above formula, we can factor out the term $\sqrt{|\det(E_j^a(u))|}$ since, in the first-order approximation that we are considering, they turn out to be the same for each vertex. Such an approximation is justified by the analysis performed in Section (2.2). We

then obtain

$$V_R = \delta^3 2\sqrt{2} \sqrt{|\det(E_j^a(u))|} \left(1 + \frac{1}{4} (-\alpha_{e_8,10,e_8,11}^2 - \alpha_{e_8,10,e_8,12}^2 - \alpha_{e_8,10,e_8,5}^2 - \alpha_{e_8,11,e_8,12}^2 - \alpha_{e_8,11,e_8,5}^2 - \alpha_{e_8,12,e_8,5}^2 - \alpha_{e_{13,18},e_{13,15}}^2 - \alpha_{e_{13,19},e_{13,15}}^2 - \alpha_{e_{13,19},e_{13,18}}^2 - \alpha_{e_{13,3},e_{13,15}}^2 - \alpha_{e_{13,3},e_{13,18}}^2 - \alpha_{e_{13,3},e_{13,19}}^2 - \right. \quad (3.21)$$

$$\left. \alpha_{e_{2,0},e_{2,5}}^2 - \alpha_{e_{2,0},e_{2,6}}^2 - \alpha_{e_{2,0},e_{2,7}}^2 - \alpha_{e_{2,5},e_{2,6}}^2 - \alpha_{e_{2,5},e_{2,7}}^2 - \alpha_{e_{2,6},e_{2,7}}^2) \right) \quad (3.22)$$

$$= \delta^3 \sqrt{|\det(E_j^a(u))|} 2\sqrt{2} \left(1 + \frac{1}{4} \left(- \sum_{i,j=1;j \neq i}^{\frac{n}{2}(n-1)} \alpha_{ji}^2 \right) \left| \det \left(\frac{\delta X_S^a}{\delta(s, u^1, u^2)} \right) \right| \right) \quad (3.23)$$

The term $\frac{1}{2}(-\sum_{i,j=1;j \neq i}^{\frac{n}{2}(n-1)} \alpha_{ji}^2)$ represents l/δ -corrections. Each term $\alpha_{i,j}$ is proportional to $C_{\frac{l'}{\delta}}$ for $l' < l$; C is a constant that depends on the Euler angles we chose. On the other hand the geometric factors G_{γ, V_i} for cases (3.19) coincide with the geometric factors as computed for any of the sub-cases in Table 2, i.e., $G_{\gamma, V_i} = 2\sqrt{2}$. This implies that although for such cases the expectation value of the volume operator is rotational invariant in zeroth-order, nonetheless, it does *not* reproduce the correct semiclassical limit.

For those embeddings whose measure is *zero* in $SO(3)$, the geometric factor turns out to be different and, in zeroth-order in l/δ , leads to a different value of the expectation value of the volume operator as computed for 4-valent graphs.

3.2.3 Expectation value of the volume operator for a translated 4-valent graph

In this Section we will analyse whether the expectation value of the volume operator for the 4-valent graph is translational invariant with respect to the plaquette.

To perform this analysis we consider our original aligned graph and translate it by an arbitrary vector $\vec{p} = (\epsilon_x, \epsilon_y, \epsilon_z)$. The new coordinates for the vertices are:

$$V_0'' = (\epsilon_x, \epsilon_y, \epsilon_z) \text{ with } \epsilon_x > \epsilon_y > \epsilon_z \quad (3.24)$$

$$V_2'' = \left(-\frac{\delta}{\sqrt{3}} + \epsilon_x, \epsilon_y + \frac{\delta}{\sqrt{3}}, \epsilon_z + \frac{\delta}{\sqrt{3}} \right) \quad (3.25)$$

$$V_8'' = \left(\frac{\delta}{\sqrt{3}} + \epsilon_x, \epsilon_y + 3\frac{\delta}{\sqrt{3}}, \epsilon_z + \frac{\delta}{\sqrt{3}} \right) \quad (3.26)$$

$$V_{13}'' = \left(\epsilon_x, \epsilon_y + 2\frac{\delta}{\sqrt{3}}, \epsilon_z - 2\frac{\delta}{\sqrt{3}} \right) \quad (3.27)$$

Similarly to the analysis for rotational invariance, the computation of the expectation value of the volume operator can be divided into different sub-cases, each of which would lead to different outcomes.

The first division is given by the choice of the signs and the relations between ϵ_x, ϵ_y and ϵ_z , i.e., whether they are positive or negative and whether one coordinate is bigger or equal to another. Each of these cases can be ultimately subdivided into sub-cases depending on the relation between the ratio $b = \frac{\delta}{\sqrt{3}}$ and the coordinates of the translational vector.

To carry out our calculations we choose the following:

- 1) $b > \epsilon_x > \epsilon_y > \epsilon_z > 0$
- 2) $|V_k^i| - |V_k^j| > n_k^i l - n_k^j l$ for all $|V_k^i| > |V_k^j|$

Altogether, such conditions will allow to determine both the sign of the coordinates for each of the vertices of the translated graph and also the magnitude relation between the coordinates of each vertex.

However, it will transpire that our result is independent of which case we decide to use to perform the calculations. In fact, as we will see, in zeroth-order, the expectation value of the volume operator for a

4-valent graph is translation invariant up to combinations of measure *zero* in $SO(3)$. However, for higher orders of approximation this will no longer be true.

As a first step in our calculations we need to specify the allowed positions for each of the translated vertices. Due to the highly symmetrical structure of the 4-valent graph, in order to determine the allowed positions of each vertex, it suffices to find the allowed positions of one reference vertex. We choose such a reference vertex to be V_0 , whose new coordinates are $V_0 = (\epsilon_x, \epsilon_y, \epsilon_z)$.

The number of stacks intersected by the vector that represents vertex V_0 in the x , y and z -directions are, respectively, $n = [\frac{\epsilon_x}{l}]$, $m = [\frac{\epsilon_y}{l}]$ and $p = [\frac{\epsilon_z}{l}]$ (where $[\]$ indicates the Gauss bracket). It follows that the allowed positions for vertex V_0 are given by the following ranges of each coordinate: $nl < \epsilon_x < nl + l$, $ml < \epsilon_y < ml + l$ and $pl < \epsilon_z < pl + l$.

It turns out that to carry out the calculations for the expectation value of the volume operator we have to restrict the value-range of the coordinates ϵ_x , ϵ_y and ϵ_z . We choose $nl < \epsilon_x < nl + \frac{l}{6}$, $ml < \epsilon_y < ml + \frac{l}{6}$ and $pl < \epsilon_z < pl + \frac{l}{6}$.

We will now compute the expectation value of the volume operator of the periodicity lattice of the 4-valent graph. We will not give the details of all the calculations involved since they are quite lengthy. However, the method utilised is the same as for the non-translated case, namely, for each of the four vertices comprising the periodicity cell we consider the sub-matrix of \sqrt{A}^{-1} labelled by the four edges intersecting at the vertex. For each of these sub-matrices, call them M , we compute the determinant of the four 3×3 sub-matrices of M defined by the triplets of linearly-independent edges. We then sum up the contributions coming from each of the vertices. Similarly as for the aligned 4-valent graph we have

$$T_{e_i}^{\{x,y\}} = F_{e_i}^{\{x,y\}} = Z_{e_i}^{\{x,y\}} = 1 \quad \forall e_i \in \gamma \quad (3.28)$$

The expression for the matrix \sqrt{A}^{-1} is

$$\begin{pmatrix} 1 & \frac{-C_0}{2} & \frac{-B_0}{2} & \frac{-C_0}{2} & 0 & 0 & 0 & 0 & 0 & 0 & 0 & 0 & 0 & 0 & 0 \\ \frac{-C_0}{2} & 1 & \frac{-C_0}{2} & \frac{-B_0}{2} & \frac{-A_2}{2} & \frac{-C_2}{2} & \frac{-A_2}{2} & 0 & 0 & 0 & 0 & 0 & 0 & 0 & 0 \\ \frac{-B_0}{2} & \frac{-C_0}{2} & 1 & \frac{-C_0}{2} & 0 & 0 & 0 & 0 & 0 & 0 & 0 & 0 & 0 & 0 & 0 \\ \frac{-C_0}{2} & \frac{-B_0}{2} & \frac{-C_0}{2} & 1 & 0 & 0 & 0 & 0 & 0 & 0 & 0 & 0 & 0 & 0 & 0 \\ 0 & \frac{-A_2}{2} & 0 & 0 & 1 & \frac{-A_2}{2} & \frac{-C_2}{2} & 0 & 0 & 0 & 0 & 0 & 0 & 0 & 0 \\ 0 & \frac{-C_2}{2} & 0 & 0 & \frac{-A_2}{2} & 1 & \frac{-A_2}{2} & 0 & 0 & 0 & 0 & 0 & 0 & 0 & 0 \\ 0 & \frac{-A_2}{2} & 0 & 0 & \frac{-C_2}{2} & \frac{-A_2}{2} & 1 & 0 & 0 & 0 & 0 & 0 & 0 & 0 & 0 \\ 0 & 0 & 0 & 0 & 0 & 0 & 0 & 1 & \frac{-A_{13}}{2} & \frac{-C_{13}}{2} & \frac{-A_{13}}{2} & 0 & 0 & 0 & 0 \\ 0 & 0 & 0 & 0 & 0 & 0 & 0 & \frac{-A_{13}}{2} & 1 & \frac{-A_{13}}{2} & \frac{-C_{13}}{2} & 0 & 0 & 0 & 0 \\ 0 & 0 & 0 & 0 & 0 & 0 & 0 & \frac{-C_{13}}{2} & \frac{-A_{13}}{2} & 1 & \frac{-A_{13}}{2} & 0 & 0 & 0 & 0 \\ 0 & 0 & 0 & 0 & 0 & 0 & 0 & \frac{-A_{13}}{2} & \frac{-C_{13}}{2} & \frac{-A_{13}}{2} & 1 & 0 & 0 & 0 & 0 \\ 0 & 0 & 0 & 0 & 0 & 0 & 0 & 0 & 0 & 0 & 0 & 1 & \frac{-A_8}{2} & \frac{-C_8}{2} & \frac{-C_8}{2} \\ 0 & 0 & 0 & 0 & 0 & 0 & 0 & 0 & 0 & 0 & 0 & \frac{-A_8}{2} & 1 & \frac{-C_8}{2} & \frac{-C_8}{2} \\ 0 & 0 & 0 & 0 & 0 & 0 & 0 & 0 & 0 & 0 & 0 & \frac{-C_8}{2} & \frac{-C_8}{2} & 1 & \frac{-A_8}{2} \\ 0 & 0 & 0 & 0 & 0 & 0 & 0 & 0 & 0 & 0 & 0 & \frac{-C_8}{2} & \frac{-C_8}{2} & \frac{-A_8}{2} & 1 \end{pmatrix}$$

where $A_i = (x_{V_i} - n_i l) \frac{1}{\delta \sqrt{3}}$, $B_i = (y_{V_i} - m_i l) \frac{1}{\delta \sqrt{3}}$, $C_i = (z_{V_i} - p_i l) \frac{1}{\delta \sqrt{3}}$.

Applying the method described above we compute the expectation value for the volume operator for one

periodicity cell to be

$$V_R = \sqrt{\frac{1}{8}} \delta^3 \left| \det \left(\frac{\delta X_S^a}{\delta(s, u^1, u^2)} \right) \right| 2 \times \quad (3.29)$$

$$\left(\sqrt{|\det(E_j^a(u))|} \sqrt{|4 - B_0^2 - 2C_0^2 - B_0 C_0^2|} + \sqrt{|\det(E_j^a(u))|} \sqrt{|4 - 2A_2^2 - A_2^2 C_2 - C_2^2|} + \right. \\ \left. \sqrt{|\det(E_j^a(u))|} \sqrt{|4 - 2A_{13}^2 - A_{13}^2 C_{13} - C_{13}^2|} + \sqrt{|\det(E_j^a(u))|} \sqrt{|4 - A_8^2 - 2C_8^2 - A_8 C_8^2|} \right) \quad (3.30)$$

In first-order approximation we then obtain

$$V_R = 2 \sqrt{\frac{1}{8}} \delta^3 \sqrt{|\det(E_j^a(u))|} \left(4 - \frac{1}{8} (B_0^2 + 2C_0^2 + B_0 C_0^2 + 2A_2^2 + A_2^2 C_2 + C_2^2 + 2A_{13}^2 + A_{13}^2 C_{13} + C_{13}^2 + \right. \\ \left. A_8^2 + 2C_8^2 + A_8 C_8^2) \right) + \mathcal{O}(4) \left| \det \left(\frac{\delta X_S^a}{\delta(s, u^1, u^2)} \right) \right| \\ = 2\sqrt{2} \delta^3 \sqrt{|\det(E_j^a(u))|} \left(1 - \frac{1}{32} (B_0^2 + 2C_0^2 + 2A_2^2 + C_2^2 + 2A_{13}^2 + C_{13}^2 + A_8^2 + 2C_8^2) + \mathcal{O}(3) \right) \left| \det \left(\frac{\delta X_S^a}{\delta(s, u^1, u^2)} \right) \right| \quad (3.31)$$

where in the last equation we have only considered first-order contributions obtained by the usual Taylor series of the square root (see Section 2.2). Thus, we were able to factor out the term $\sqrt{|\det(E_j^a(u))|}$. As it is evident, the corrections of second order in l/δ are not translationally invariant.

3.3 Analysis of the expectation value of the volume operator for 6-valent graphs

In this Section we will calculate the expectation value of the volume operator for a 6-valent graph. First we consider the non-rotated graph, then we will analyse the rotational and translational dependence of the expectation value by performing a rotation of the graph, followed by a translation of the graph. We will then recalculate the expectation value.

3.3.1 Expectation value of the volume operator for a general 6-valent graph

Similarly as for the 4-valent graph, we will analyse the case for which $\frac{\delta}{l} > 0$; the motivation for such a choice was given in Section 2.2. For computational simplicity we will position the graph so that the $(0, 0, 0)$ coordinates of the graph coincide with the $(0, 0, 0)$ coordinates of the plaquette. We also need to align the graph in such a way that each vertex is symmetrical with respect to the axis. Therefore we will choose, for each vertex V_k , the value $\phi_{e_{k,i}} = 45$ for all edges $e_{k,i}$ incident at V_k and $\theta_{e_{k,i}} = 45$ for four edges, while the remaining two will have $\theta_{e_{k,i}} = 0$. This edge orientation corresponds to the limiting case (2) described in Section 2.4.1.

As for the diamond lattice, we choose the vertex V_2 as our reference vertex with respect to which we determine the allowed positions of all the remaining vertices of the graph. We also choose the allowed values of the x -coordinate of V_2 to be $nl < x_{V_2} < nl + \frac{l}{6}$, where, in this case, $n = \lfloor \frac{\delta \sqrt{2}}{2l} \rfloor$. Using the same method used in Section 3.1 we can compute all the terms $\frac{t_{e_i e_j}}{\sqrt{t_{e_i} t_{e_j}}}$ for the periodicity cell of the 6-valent graph that contains nine vertices. Given the geometry of the 6-valent graph we have the following values for the term

in equations (3.4)–(3.6)

$$\begin{aligned}
Z_{e_i}^{\{x,y\}} &= \begin{cases} \frac{2}{\sqrt{2}} & \text{iff } \theta_{e_i} \neq 0 \\ 1 & \text{iff } \theta_{e_i} = 0 \end{cases} & T_{e_i}^{\{x,y\}} &= \begin{cases} \frac{\sqrt{2}}{2} & \text{iff } \theta_{e_i} \neq 0 \\ 1 & \text{iff } \theta_{e_i} = 0 \end{cases} \\
F_{e_i}^x &= \begin{cases} 1 & \text{iff } \theta_{e_i} \neq 0 \\ \infty & \text{iff } \theta_{e_i} = 0 \end{cases} & F_{e_i}^x &= 1 & \forall e_i \in \gamma
\end{aligned} \tag{3.32}$$

The coordinates of the vertices of the periodicity cell are

$$\begin{aligned}
V_0 &= (0, 0, 0) \\
V_2 &= \left(\delta \frac{\sqrt{2}}{2}, 0, \delta \frac{\sqrt{2}}{2}\right) \\
V_3 &= \left(\left(\delta \frac{\sqrt{2}}{2} - \left(\delta \frac{1}{2}, -\delta \frac{1}{2}, 2\delta \frac{\sqrt{2}}{2}\right)\right)\right) \\
V_4 &= \left(2\delta \frac{\sqrt{2}}{2}, -2\delta \frac{1}{2}, 2\delta \frac{\sqrt{2}}{2}\right) \\
V_5 &= \left(0, -2\delta \frac{1}{2}, 0\right) \\
V_{13} &= \left(\delta \frac{\sqrt{2}}{2}, -2\delta \frac{1}{2}, \delta \frac{\sqrt{2}}{2}\right) \\
V_{18} &= \left(2\delta \frac{\sqrt{2}}{2} + \delta \frac{1}{2}, -1\delta \frac{1}{2}, \delta \frac{\sqrt{2}}{2}\right) \\
V_{15} &= \left(\delta \frac{\sqrt{2}}{2} - \delta, -2\delta \frac{1}{2}, 3\delta \frac{\sqrt{2}}{2}\right) \\
V_{14} &= \left(\delta \frac{\sqrt{2}}{2} + \delta \frac{1}{2}, -3\delta \frac{1}{2}, 0\right)
\end{aligned}$$

The values for the terms $\frac{t_{e_i e_j}}{\sqrt{t_{e_i} t_{e_j}}}$ are given in the section A.2.1 of the appendix

The value for the expectation value of the volume operator for one periodicity cell consisting of *nine*

vertices is computed to be

$$\begin{aligned}
V_R = & \frac{1}{8}\delta^3 \left| \det \left(\frac{\delta X_S^a}{\delta(s, u^1, u^2)} \right) \right| 2 \left(\sqrt{8} \sqrt{|\det(E_j^a(u))|} + \sqrt{\left| 8 - \frac{\alpha^2}{2} - \frac{23(\alpha')^2}{4} - \frac{\alpha(\alpha')^2}{4} - \frac{3\alpha(\alpha')^2}{4\sqrt{2}} \right|} 2 \sqrt{|\det(E_j^a(u))|} \right) \\
& + \sqrt{\left| 8 - \frac{5(A'_3)^2}{2} - \frac{(A'_3)^2 A_3}{4} - \frac{5A_3^2}{2} - \sqrt{2}A_3^2 - \frac{A'_3 A_3 \alpha'}{2} - (\alpha')^2 - \frac{(A'_3)^2 \beta}{4} - \frac{(A'_3)^2 \beta}{2\sqrt{2}} - \frac{3\beta^2}{2} - \sqrt{2}\beta^2 - \frac{3A'_3 A_3 \beta'}{2} \right|} \\
& - \sqrt{2}A'_3 A_3 \beta' - \frac{\alpha' \beta \beta'}{2} - \frac{\alpha' \beta \beta'}{2\sqrt{2}} - \frac{7(\beta')^2}{2} - \frac{A_3(\beta')^2}{2\sqrt{2}} \left| \sqrt{|\det(E_j^a(u))|} + \sqrt{\left| 8 - 12\beta^2 - 8\sqrt{2}\beta^2 \right|} \sqrt{|\det(E_j^a(u))|} \right) \\
& + \sqrt{\left| 8 - 2\alpha^2 - 9(\alpha')^2 - 2\sqrt{2}\alpha(\alpha')^2 - 12\beta^2 - 8\sqrt{2}\beta^2 - 12\alpha' \beta \beta' - 9\sqrt{2}\alpha' \beta \beta' - 12(\beta')^2 - 4\alpha(\beta')^2 \right|} \sqrt{|\det(E_j^a(u))|} \\
& + \sqrt{\left| 8 - \frac{7\alpha^2}{4} - \frac{7(\alpha')^2}{2} - \frac{13\alpha(\alpha')^2}{8\sqrt{2}} - 2\alpha\beta - 2\sqrt{2}\alpha\beta - \frac{(\alpha')^2 \beta}{2} - \frac{3(\alpha')^2 \beta}{2\sqrt{2}} - 6\beta^2 - \frac{5\alpha\alpha' \beta'}{2\sqrt{2}} - 2\alpha' \beta \beta' - 4(\beta')^2 \right|} \\
& \times \sqrt{|\det(E_j^a(u))|} + \sqrt{\left| 8 - \frac{3(A'_{18})^2}{2} - \alpha^2/2 - \frac{A'_{18}\alpha\alpha'}{2\sqrt{2}} - \frac{3(\alpha')^2}{4} - 3\beta^2 - 2\sqrt{2}\beta^2 - A'_{18}\beta\beta' - \frac{3A'_{18}\beta\beta'}{2\sqrt{2}} - \frac{\alpha' \beta \beta'}{2} - \right.} \\
& \left. - \frac{3\alpha' \beta \beta'}{4\sqrt{2}} - 3(\beta')^2 - \frac{\alpha(\beta')^2}{2} \right|} \sqrt{|\det(E_j^a(u))|} + \sqrt{\left| 8 - 3(A'_{15})^2 - \frac{(A'_{15})^2 A_{15}}{\sqrt{2}} - 2A_{15}^2 - \frac{3A'_{15} A_{15} \alpha'}{\sqrt{2}} - 9(\alpha')^2 \right|} \\
& - \frac{9A_{15}(\alpha')^2}{4\sqrt{2}} - \frac{3(A'_{15})^2 \beta}{2} - \frac{(A'_{15})^2 \beta}{\sqrt{2}} - 3\sqrt{2}A_{15}\beta - \frac{9(\alpha')^2 \beta}{2} - 10\beta^2 - 4\sqrt{2}\beta^2 - \frac{A'_{15} A_{15} \beta'}{\sqrt{2}} - 3\alpha' \beta \beta' - 3\sqrt{2}\alpha' \beta \beta' \\
& - 2(\beta')^2 \left| \sqrt{|\det(E_j^a(u))|} + \sqrt{\left| 8 - 2(A'_{14})^2 - A_{14}^2 - \frac{3(A'_{14})^2 \beta}{4} - \frac{3(A'_{14})^2 \beta}{2\sqrt{2}} - 3\sqrt{2}A_{14}\beta \right.} \right. \\
& \left. - 18\beta^2 - 9\sqrt{2}\beta^2 - \frac{3A'_{14} A_{14} \beta'}{\sqrt{2}} - \frac{9A'_{14} \beta \beta'}{2} - 9(\beta')^2 \right|} \sqrt{|\det(E_j^a(u))|} \Big) \tag{3.33}
\end{aligned}$$

Expanding the square root (see the analysis in Section 2.2) and considering first-order terms we obtain

$$\begin{aligned}
V_R = & 2\delta^3 \sqrt{|\det(E_j^a(u))|} \left| \det \left(\frac{\delta X_S^a}{\delta(s, u^1, u^2)} \right) \right| \left(9 + \frac{1}{2} \times \frac{1}{8} \left(-2(A'_{14})^2 - 3(A'_{15})^2 - \frac{3(A'_{18})^2}{2} - \frac{5(A'_3)^2}{2} - A_{14}^2 \right. \right. \\
& \left. \left. - 2A_{15}^2 - \frac{5A_3^2}{2} - \sqrt{2}A_3^2 - \frac{19\alpha^2}{4} - 29(\alpha')^2 - 3\sqrt{2}A_{14}\beta - 3\sqrt{2}A_{15}\beta - 2\alpha\beta - 2\sqrt{2}\alpha\beta - \frac{125\beta^2}{2} - 32\sqrt{2}\beta^2 - \frac{67(\beta')^2}{2} \right) \right) \tag{3.34}
\end{aligned}$$

Contrary to [23] we find that, to zeroth-order in l/δ , the expectation value of the volume operator for a 6-valent graph does *not* have the correct semiclassical limit. On the other hand, if the graph is aligned to the orientation of the plaquette we *do* obtain the correct semiclassical value. However, this embedding has measure *zero* in $SO(3)$.

3.3.2 Expectation value of the volume operator for a rotated 6-valent graph

We will now analyse the expectation value of the volume operator for a rotated 6-valent graph. As for the 4-valent graph, different choices of Euler angles in the rotation give different values of $t_{e_i e_j}$. Therefore, we will once again have to define sub-cases which are defined according to the possible ranges of values for the angles ϕ_{e_i} and θ_{e_i} for each edge e_i . Because of the geometry of the 6-valent lattice, we know that for any edge, e , of a given vertex there exists a co-linear edge, e' , which intersects the same vertex. This implies that, given two co-linear edges e and e' , we can define the angles of e (respectively e') in terms of e' (respectively

e) as follows: $\phi_e = 180^\circ - \phi_{e'}$ and $\theta_e = 180^\circ - \theta_{e'}$. Such relations reduce the number of cases that need to be analysed.

We choose the vertex V'_0 as our reference vertex. The relations for the angles of the edges incident at V'_0 are:

$$\begin{aligned}
\phi_{e_{0,7}} &= 180^\circ - \phi_{e_{0,2}} \\
\phi_{e_{0,1}} &= 180^\circ - \phi_{e_{0,17}} \\
\phi_{e_{0,6}} &= 180^\circ - \phi_{e_{0,8}} \\
\theta_{e_{0,8}} &= 180^\circ - \theta_{e_{0,6}} \\
\theta_{e_{0,17}} &= 180^\circ - \theta_{e_{0,1}} \\
\theta_{e_{0,2}} &= 180^\circ - \theta_{e_{0,7}}
\end{aligned} \tag{3.35}$$

These relations imply that the allowed values of the angles of the edges at a given vertex fall into one of the following groups:

1. A given triplet of edges points upwards, i.e., their angle ϕ lies between $-\frac{\pi}{2}$ and $\frac{\pi}{2}$, and the triplet formed by their co-linear edges points downwards, i.e., their angle ϕ lies between $\frac{\pi}{2}$ and $\frac{3\pi}{2}$. This situation arises when none of the edges is aligned with one of the x , y , z -coordinates. However we have two distinct sub-cases which satisfy this arrangement of edges
 - a. No edge lies in any plaquette.
 - b. Only one edge and its co-planar lie in a given plaquette (Figure 3).
2. A given couple of edges points upwards i.e., their angle ϕ lies between $-\frac{\pi}{2}$ and $\frac{\pi}{2}$, and their co-linear edges point downwards i.e., their angle ϕ lies between $\frac{\pi}{2}$ and $\frac{3\pi}{2}$. This situation arises when one edge (and subsequently its collinear edge) is aligned with one of the coordinates axis and, subsequently, the remaining two edges and their co-linear lie in two different plaquettes in the same direction (Figure 5)
3. Only one edge points upwards, i.e., its angle ϕ lies between $-\frac{\pi}{2}$ and $\frac{\pi}{2}$, and the co-linear edge points downwards i.e., its angle ϕ lies between $\frac{\pi}{2}$ and $\frac{3\pi}{2}$. This situation arises when all of the edges are aligned with the coordinate axis (Figure 6).

A discussion of each of these cases and the respective value for the geometric factor was carried out in Section 2.4.1. There it was shown that only case 1a above has *non-zero* measure in $SO(3)$, therefore we will restrict our analysis to such a case.

It is straight forward to see that case 1a can be divided into further sub-cases according to the values of the θ -angles and the relations between the ϕ -angles of each of the up/down couples. In what follows, we will not give the results for all possible choices. Instead, we will choose a particular sub-case and perform the calculations for the expectation value of the volume operator with respect to this sub-case. As we will see, these calculations show that, up to embeddings of measure zero in $SO(3)$, the semiclassical behavior of the volume operator, in zeroth-order, does not depend on how the graph is rotated: *a fortiori*, it is independent of the particular case we analysed.

In order to carry out a proper comparison between the semiclassical behavior of the volume operator as applied to graphs of different valence, we will apply the same Euler transformations (i.e., with the same Euler angles) to each of the graphs we consider. Since we have not specified the values of the Euler angles, the only way to do this is to assume that after a rotation, those edges which had the same angles used in both the aligned 4-valent and 6-valent case will end up in the same octant. For example, consider Figures 17 and 18 which depict both 6-valent and 4-valent vertices respectively. From such pictures it is easy to see that the edges $e_{0,2}$ and $e_{0,3}$ of the 4-valent graph have the same θ - and ϕ -angles as the edges, $e_{0,8}$, and, $e_{0,1}$, of the 6-valent graph. Therefore, in the rotated case we will assume that $e_{0,8}$, and, $e_{0,1}$ lie in the same

octants as $e_{0,2}$ and $e_{0,3}$ respectively. It follows that the angle-ranges for the edges incident at vertex V_0 for a 6-valent graph are:

$$\begin{array}{ll}
 \frac{3\pi}{2} < \theta_{e_{0,2}} < \frac{7\pi}{4} & \frac{3\pi}{2} < \phi_{e_{0,2}} < 2\pi \\
 \frac{\pi}{4} < \theta_{e_{0,8}} < \frac{\pi}{2} & 0 < \phi_{e_{0,8}} < \frac{\pi}{2} \\
 \frac{3\pi}{4} < \theta_{e_{0,17}} < \pi & 0 < \phi_{e_{0,17}} < \frac{\pi}{2} \\
 \frac{\pi}{2} < \theta_{e_{0,7}} < \frac{3\pi}{4} & \frac{\pi}{2} < \phi_{e_{0,7}} < \pi \\
 \frac{\pi}{2} < \theta_{e_{0,6}} < \frac{3\pi}{4} & \pi < \phi_{e_{0,6}} < \frac{3\pi}{2} \\
 \frac{7\pi}{4} < \theta_{e_{0,1}} < 2\pi & \pi < \phi_{e_{0,1}} < \frac{3\pi}{2}
 \end{array} \tag{3.36}$$

Such conditions of the angles implies that the edges $e_{0,1}$, $e_{0,2}$, $e_{0,6}$, $e_{0,7}$, $e_{0,7}$ and $e_{0,17}$ lie in the octants H , D , G , F , A and B respectively.

Since we are considering a regular 6-valent lattice, the above ranges of angles induce a relation on all the other angle-ranges of the edges for each vertex in the graph. The coordinates of the rotated vertices are:

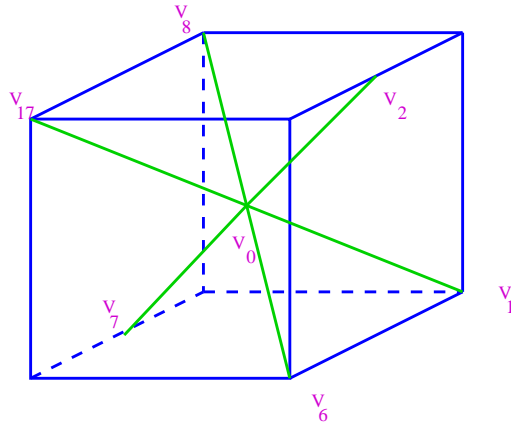


Figure 17: 6-valent vertex

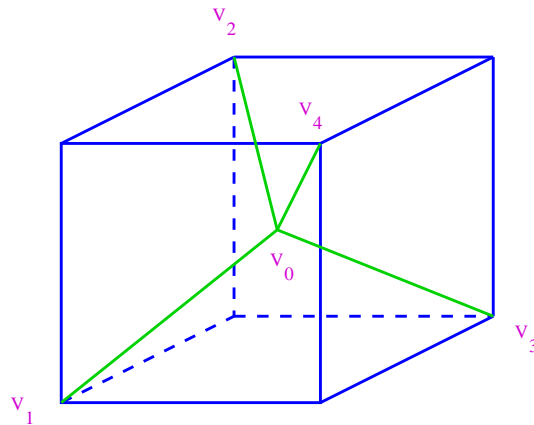


Figure 18: 4-valent vertex

$$\begin{aligned}
V'_0 &= (0, 0, 0) \\
V'_2 &= \left((R_{11} + R_{13})\frac{\delta\sqrt{2}}{2}, (R_{21} + R_{23})\frac{\delta\sqrt{2}}{2}, (R_{31} + 2R_{33})\frac{\delta\sqrt{2}}{2} \right) \\
V'_3 &= \left((R_{11}\left(\frac{\sqrt{2}-1}{2}\right) - \frac{R_{12}}{2} + R_{13}\sqrt{2})\delta, (R_{21}\left(\frac{\sqrt{2}-1}{2}\right) - \frac{R_{22}}{2} + R_{23}\sqrt{2})\delta, (R_{31}\left(\frac{\sqrt{2}-1}{2}\right) - \frac{R_{32}}{2} + R_{33}\sqrt{2})\delta \right) \\
V'_4 &= \left((\sqrt{2}R_{11} - R_{12} + \sqrt{2}R_{13})\delta, (\sqrt{2}R_{21} - R_{22} + \sqrt{2}R_{23})\delta, (\sqrt{2}R_{31} - R_{32} + \sqrt{2}R_{33})\delta \right) \\
V'_5 &= \left(-R_{12}\delta, R_{22}\delta, R_{32}\delta \right) \\
V'_{13} &= \left(\left(-\frac{\sqrt{2}}{2}R_{11} - R_{12} + \frac{\sqrt{2}}{2}R_{13}\right)\delta, \left(-\frac{\sqrt{2}}{2}R_{21} - R_{22} + \frac{\sqrt{2}}{2}R_{23}\right)\delta, \left(-\frac{\sqrt{2}}{2}R_{31} - R_{32} + \frac{\sqrt{2}}{2}R_{33}\right)\delta \right) \\
V'_{18} &= \left(\left(\left(\sqrt{2} + \frac{1}{2}\right)R_{11} - \frac{1}{2}R_{12} + \frac{\sqrt{2}}{2}R_{13}\right)\delta, \left(\left(\sqrt{2} + \frac{1}{2}\right)R_{21} - \frac{1}{2}R_{22} + \frac{\sqrt{2}}{2}R_{23}\right)\delta, \left(\left(\sqrt{2} + \frac{1}{2}\right)R_{31} - \frac{1}{2}R_{32} + \frac{\sqrt{2}}{2}R_{33}\right)\delta \right) \\
V'_{15} &= \left(\left(\left(\frac{\sqrt{2}}{2} - 1\right)R_{11} - R_{12} + \frac{3\sqrt{2}}{2}R_{13}\right)\delta, \left(\left(\frac{\sqrt{2}}{2} - 1\right)R_{21} - R_{22} + \frac{3\sqrt{2}}{2}R_{23}\right)\delta, \left(\left(\frac{\sqrt{2}}{2} - 1\right)R_{31} - R_{32} + \frac{3\sqrt{2}}{2}R_{33}\right)\delta \right) \\
V'_{14} &= \left(\left(\frac{\sqrt{2}+1}{2}R_{11} - \frac{3}{2}R_{12}\right)\delta, \left(\frac{\sqrt{2}+1}{2}R_{21} - \frac{3}{2}R_{22}\right)\delta, \left(\frac{\sqrt{2}+1}{2}R_{31} - \frac{3}{2}R_{32}\right)\delta \right) \tag{3.37}
\end{aligned}$$

Similarly, as was done for the 4-valent case, different choices of combination of angles satisfying conditions (3.36) above will lead to different values for the terms $\frac{t_{e_i, e_j}}{\sqrt{t_{e_i} t_{e_j}}}$. However, the couples of edges commonly

intersecting a given stack will coincide for any such combination. This implies that the matrix \sqrt{A}^{-1} will have the same entries for any sub-case of (3.36) but their specific values will be different.

Moreover, the geometric factor $G_{\gamma, V}$ of any sub-case of (3.36) will coincide. It follows that any combination of angles that satisfies conditions (3.36) will lead to the same value in zeroth-order in $\frac{1}{\delta}$ of the expectation value for the volume operator. Therefore, as was done for the 4-valent case, in order to compute the expectation value for the volume operator, we will not specify a particular sub-case of (3.36), but leave the result as general as possible.

Given conditions 3.36 the expectation value of the volume for the periodicity cell is

$$\begin{aligned}
V_R = & \delta^3 \sqrt{\frac{1}{8}} \left| \det \left(\frac{\delta X_S^a}{\delta(s, u^1, u^2)} \right) \right| 2 \left\{ 2\sqrt{2} \times \sqrt{|\det(E_j^a(u))|} \right. \\
& + \sqrt{\left| 8 + \frac{1}{2} \left(-\rho_{63,83}^2 - \rho_{63,23}^2 - \rho_{113,63}^2 - \rho_{113,83}^2 - \rho_{113,133}^2 - \rho_{113,23}^2 - \rho_{173,63}^2 - \rho_{173,83}^2 - \rho_{173,133}^2 - \rho_{173,23}^2 \right. \right. \\
& \quad \left. \left. - \rho_{133,83}^2 - \rho_{133,23}^2 \right) \right|} \times \sqrt{|\det(E_j^a(u))|} \\
& + \sqrt{\left| 8 + \frac{1}{2} \left(-\rho_{1413,2113}^2 - \rho_{913,1413}^2 - \rho_{313,2113}^2 - \rho_{313,913}^2 - \rho_{413,913}^2 - \rho_{413,2113}^2 - \rho_{413,313}^2 - \rho_{413,1413}^2 - \rho_{513,913}^2 \right. \right. \\
& \quad \left. \left. - \rho_{513,2113}^2 - \rho_{513,313}^2 - \rho_{513,1413}^2 \right) \right|} \times \sqrt{|\det(E_j^a(u))|} \\
& + \sqrt{\left| 8 + \frac{1}{2} \left(-\rho_{02,102}^2 - \rho_{02,112}^2 - \rho_{02,32}^2 - \rho_{02,92}^2 - \rho_{112,32}^2 - \rho_{122,102}^2 - \rho_{122,112}^2 - \rho_{122,32}^2 - \rho_{122,92}^2 - \rho_{92,102}^2 \right. \right. \\
& \quad \left. \left. - \rho_{112,102}^2 - \rho_{92,32}^2 \right) \right|} \times \sqrt{|\det(E_j^a(u))|} \\
& + \sqrt{\left| 8 + \frac{1}{2} \left(-\rho_{1212,412}^2 - \rho_{1212,f12}^2 - \rho_{912,1212}^2 - \rho_{912,412}^2 - \rho_{912,e12}^2 - \rho_{912,f12}^2 - \rho_{d12,1212}^2 - \rho_{d12,412}^2 - \rho_{d12,e12}^2 \right. \right. \\
& \quad \left. \left. - \rho_{d12,f12}^2 - \rho_{e12,412}^2 - \rho_{e12,f12}^2 \right) \right|} \times \sqrt{|\det(E_j^a(u))|} \\
& + \sqrt{\left| 8 + \frac{1}{2} \left(-2\rho_{c'15,315}^2 - \rho_{d'15,315}^2 - \rho_{d'15,c15}^2 - \rho_{d'15,e'15}^2 - \rho_{d'15,f'15}^2 - \rho_{e'15,c'15}^2 - \rho_{f'15,315}^2 - \rho_{f'15,e'15}^2 - \rho_{a'15,315}^2 - \rho_{a'15,c'15}^2 \right. \right. \\
& \quad \left. \left. - \rho_{a'15,e'15}^2 - \rho_{a'15,f'15}^2 \right) \right|} \times \sqrt{|\det(E_j^a(u))|} \\
& + \sqrt{\left| 8 + \frac{1}{2} \left(-\rho_{134,184}^2 - \rho_{134,c4}^2 - \rho_{164,134}^2 - \rho_{164,184}^2 - \rho_{164,b4}^2 - \rho_{b4,184}^2 - \rho_{b4,c4}^2 - \rho_{a4,134}^2 - \rho_{a4,184}^2 - \rho_{a4,b4}^2 - \rho_{a4,c4}^2 \right. \right. \\
& \quad \left. \left. - \rho_{c4,164}^2 \right) \right|} \times \sqrt{|\det(E_j^a(u))|} \\
& + \sqrt{\left| 8 + \frac{1}{2} \left(-\rho_{1314,a14}^2 - \rho_{1314,h14}^2 - \rho_{1314,l14}^2 - \rho_{h14,a14}^2 - \rho_{j14,a14}^2 - \rho_{j14,h14}^2 - \rho_{j14,l14}^2 - \rho_{k14,1314}^2 - \rho_{k14,h14}^2 - \rho_{k14,j14}^2 \right. \right. \\
& \quad \left. \left. - \rho_{k14,l14}^2 - \rho_{l14,a14}^2 \right) \right|} \times \sqrt{|\det(E_j^a(u))|} \\
& + \sqrt{\left| 8 + \frac{1}{2} \left(-\rho_{175,65}^2 - \rho_{175,135}^2 - \rho_{175,r5}^2 - \rho_{135,65}^2 - \rho_{p5,175}^2 - \rho_{p5,65}^2 - \rho_{p5,q5}^2 - \rho_{p5,r5}^2 - \rho_{q5,65}^2 - \rho_{q5,135}^2 \right. \right. \\
& \quad \left. \left. - \rho_{q5,r5}^2 - \rho_{r5,135}^2 \right) \right|} \times \sqrt{|\det(E_j^a(u))|} \left. \right\} \tag{3.38}
\end{aligned}$$

Expanding the square roots (see Section 2.2) and considering just first-order terms we obtain

$$\begin{aligned}
V_R &= \delta^3 \sqrt{|\det(E_j^a(u))|} 2 \left(9 + \frac{1}{2} \times \frac{1}{16} \left(-\rho_{63,83}^2 - \rho_{63,23}^2 - \rho_{113,63}^2 - \rho_{113,83}^2 - \rho_{113,133}^2 - \rho_{113,23}^2 - \rho_{173,63}^2 - \rho_{173,83}^2 - \right. \right. \\
&\quad - \rho_{173,133}^2 - \rho_{173,23}^2 - \rho_{133,83}^2 - \rho_{133,23}^2 - \rho_{1413,2113}^2 - \rho_{913,1413}^2 - \rho_{313,2113}^2 - \rho_{313,913}^2 - \rho_{413,913}^2 - \rho_{413,2113}^2 - \rho_{413,313}^2 \\
&\quad - \rho_{413,1413}^2 - \rho_{513,913}^2 - \rho_{513,2113}^2 - \rho_{513,313}^2 - \rho_{513,1413}^2 - \rho_{02,102}^2 - \rho_{02,112}^2 - \rho_{02,32}^2 - \rho_{02,92}^2 - \rho_{112,32}^2 - \rho_{122,102}^2 \\
&\quad - \rho_{122,112}^2 - \rho_{122,32}^2 - \rho_{122,92}^2 - \rho_{92,102}^2 - \rho_{112,102}^2 - \rho_{92,32}^2 - \rho_{1212,412}^2 - \rho_{1212,f12}^2 - \rho_{912,1212}^2 - \rho_{912,412}^2 - \rho_{912,e12}^2 \\
&\quad - \rho_{912,f12}^2 - \rho_{d12,1212}^2 - \rho_{d12,412}^2 - \rho_{d12,e12}^2 - \rho_{d12,f12}^2 - \rho_{e12,412}^2 - \rho_{e12,f12}^2 - 2\rho_{c'15,315}^2 - \rho_{d'15,315}^2 - \rho_{d'15,c15}^2 - \rho_{d'15,e'15}^2 \\
&\quad - \rho_{d'15,f'15}^2 - \rho_{e'15,c'15}^2 - \rho_{f'15,315}^2 - \rho_{f'15,e'15}^2 - \rho_{a'15,315}^2 - \rho_{a'15,c'15}^2 - \rho_{a'15,e'15}^2 - \rho_{a'15,f'15}^2 - \rho_{134,184}^2 - \rho_{134,c4}^2 - \rho_{164,134}^2 \\
&\quad - \rho_{164,184}^2 - \rho_{164,b4}^2 - \rho_{b4,184}^2 - \rho_{b4,c4}^2 - \rho_{a4,134}^2 - \rho_{a4,184}^2 - \rho_{a4,b4}^2 - \rho_{a4,c4}^2 - \rho_{c4,164}^2 - \rho_{1314,a14}^2 - \rho_{1314,h14}^2 - \rho_{1314,l14}^2 \\
&\quad - \rho_{h14,a14}^2 - \rho_{j14,a14}^2 - \rho_{j14,h14}^2 - \rho_{j14,l14}^2 - \rho_{k14,1314}^2 - \rho_{k14,h14}^2 - \rho_{k14,j14}^2 - \rho_{k14,l14}^2 - \rho_{l14,a14}^2 - \rho_{175,65}^2 - \rho_{175,135}^2 \\
&\quad \left. - \rho_{175,r5}^2 - \rho_{135,65}^2 - \rho_{p5,175}^2 - \rho_{p5,65}^2 - \rho_{p5,q5}^2 - \rho_{p5,r5}^2 - \rho_{q5,65}^2 - \rho_{q5,135}^2 - \rho_{q5,r5}^2 - \rho_{r5,135}^2 \right) \left| \det \left(\frac{\delta X_S^a}{\delta(s, u^1, u^2)} \right) \right| \\
&= 2\delta^3 \sqrt{|\det(E_j^a(u))|} \left(9 + \frac{1}{2} \left(-\frac{1}{16} \sum_{i,j=1;j \neq i}^{\frac{n}{2}(n-1)} \rho_{jk,i_k}^2 \right) \right) \left| \det \left(\frac{\delta X_S^a}{\delta(s, u^1, u^2)} \right) \right| \tag{3.39}
\end{aligned}$$

Here ρ_{l_i, k_i} represent the off-diagonal entries of the matrix \sqrt{A}^{-1} (see Section A.2.2) which denote the value of the term $\frac{\sqrt{t_{e_{i,l}, e_{i,k}}}}{t_{e_{i,l}} t_{e_{i,k}}}$ for the edges $e_{i,l}$ and $e_{i,k}$ incident at the vertex V_i .

The term proportional to ρ_{j_k, i_k}^2 represents the higher-order corrections to the expectation value of the volume operator. Each term ρ_{i_k, j_k} is proportional to $C \times \frac{l'}{\delta}$ for $l' < l$ where C is a constant that depends on the Euler angles we choose. It follows that only the zeroth-order of the expectation value of the volume operator for the 6-valent graph is rotationally invariant, up to embeddings with measure zero in $SO(3)$. However, only embeddings which have measure *zero* in $SO(3)$ (when the edges are aligned to the plaquettes) give the correct semiclassical limit.

3.3.3 Expectation value of the volume operator for a translated 6-valent graph

In this Section we will calculate the expectation value of the volume operator for a translated 6-valent graph. To make the comparison as accurate as possible, we translate the 6-valent graph by a vector with more or less the same properties as the vector with respect to which we translated the 4-valent graph, namely:

- 1) $\frac{\delta}{2} \geq \epsilon_x \geq \epsilon_y \geq \epsilon_z \geq 0$
- 2) $\frac{\delta\sqrt{2}}{2} < \epsilon_i + \epsilon_j$
- 3) $\frac{\delta\sqrt{2}}{2} - \frac{\delta 1}{2} < \epsilon_z$
- 4) $|V_k^i| - |V_k^j| > n_k^i l - n_k^j l$ for all $|V_k^i| > |V_k^j|$

The coordinates of the translated vertices are

$$V_0'' = (\epsilon_x, \epsilon_y, \epsilon_z) \quad (3.40)$$

$$V_2'' = \left(\frac{\delta\sqrt{2}}{2} + \epsilon_x, \epsilon_y, \frac{\delta\sqrt{2}}{2} + \epsilon_z \right) \quad (3.41)$$

$$V_3'' = \left(\epsilon_x + \frac{\delta\sqrt{2}}{2} - \frac{\delta}{2}, \epsilon_y - \frac{\delta}{2}, \delta\sqrt{2} + \epsilon_z \right) \quad (3.42)$$

$$V_4'' = \left(\delta\sqrt{2} + \epsilon_x, \epsilon_y - \delta, \delta\sqrt{2} + \epsilon_z \right) \quad (3.43)$$

$$V_5'' = (\epsilon_x, \epsilon_y - \delta, \epsilon_z) \quad (3.44)$$

$$V_{13}'' = \left(\frac{\delta\sqrt{2}}{2} + \epsilon_x, \epsilon_y - \delta, \frac{\delta\sqrt{2}}{2} + \epsilon_z \right) \quad (3.45)$$

$$V_{18}'' = \left(\delta\sqrt{2} + \frac{\delta}{2} + \epsilon_x, \epsilon_y - \frac{\delta}{2}, \epsilon_z + \frac{\delta\sqrt{2}}{2} \right) \quad (3.46)$$

$$V_{15}'' = \left(\frac{\delta\sqrt{2}}{2} - \frac{\delta 2}{2} + \epsilon_x, \epsilon_y - \delta, 3\frac{\delta\sqrt{2}}{2} + \epsilon_z \right) \quad (3.47)$$

$$V_{14}'' = \left(\frac{\delta\sqrt{2}}{2} + \frac{\delta}{2} + \epsilon_x, \epsilon_y - 3\frac{\delta}{2}, \epsilon_z \right) \quad (3.48)$$

Similarly as for the aligned case we have

$$\begin{aligned} Z_{e_i}^{\{x,y\}} &= \begin{cases} \frac{2}{\sqrt{2}} & \text{iff } \theta_{e_i} \neq 0 \\ 1 & \text{iff } \theta_{e_i} = 0 \end{cases} & T_{e_i}^{\{x,y\}} &= \begin{cases} \frac{\sqrt{2}}{2} & \text{iff } \theta_{e_i} \neq 0 \\ 1 & \text{iff } \theta_{e_i} = 0 \end{cases} \\ F_{e_i}^x &= \begin{cases} 1 & \text{iff } \theta_{e_i} \neq 0 \\ \infty & \text{iff } \theta_{e_i} = 0 \end{cases} & F_{e_i}^x &= 1 \quad \forall e_i \in \gamma \end{aligned} \quad (3.49)$$

The expression for the matrix \sqrt{A}^{-1} is given in Table A.2.3 in the Appendix.

Given the conditions above we obtain the following value for the expectation value of the volume operator as applied to the periodicity cell:

$$\begin{aligned}
V_R = & \sqrt{\frac{4}{8}}\delta^3 \left(\sqrt{\left| 8 - \frac{3(A'_0)^2}{2} - \frac{5B_0^2}{2} - \sqrt{2}B_0^2 - A'_0B_0B'_0 - \frac{A'_0B_0B'_0}{\sqrt{2}} - 2(B'_0)^2 - B_0C_0 - \frac{A'_0B'_0C_0}{4} - \frac{3C_0^2}{4} - \frac{A'_0C_0C'_0}{2\sqrt{2}} \right.} \right. \\
& \left. \frac{B'_0C_0C'_0}{4} - \frac{B'_0C_0C'_0}{4\sqrt{2}} - \frac{3(C'_0)^2}{2} - \frac{B_0(C'_0)^2}{4} - \frac{3B_0(C'_0)^2}{4\sqrt{2}} - \frac{C_0(C'_0)^2}{8\sqrt{2}} \right) \times \sqrt{|\det(E_j^a(u))|} \\
& + \sqrt{\left| 8 - \frac{3(A'_2)^2}{2} - \frac{7(B'_2)^2}{2} - A'_2B'_2B_2 - \frac{3A'_2B'_2B_2}{2\sqrt{2}} - 3B_2^2 - 2\sqrt{2}B_2^2 - \frac{3B'_2B_2C'_2}{4} - \frac{5B'_2B_2C'_2}{4\sqrt{2}} - (C'_2)^2 - \frac{(B'_2)^2C_2}{4} \right.} \\
& \left. \frac{(B'_2)^2C_2}{2\sqrt{2}} - \frac{A'_2C'_2C_2}{2\sqrt{2}} - C_2^2/2 \right) \times \sqrt{|\det(E_j^a(u))|} + \sqrt{\left| 8 - \frac{3(A'_3)^2}{2} - A_3^2 - \frac{5(B'_3)^2}{2} - \frac{A_3(B'_3)^2}{\sqrt{2}} - \frac{B'_3B_3}{2} - \frac{3A'_3B'_3B_3}{4} \right.} \\
& \left. \frac{A'_3B'_3B_3}{\sqrt{2}} - 3B_3^2 - 2\sqrt{2}B_3^2 - \frac{A'_3B_3^2}{4} - \frac{A'_3B_3^2}{2\sqrt{2}} - \frac{A'_3A_3C'_3}{2} - \frac{B'_3B_3C'_3}{2} - \frac{3B'_3B_3C'_3}{4\sqrt{2}} - \frac{3(C'_3)^2}{4} \right) \times \sqrt{|\det(E_j^a(u))|} \\
& + \sqrt{\left| 8 - \frac{3(A'_4)^2}{2} - \frac{A_4^2}{2} - 3(B'_4)^2 - \frac{A_4(B'_4)^2}{\sqrt{2}} - A'_4B'_4B_4 - \frac{3A'_4B'_4B_4}{2\sqrt{2}} - 3B_4^2 - 2\sqrt{2}B_4^2 - \frac{B'_4B_4C'_4}{2} - \frac{3B'_4B_4C'_4}{4\sqrt{2}} \right.} \\
& \left. \frac{3(C'_4)^2}{4} - \frac{A'_4C'_4C_4}{2\sqrt{2}} - \frac{C_4^2}{4} \right) \times \sqrt{|\det(E_j^a(u))|} + \sqrt{\left| 8 - 3(A'_5)^2 - \frac{(A'_5)^2A_5}{\sqrt{2}} - A_5^2 - \frac{(A'_5)^2B_5}{2} - \frac{(A'_5)^2B_5}{2\sqrt{2}} - \sqrt{2}A_5B_5 \right.} \\
& \left. \frac{3B_5^2}{2} - \frac{13(C'_5)^2}{8} - \frac{A'_5(C'_5)^2}{4\sqrt{2}} - \frac{A_5(C'_5)^2}{2\sqrt{2}} - \frac{B_5(C'_5)^2}{4} - \frac{B_5(C'_5)^2}{4\sqrt{2}} - \frac{(A'_5)^2C_5}{4\sqrt{2}} - B_5C_5 - \frac{3A'_5C'_5C_5}{4\sqrt{2}} - \frac{(C'_5)^2C_5}{8\sqrt{2}} - \frac{5C_5^2}{8} \right|} \\
& \times \sqrt{|\det(E_j^a(u))|} + \sqrt{\left| 8 - \frac{3(A'_{13})^2}{2} - \frac{11(B'_{13})^2}{4} - A'_{13}B'_{13}B_{13} - \frac{A'_{13}B'_{13}B_{13}}{\sqrt{2}} - 3B_{13}^2 - 2\sqrt{2}B_{13}^2 - \frac{B'_{13}B_{13}C'_{13}}{2} \right.} \\
& \left. \frac{3B'_{13}B_{13}C'_{13}}{4\sqrt{2}} - \frac{3(C'_{13})^2}{4} - \frac{(B'_{13})^2C_{13}}{2} - \frac{A'_{13}C'_{13}C_{13}}{2\sqrt{2}} - \frac{C_{13}^2}{2} \right) \times \sqrt{|\det(E_j^a(u))|} + \sqrt{\left| 8 - \frac{5(A'_{18})^2}{4} - \frac{A_{18}^2}{4} - 3(B'_{18})^2 \right.} \\
& \left. - A'_{18}B'_{18}B_{18} - \frac{3A'_{18}B'_{18}B_{18}}{2\sqrt{2}} - 3B_{18}^2 - 2\sqrt{2}B_{18}^2 - \frac{B'_{18}B_{18}C'_{18}}{2} - \frac{3B'_{18}B_{18}C'_{18}}{4\sqrt{2}} - \frac{3(C'_{18})^2}{4} - \frac{(B'_{18})^2C_{18}}{2} - \frac{A'_{18}C'_{18}C_{18}}{4\sqrt{2}} \right.} \\
& \left. \frac{A_{18}C'_{18}C_{18}}{4\sqrt{2}} - \frac{C_{18}^2}{2} \right) \times \sqrt{|\det(E_j^a(u))|} + \sqrt{\left| 8 - 3(A'_{15})^2 - \frac{(A'_{15})^2A_{15}}{\sqrt{2}} - 2A_{15}^2 - \frac{A'_{15}A_{15}B'_{15}}{2\sqrt{2}} - \frac{B'_{15}^2}{2} - \frac{3(A'_{15})^2B_{15}}{4} \right.} \\
& \left. \frac{(A'_{15})^2B_{15}}{2\sqrt{2}} - \sqrt{2}A_{15}B_{15} - 2B_{15}^2 - \sqrt{2}B_{15}^2 - \frac{A'_{15}A_{15}C_{15}}{\sqrt{2}} - \frac{B'_{15}B_{15}C_{15}}{4} - \frac{B'_{15}B_{15}C_{15}}{2\sqrt{2}} - C_{15}^2 - \frac{A_{15}C_{15}^2}{4\sqrt{2}} - \frac{B_{15}C_{15}^2}{8} \right|} \\
& \times \sqrt{|\det(E_j^a(u))|} + \sqrt{\left| 8 - \frac{3(A'_{14})^2}{2} - 2(B'_{14})^2 - A'_{14}B'_{14}B_{14} - \frac{A'_{14}B'_{14}B_{14}}{\sqrt{2}} - \frac{5B_{14}^2}{2} - \sqrt{2}B_{14}^2 - \frac{3(C'_{14})^2}{2} \right.} \\
& \left. \frac{B_{14}(C'_{14})^2}{4} - \frac{3B_{14}(C'_{14})^2}{4\sqrt{2}} - \frac{A'_{14}B'_{14}C_{14}}{4} - B_{14}C_{14} - \frac{A'_{14}C'_{14}C_{14}}{2\sqrt{2}} - \frac{B'_{14}C'_{14}C_{14}}{4} - \frac{B'_{14}C'_{14}C_{14}}{4\sqrt{2}} - \frac{(C'_{14})^2C_{14}}{8\sqrt{2}} - \frac{3C_{14}^2}{4} \right|} \\
& \times \sqrt{|\det(E_j^a(u))|} \left| \det\left(\frac{\delta X_S^a}{\delta(s, u^1, u^2)}\right) \right| \tag{3.50}
\end{aligned}$$

Expanding the square root and considering only first-order contributions (see Section 2.2) we obtain

$$\begin{aligned}
V_R = & \delta^3 \sqrt{|\det(E_j^a(u))|} \left| \det\left(\frac{\delta X_S^a}{\delta(s, u^1, u^2)}\right) \right| 2 \left(9 + \frac{1}{16} \left(-\frac{3(A'_0)^2}{2} - \frac{5B_0^2}{2} - \sqrt{2}B_0^2 - 2(B'_0)^2 - B_0C_0 - \frac{3C_0^2}{4} \right. \right. \\
& - \frac{3(C'_0)^2}{2} - \frac{3(A'_2)^2}{2} - \frac{7(B'_2)^2}{2} - 3B_2^2 - 2\sqrt{2}B_2^2 - (C'_2)^2 - \frac{C_2^2}{2} - \frac{3(A'_3)^2}{2} - A_3^2 - \frac{5(B'_3)^2}{2} - \frac{B'_3B_3}{2} \\
& - 3B_3^2 - 2\sqrt{2}B_3^2 - \frac{3(C'_3)^2}{4} - \frac{3(A'_4)^2}{2} - \frac{A_4^2}{2} - 3(B'_4)^2 - 3B_4^2 - 2\sqrt{2}B_4^2 - \frac{3(C'_4)^2}{4} - \frac{C_4^2}{4} - 3(A'_5)^2 \\
& - A_5^2 - \sqrt{2}A_5B_5 - \frac{3B_5^2}{2} - \frac{13(C'_5)^2}{8} - B_5C_5 - \frac{5C_5^2}{8} - \frac{3(A'_{13})^2}{2} - \frac{11(B'_{13})^2}{4} - 3B_{13}^2 - 2\sqrt{2}B_{13}^2 - \frac{3(C'_{13})^2}{4} \\
& - \frac{C_{13}^2}{2} - \frac{5(A'_{18})^2}{4} - \frac{A_{18}^2}{4} - 3(B'_{18})^2 - 3B_{18}^2 - 2\sqrt{2}B_{18}^2 - \frac{3(C'_{18})^2}{4} - \frac{C_{18}^2}{2} - 3(A'_{15})^2 - 2A_{15}^2 - \frac{B'_{15})^2}{2} \\
& - \sqrt{2}A_{15}B_{15} - 2B_{15}^2 - \sqrt{2}B_{15}^2 - C_{15}^2 - \frac{B_{15}C_{15}^2}{8} - \frac{3(A'_{14})^2}{2} - 2(B'_{14})^2 - \frac{5B_{14}^2}{2} - \sqrt{2}B_{14}^2 - \frac{3(C'_{14})^2}{2} \\
& \left. \left. - B_{14}C_{14} - \frac{3C_{14}^2}{4} \right) \right) \tag{3.51}
\end{aligned}$$

where the terms

$$\begin{aligned}
A'_i &= \frac{|x_{V_i}| - n_i}{\delta(\sqrt{\sqrt{2} + 1})} & A_i &= \frac{(|x_{V_i}| - n_i)l}{\delta_e(1 + \frac{\sqrt{2}}{2})} \\
B'_i &= \frac{(|y_{V_i}| - m_i)l}{\delta(\sqrt{\sqrt{2} + 1})} & B_i &= \frac{(|y_{V_i}| - m_i)l}{\delta_e(1 + \frac{\sqrt{2}}{2})} \\
C'_i &= \frac{(|z_{V_i}| - p_i)l}{\delta(\sqrt{\sqrt{2} + 1})} & C_i &= \frac{(|z_{V_i}| - p_i)l}{\delta_e(1 + \frac{\sqrt{2}}{2})} \tag{3.52}
\end{aligned}$$

are the off-diagonal matrix elements of \sqrt{A}^{-1} (see Section A.2.3). The quantities x_{V_i} , y_{V_i} , z_{V_i} represent are the x , y , z -coordinates of the vertex V_i respectively.

In the last line of the equation above we have performed a Taylor expansion and factored out the term $\sqrt{|\det(E_j^a(u))|}$, since we can assume that, although it is vertex dependent, the values of this term to first-order will be the same for each vertex. Due to the appearance of the terms (3.52), which are proportional to the Euler angles, equation (3.50) is translational invariant (up to embeddings of measure zero in $SO(3)$), only at zeroth-order.

3.4 Analysis of the expectation value of the volume operator for 8-valent graphs

In this Section we will calculate the expectation value of the volume operator for an 8-valent graph. As in the case of 4- and 6-valent graphs, we first consider the non-rotated graph. We then analyse the rotational and translational dependence of the expectation value by performing a rotation and then a translation of the graph; we then repeat the calculation. It transpires that, even for the 8-valent graph, the off-diagonal elements of the matrix have non-trivial contributions that cause the expectation value of the volume operator to be translationally and rotationally dependent, for higher orders than the zeroth-one.

3.4.1 Expectation value of the volume operator for a general 8-valent graph

As in the previous cases, we take the $(0,0,0)$ point of the lattice to coincide with the $(0,0,0)$ point of the plaquette, and each vertex to be symmetric with respect to the axis. The coordinates of the vertices

comprising the periodicity cell are the following:

$$V_1 = \left(\frac{-\delta}{\sqrt{3}}, \frac{-\delta}{\sqrt{3}}, \frac{\delta}{\sqrt{3}} \right) \quad (3.53)$$

$$V_9 = \left(0, \frac{-2\delta}{\sqrt{3}}, 0 \right) \quad (3.54)$$

$$V_{12} = \left(0, \frac{-2\delta}{\sqrt{3}}, \frac{2\delta}{\sqrt{3}} \right) \quad (3.55)$$

$$V_4 = \left(\frac{-\delta}{\sqrt{3}}, \frac{-\delta}{\sqrt{3}}, \frac{3\delta}{\sqrt{3}} \right) \quad (3.56)$$

For the 8-valent lattice we choose V_1 as our reference vertex. The allowed value for its x -coordinate is $nl < |x_{V_2}| < nl + \frac{l}{4}$, where $n = \lfloor \frac{\delta}{\sqrt{3}l} \rfloor$. Similarly to the cases of 4- and 6-valent graphs, the allowed positions of the remaining vertices in the periodicity cell can be computed from the allowed positions of V_1 . Because of the geometry of the 8-valent graph we obtain

$$T_{e_i}^{\{x,y\}} = F_{e_i}^{\{x,y\}} = Z_{e_i}^{\{x,y\}} = 1 \quad \forall e_i \in \gamma \quad (3.57)$$

This results in the following values for the terms $\frac{t_{e_i e_j}}{\sqrt{t_{e_i} t_{e_j}}}$ as computed for the above five vertices.

V_0	all $\frac{t_{e_i e_j}}{\sqrt{t_{e_i} t_{e_j}}} = 0$
V_1	14 terms equal to β ; 12 terms equal to 2β
V_9	8 terms equal to 2β
V_{12}	8 terms equal to 4β ; 4 terms equal to 2β
V_e	1 term equal to 6β ; 9 terms equal to 2β ; 12 terms equal to β ; 2 terms equal to 4β

Here $\beta := \left(\frac{\delta}{\sqrt{3}} - nl \right) \frac{1}{\sqrt{3}\delta}$ and it is proportional to the off-diagonal entries of the matrix \sqrt{A}^{-1} whose values are given in Section A.3.1 in the Appendix.

The expectation value of the volume operator is:

$$\begin{aligned}
V_R = & \sqrt{\frac{1}{8}} \delta^3 \left| \det \left(\frac{\delta X_S^a}{\delta(s, u^1, u^2)} \right) \right| 2 \left(\sqrt{32} \sqrt{|\det(E_j^a(u))|} + \sqrt{|\det(E_j^a(u))|} \times \sqrt{|32 - 60\beta^2 - 28\beta^3|} \right. \\
& + \sqrt{|\det(E_j^a(u))|} \times \sqrt{|32 - 16\beta^2|} + \sqrt{|\det(E_j^a(u))|} \times \sqrt{|32 - 144b^2 - 64\beta^3|} \\
& \left. + \sqrt{|\det(E_j^a(u))|} \sqrt{|32 - 104\beta^2 - 32\beta^3|} \right) \quad (3.58)
\end{aligned}$$

By approximating to first-order (see Section 2.2) we obtain

$$V_R = 4\delta^3 \sqrt{|\det(E_j^a(u))|} \left| \det \left(\frac{\delta X_S^a}{\delta(s, u^1, u^2)} \right) \right| \left(5 + \frac{1}{2} \times \frac{1}{32} (324\beta^2) \right) \quad (3.59)$$

In this case, the deviation from the classical value of the volume of a region, R , is of the order four, even to zeroth-order in l/δ .

3.4.2 Expectation value of the volume operator for a rotated 8-valent graph

We will now analyse the expectation value of the volume operator for a rotated 8-valent graph. In order to make the comparison with the 4- and 6-valent graphs as accurate as possible, we will rotate the 8-valent graph by the same amount the other valence graphs were rotated. It follows that the angles of the edges incident at V_0 will satisfy the following conditions:

- 1) $0 < \theta_{0,2}, \theta_{e_{0,8}} < \frac{\pi}{2}, \frac{3\pi}{2} < \theta_{0,3}, \theta_{0,7} < 2\pi, \frac{\pi}{2} < \theta_{0,1}, \theta_{0,6} < \pi$ and $\pi < \theta_{0,4}, \theta_{0,5} < \frac{5\pi}{4}$.
- 2) $\frac{3\pi}{2} < \phi_{e_{0,2}}, \phi_{e_{0,3}} < 2\pi - \sin^{-1}\frac{1}{3}, \pi + \sin^{-1}(\frac{1}{3}) < \phi_{e_{0,7}}, \phi_{e_{0,8}} < \frac{3\pi}{2}, \frac{3\pi}{2} < \phi_{e_{0,6}}, \phi_{e_{0,5}} < \pi - \sin^{-1}(\frac{1}{3})$ and $\sin^{-1}(\frac{1}{3}) < \phi_{e_{0,4}}, \phi_{e_{0,1}} < \frac{\pi}{2}$

The angles for the co-linear edges are defined through the formula $\theta_e = 180^\circ - \theta_{e_{\text{collinear}}}$ and $\phi_e = 180^\circ - \phi_{e_{\text{collinear}}}$ respectively. It follows that the edges $e_{0,1}, e_{0,2}, e_{0,3}, e_{0,4}, e_{0,5}, e_{0,6}, e_{0,7}$ and $e_{0,8}$ lie in the octants B, A, D, C, G, F, H and E respectively. The coordinates of the rotated vertices are

$$V'_1 = \left((-R_{11} - R_{12} + R_{13})\frac{\delta}{\sqrt{3}}, (-R_{21} - R_{22} + R_{23})\frac{\delta}{\sqrt{3}}, (-R_{31} - R_{32} + R_{33})\frac{\delta}{\sqrt{3}} \right) \quad (3.60)$$

$$V'_9 = \left(-2R_{12}\frac{\delta}{\sqrt{3}}, -2R_{22}\frac{\delta}{\sqrt{3}}, -2R_{32}\frac{\delta}{\sqrt{3}} \right) \quad (3.61)$$

$$V'_{12} = \left((-R_{12} + 2R_{13})\frac{\delta}{\sqrt{3}}, (-R_{22} + 2R_{23})\frac{\delta}{\sqrt{3}}, (-2R_{32} + 2R_{33})\frac{\delta}{\sqrt{3}} \right) \quad (3.62)$$

$$V'_e = \left((-R_{11} - R_{12} + 3R_{13})\frac{\delta}{\sqrt{3}}, (-R_{21} - R_{22} + 3R_{23})\frac{\delta}{\sqrt{3}}, (-R_{31} - R_{32} + 3R_{33})\frac{\delta}{\sqrt{3}} \right) \quad (3.63)$$

As was done for the 4- and 6-valent graphs, in order to carry out the calculations for the expectation value of the volume operator we would have to specify a particular combinations of angles satisfying conditions 1) and 2) above. However, all combinations satisfying 1) and 2) above lead to the same value, in zeroth-order in $\frac{l}{\delta}$, of the expectation value of the volume operator. Rotational dependence will only appear for higher orders in $\frac{l}{\delta}$. Moreover any sub-case of 1) and 2) will lead to the same couples of edges commonly intersecting surfaces $s^I_{\alpha,t}$ in a given stack. Therefore, to leave the result as general as possible, we will not specify a particular sub-case of 1) and 2) but simply derive a general expression for the expectation value of the volume operator given conditions 1) and 2).

The expectation value of the volume operator for a periodicity region, R , is then computed as

$$\delta^3 \sqrt{|\det(E_j^a(u))|} 4 \left(5 + \frac{1}{2} \left(-\frac{1}{32} \sum_{i,j=1;j \neq i}^{\frac{n}{2}(n-1)} \alpha_{ji}^2 \right) \left| \det \left(\frac{\delta X_S^a}{\delta(s, u^1, u^2)} \right) \right| \right) \quad (3.64)$$

where the terms α_{ij} are the off-diagonal entries of the matrix \sqrt{A}^{-1} (See Section A.3.2 in the Appendix) Evidently, the higher-order corrections are angle dependent, while the zeroth-ones are not. Therefore, as for the 4- and 6-valent case, the expectation value of the volume operator for the 8-valent graph is rotational invariant, in zeroth-order up to measure *zero* in $SO(3)$. However, it does *not* reproduce the correct semiclassical limit.

3.4.3 Expectation value of the volume operator for a translated 8-valent graph

We now consider the translated 8-valent graph. As for the 4- and 6-valent graphs we choose the following conditions on the components of the translation vector:

- 1) $b > \epsilon_x > \epsilon_y > \epsilon_z > 0$
- 2) $|V_k^i| - |V_k^j| > n_k^i l - n_k^j l$ for all $|V_k^i| > |V_k^j|$

Similarly as for the aligned 8-valent graph we have

$$T_{e_i}^{\{x,y\}} = F_{e_i}^{\{x,y\}} = Z_{e_i}^{\{x,y\}} = 1 \quad \forall e_i \in \gamma \quad (3.65)$$

The coordinates of the translated vertices are

$$V'_0 = (\epsilon_x, \epsilon_y, \epsilon_z) \quad (3.66)$$

$$V'_1 = \left(-\frac{\delta}{\sqrt{3}} + \epsilon_x, -\frac{\delta}{\sqrt{3}} + \epsilon_y, \frac{\delta}{\sqrt{3}} + \epsilon_z \right) \quad (3.67)$$

$$V'_9 = \left(\epsilon_x, -2\frac{\delta}{\sqrt{3}} + \epsilon_y, \frac{\delta}{\sqrt{3}} + \epsilon_z \right) \quad (3.68)$$

$$V'_{12} = \left(\epsilon_x, -\frac{\delta}{\sqrt{3}} + \epsilon_y, 2\frac{\delta}{\sqrt{3}} + \epsilon_z \right) \quad (3.69)$$

$$V'_e = \left(-\frac{\delta}{\sqrt{3}} + \epsilon_x, -\frac{\delta}{\sqrt{3}} + \epsilon_y, 3\frac{\delta}{\sqrt{3}} + \epsilon_z \right) \quad (3.70)$$

The expression for the matrix \sqrt{A}^{-1} is given in Section A.3.3 in the Appendix.

The value obtained for the volume of a region R is:

$$\begin{aligned} V_R = & \sqrt{\frac{1}{8}} \delta^3 \left| \det \left(\frac{\delta X_S^a}{\delta(s, u^1, u^2)} \right) \right| \times \\ & \left\{ \sqrt{\left| 4 \left(32 - 4A_0^2 - 12B_0^2 - 2A_0B_0^2 - \frac{45C_0^2}{2} - 2A_0C_0^2 - 6B_0C_0^2 - \frac{5C_0^2D_0}{2} - 3D_0^2 - \frac{B_0D_0^2}{2} - C_0^2E \right. \right. \right. \\ & \left. \left. \left. - \frac{B_0D_0E_0}{2} - E_0^2 - B_0^2F_0 - C_0^2F_0 - F_0^2 \right) \right| \times \sqrt{\left| \det \left(E_j^a(u) \right) \right|} \right. \\ & + \sqrt{\left| 4 \left(32 - 16A_1^2 - 2A_1^3 - 24B_1^2 - 8A_1B_1^2 - B_1^2D_1 - D_1^2 - A_1^2E_1 - B_1^2E_1 - E_1^2 - 3B_1^2F_1 - \right. \right. \\ & \left. \left. \left. - \frac{A_1D_1F_1}{2} - 3F_1^2 - \frac{A_1F_1^2}{2} \right) \right| \times \sqrt{\left| \det \left(E_j^a(u) \right) \right|} \right. \\ & + \sqrt{\left| 4 \left(32 - 24B_9^2 - 4B_9^2C_9 - 8C_9^2 - 6B_9^2D_9 - \frac{9D_9^2}{2} - \frac{C_9D_9^2}{2} - C_9^2E_9 - \frac{3E_9^2}{2} - \frac{C_9E_9^2}{2} - B_9^2F_9 - \right. \right. \\ & \left. \left. \left. - \frac{C_9D_9F_9}{2} - F_9^2 \right) \right| \times \sqrt{\left| \det \left(E_j^a(u) \right) \right|} \right. \\ & + \sqrt{\left| 4 \left(32 - 24A_{12}^2 - 6A_{12}^2B_{12} - 12B_{12}^2 - 2A_{12}^2C_{12} - 2B_{12}^2C_{12} - 4C_{12}^2 - A_{12}^2D_{12} - B_{12}^2D_{12} - D_{12}^2 - A_{12}^2E_{12} - E_{12}^2 \right. \right. \\ & \left. \left. \left. - 3A_{12}^2F_{12} - \frac{B_{12}E_{12}F_{12}}{2} - 3F_{12}^2 - \frac{B_{12}F_{12}^2}{2} \right) \right| \times \sqrt{\left| \det \left(E_j^a(u) \right) \right|} \right. \\ & \left. + \sqrt{\left| 4 \left(32 - \frac{29A_e^2}{2} - \frac{43B_e^2}{2} - 6A_eB_e^2 - 2A_e^2C_e - 2C_e^2 - B_e^2D_e - D_e^2 - 2A_e^2E_e - B_e^2E_e - \frac{3E_e^2}{2} - 3B_e^2F_e - \right. \right. \right. \\ & \left. \left. \left. \frac{A_eD_eF_e}{2} - 3F_e^2 - \frac{A_eF_e^2}{2} \right) \right| \times \sqrt{\left| \det \left(E_j^a(u) \right) \right|} \right\} \quad (3.71) \end{aligned}$$

Considering only contributions of first-order in $\frac{1}{\delta}$ (see Section 2.2) we obtain

$$\begin{aligned}
V_R &= 4\delta^3 \sqrt{|\det(E_j^a(u))|} \left| \det\left(\frac{\delta X_S^a}{\delta(s, u^1, u^2)}\right) \right| \times \left\{ \sqrt{1 + \frac{1}{32} \left(-4A_0^2 - 12B_0^2 - \frac{45C_0^2}{2} - 3D_0^2 - E_0^2 - F_0^2 \right)} \right. \\
&+ \sqrt{1 + \frac{1}{32} \left(-16A_1^2 - 24B_1^2 - D_1^2 - E_1^2 - 3F_1^2 \right)} + \sqrt{1 + \frac{1}{32} \left(-24B_9^2 - 8C_9^2 - \frac{9D_9^2}{2} - \frac{3E_9^2}{2} - F_9^2 \right)} \\
&+ \left. \sqrt{1 + \frac{1}{32} \left(-24A_{12}^2 - 12B_{12}^2 - 4C_{12}^2 - D_{12}^2 - E_{12}^2 - 3F_{12}^2 \right)} + \sqrt{1 + \frac{1}{32} \left(-\frac{29A_e^2}{2} - \frac{43B_e^2}{2} - 2C_e^2 - D_e^2 - \frac{3E_e^2}{2} - 3F_e^2 \right)} \right\} \\
&= 4\delta^3 \sqrt{|\det(E_j^a(u))|} \left| \det\left(\frac{\delta X_S^a}{\delta(s, u^1, u^2)}\right) \right| \times \left\{ 5 + \frac{1}{2} \times \frac{1}{32} \left(-4A_0^2 - 12B_0^2 - \frac{45C_0^2}{2} - 3D_0^2 - E_0^2 - F_0^2 \right) \right. \\
&- 16A_1^2 - 24B_1^2 - D_1^2 - E_1^2 - 3F_1^2 - 24B_9^2 - 8C_9^2 - \frac{9D_9^2}{2} - \frac{3E_9^2}{2} - F_9^2 \\
&- \left. 24A_{12}^2 - 12B_{12}^2 - 4C_{12}^2 - D_{12}^2 - E_{12}^2 - 3F_{12}^2 - \frac{29A_e^2}{2} - \frac{43B_e^2}{2} - 2C_e^2 - D_e^2 - \frac{3E_e^2}{2} - 3F_e^2 \right\} \quad (3.72)
\end{aligned}$$

where A_i, B_i, C_i, D_i, E_i and F_i are the matrix elements of \sqrt{A}^{-1} as defined in Section A.3.3 of the Appendix. Again, translational invariance holds only at zeroth-order up to measure zero in $SO(3)$. However, it does *not* reproduce the correct semiclassical limit.

4 Summary and Conclusions

We have shown that if we use semiclassical states derived from the area complexifier, then we do *not* obtain the correct semiclassical value of the volume, operator unless we perform an artificial re-scaling of the coherent state label and we restrict our calculation to the following special cases:

- 1) The edges of the graph are aligned with the orientation of the plaquettes (6-valent graph).
- 2) Two or more edges lie in a given plaquette (4-valent graph).
- 3) One edge is aligned with a given plaquette while a second edge lies in a given plaque (4-valent graph).

However, such combination of edges have measure zero in $SO(3)$. For embeddings whose measure in $SO(3)$ is non-trivial we do not obtain the correct semiclassical behavior for the volume operator for any valence of the graph.

This result suggests strongly that the area complexifier coherent states are not the correct states with which to analyse semiclassical properties in LQG. Moreover, as previously mentioned, if embedding independence (staircase problem) is to be eliminated, area complexifier coherent states should be ruled out as semiclassical states altogether.

Acknowledgments

I would like to thank very much Thomas Thiemann for illuminating discussions and useful comments on the manuscript. I am also grateful to the Perimeter Institute for Theoretical Physics for hospitality and financial support where parts of the present work were carried out. Research performed at Perimeter Institute for Theoretical Physics is supported in part by the Government of Canada through NSERC and by the Province of Ontario through MRI.

A Edge metric calculations

A.1 Edge metric components for the 4-valent graph

In this Section we list the values for each of the terms $\frac{t_{e_i e_j}}{\sqrt{t_{e_i} t_{e_j}}}$ which comprise the matrix \sqrt{A}^{-1} that appears in the computation of the expectation value of the volume operator. The method for computing such terms was described in Section 3.1 with the aid of a two-dimensional example. It is worth recalling that the term $t_{e_i e_j} = t_{e_i e_j}^x + t_{e_i e_j}^y + t_{e_i e_j}^z$ represents the total number of plaquettes in each direction that are intersected by both the edges e_i and e_j . On the other hand, the terms $t_{e_i} = t_{e_i}^x + t_{e_i}^y + t_{e_i}^z$ and $t_{e_j} = t_{e_j}^x + t_{e_j}^y + t_{e_j}^z$ represent are the total number of plaquettes in each direction intersected by the edges e_i and e_j respectively.

A.1.1 Rotated 4-valent graph

In this Section we will list the values of all the terms, $\frac{t_{e_i e_j}}{\sqrt{t_{e_i} t_{e_j}}}$, that appear in the matrix \sqrt{A}^{-1} for the rotated 4-valent graph. This is a 15×15 matrix labelled by the edges belonging to *four* vertices, as for the aligned case. At this point, we recall the meaning of the following symbols

$$\begin{aligned} Z_{e_i}^x &= \left| \frac{1}{\cos \theta_{e_i}} \cot \phi_{e_i} \right| & Z_{e_i}^y &= \left| \frac{1}{\sin \theta_{e_i}} \cot \phi_{e_i} \right| \\ F_{e_i}^x &= |\cot \theta_{e_i}| & F_{e_i}^y &= |\tan \theta_{e_i}| \\ T_{e_i}^x &= |\tan \phi_{e_i} \cos \theta_{e_i}| & T_{e_i}^y &= |\tan \phi_{e_i} \sin \theta_{e_i}| \\ t_{e_i} &= t_{e_i}^x + t_{e_i}^y + t_{e_i}^z = \delta \sin \phi_{e_i} \cos \theta_{e_i} + \delta \sin \phi_{e_i} \sin \theta_{e_i} + \delta \cos \phi_{e_i} = \alpha_{e_i} \delta \end{aligned} \quad (\text{A.1})$$

which represent the angular dependence of the terms $x t^z$, $y t^z$, $y t^x$, $x t^y$, $z t^x$ and $z t^y$ respectively (see Section 3.1).

The arrangement of angles for which we choose to perform our calculations will be such that the edges incident at vertex V_0 — $e_{0,1}$, $e_{0,2}$, $e_{0,3}$ and $e_{0,4}$ —lie in the octants F , A , H and C respectively. However, as mentioned in previous Sections, in order to compute the specific value for the terms t_{e_i, e_j} , we would need to choose a particular value for each of the edge's angles. Nonetheless, we will refrain from doing so here, since we would like to leave our result as general as possible. What we will do, instead, is to write the terms t_{e_i, e_j} as functions depending on the angles of the edges and on the position of the vertex at which they are commonly incident. Specifically, we recall from Section 3.1 that the number of plaquettes a given edge e_i intersects in direction z is given by

$$t_{e_i}^z := {}^x t_{e_i}^z \cap {}^y t_{e_i}^z := \Gamma_{e_i}^z \quad (\text{A.2})$$

where

$$x t_{e_i}^z = \begin{cases} (x_{V_j} - n_{x_{V_j}} l) Z_{e_i}^x & \text{iff the edge points in the negative } x\text{-direction} \\ (n_{x_{V_j}} l + l - x_{V_j}) Z_{e_i}^x & \text{iff the edge points in the positive } x\text{-direction} \end{cases}$$

and

$$y t_{e_i}^z = \begin{cases} (x_{V_j} - n_{x_{V_j}} l) Z_{e_i}^y & \text{iff the edge points in the negative } z\text{-direction} \\ (n_{x_{V_j}} l + l - x_{V_j}) Z_{e_i}^y & \text{iff the edge points in the positive } z\text{-direction} \end{cases}$$

Similarly, for intersections in the x - and y -direction we have the following:

$$t_{e_i}^x := {}^z t_{e_i}^x \cap {}^y t_{e_i}^x := \Gamma_{e_i}^x \quad (\text{A.3})$$

where

$$y t_{e_i}^x = \begin{cases} (y_{V_j} - n_{y_{V_j}} l) F_{e_i}^x & \text{iff the edge points in the negative } y\text{-direction} \\ (n_{y_{V_j}} l + l - y_{V_j}) F_{e_i}^x & \text{iff the edge points in the positive } y\text{-direction} \end{cases}$$

$$z t_{e_i}^x = \begin{cases} (z_{V_j} - n_{z_{V_j}} l) T_{e_i}^x & \text{iff the edge points in the negative } z\text{-direction} \\ (n_{z_{V_j}} l + l - z_{V_j}) T_{e_i}^x & \text{iff the edge points in the positive } z\text{-direction} \end{cases}$$

and

$$t_{e_i}^y := {}^z t_{e_i}^y \cap^x t_{e_i}^y := \Gamma_{e_i}^y \quad (\text{A.4})$$

where

$$x t_{e_i}^y = \begin{cases} (x_{V_j} - n_{x_{V_j}} l) F_{e_i}^y & \text{iff the edge points in the negative } y\text{-direction} \\ (n_{x_{V_j}} l + l - x_{V_j}) F_{e_i}^y & \text{iff the edge points in the positive } y\text{-direction} \end{cases}$$

$$z t_{e_i}^y = \begin{cases} (z_{V_j} - n_{z_{V_j}} l) T_{e_i}^y & \text{iff the edge points in the negative } z\text{-direction} \\ (n_{z_{V_j}} l + l - z_{V_j}) T_{e_i}^y & \text{iff the edge points in the positive } z\text{-direction} \end{cases}$$

From the above formulae it is straightforward to deduce that the precise value for the terms ${}^i t_{e_j}^k$ will differ according to which angles we choose for each edge. However, which couple of edges commonly intersect surfaces in a given direction only depends on the octant in which the edges lie. Since we do not want to restrict our calculations to any specific angle, we will simply define the terms t_{e_i, e_j} as follows

$$t_{e_i, e_j} := \Gamma_{e_i}^z \cap \Gamma_{e_j}^z + \Gamma_{e_i}^x \cap \Gamma_{e_j}^x + \Gamma_{e_i}^y \cap \Gamma_{e_j}^y := \Xi_{e_i} \cap \Xi_{e_j} \quad (\text{A.5})$$

and

$$\alpha_{e_i, e_j} := \frac{t_{e_i, e_j}}{\sqrt{t_{e_i} t_{e_j}}} := \frac{\Xi_{e_i} \cap \Xi_{e_j}}{\sqrt{t_{e_i} t_{e_j}}} \quad (\text{A.6})$$

To simplify the notation, we denote the edge, e_i , going from vertex V_k to vertex V_j as $e_{k,j}$. We can then write the terms above in the following simplified way: $\alpha_{e_{k,i}, e_{k,j}} = \alpha_{k_i, l_i}$.

Given the above, the non-zero entries of the upper-half entries of \sqrt{A}^{-1} for the rotated 4-valent graph are listed below.

$$\begin{array}{lll} (\sqrt{A})_{5,2}^{-1} = -\frac{1}{2}\alpha_{7_2,0_2} & (\sqrt{A})_{6,2}^{-1} = -\frac{1}{2}\alpha_{6_2,0_2} & (\sqrt{A})_{7,2}^{-1} = -\frac{1}{2}\alpha_{5_2,0_2} \\ (\sqrt{A})_{6,5}^{-1} = -\frac{1}{2}\alpha_{6_2,7_2} & (\sqrt{A})_{7,5}^{-1} = -\frac{1}{2}\alpha_{5_2,7_2} & (\sqrt{A})_{7,6}^{-1} = -\frac{1}{2}\alpha_{5_2,6_2} \\ (\sqrt{A})_{9,8}^{-1} = -\frac{1}{2}\alpha_{5_8,12_8} & (\sqrt{A})_{10,8}^{-1} = -\frac{1}{2}\alpha_{11_8,12_8} & (\sqrt{A})_{11,8}^{-1} = -\frac{1}{2}\alpha_{10_8,12_8} \\ (\sqrt{A})_{10,9}^{-1} = -\frac{1}{2}\alpha_{11_8,5_8} & (\sqrt{A})_{11,9}^{-1} = -\frac{1}{2}\alpha_{10_8,5_8} & (\sqrt{A})_{11,10}^{-1} = -\frac{1}{2}\alpha_{10_8,11_8} \\ (\sqrt{A})_{13,12}^{-1} = -\frac{1}{2}\alpha_{15_{13},3_{13}} & (\sqrt{A})_{14,12}^{-1} = -\frac{1}{2}\alpha_{18_{13},3_{13}} & (\sqrt{A})_{15,12}^{-1} = -\frac{1}{2}\alpha_{19_{13},3_{13}} \\ (\sqrt{A})_{14,13}^{-1} = -\frac{1}{2}\alpha_{18_{13},15_{13}} & (\sqrt{A})_{15,13}^{-1} = -\frac{1}{2}\alpha_{19_{13},15_{13}} & (\sqrt{A})_{15,14}^{-1} = -\frac{1}{2}\alpha_{19_{13},18_{13}} \end{array}$$

Here $(\sqrt{A})_{i,j}^{-1}$ indicates the i -th column and the j -th row entry of the matrix $(\sqrt{A})^{-1}$.

A.1.2 Translated 4-valent graph

In this Section we give the matrix entries of \sqrt{A}^{-1} obtained after translating the 4-valent graph. As for the aligned and rotated graphs discussed above, there are four vertices in the periodicity cell. The values for the terms $t_{e_i e_j} = t_{e_i e_j}^x + t_{e_i e_j}^y + t_{e_i e_j}^z$ as obtained for each vertex are given below. The (Gauss brackets) terms $n_i = [\frac{V_i^x}{l}]$, $m_i = [\frac{V_i^y}{l}]$ and $p_i = [\frac{V_i^z}{l}]$ represent the number of stacks which each edge e_i intersects in the x -, y - and z -direction respectively (see Section 3.1).

1) $V_0'' = (\epsilon_x, \epsilon_y, \epsilon_z)$ with $\epsilon_x > \epsilon_y > \epsilon_z$

$$\frac{(V_0'')^z}{t_{e_{0,1}e_{0,3}}^z = t_{e_{0,2}e_{0,4}}^z = (\epsilon_y - m_0 l)} \mid \frac{(V_0'')^x}{t_{e_{0,3}e_{0,4}}^x = t_{e_{0,1}e_{0,2}}^x = (\epsilon_z - p_0 l)} \mid \frac{(V_0'')^y}{t_{e_{0,3}e_{0,2}}^y = t_{e_{0,1}e_{0,4}}^y = (\epsilon_z - p_0 l)}$$

2) $V_2'' = (-\frac{\delta_e}{\sqrt{3}} + \epsilon_x, \epsilon_y + \frac{\delta_e}{\sqrt{3}}, \epsilon_z + \frac{\delta_e}{\sqrt{3}})$

$$\frac{(V_2'')^z}{t_{e_{2,6}e_{2,5}}^z = t_{e_{2,0}e_{2,7}}^z = (|\epsilon_x - \frac{\delta_e}{\sqrt{3}}| - n_2l)} \quad \left| \quad \frac{(V_2'')^x}{t_{e_{2,0}e_{2,5}}^x = t_{e_{2,7}e_{2,6}}^x = (\frac{\delta_e}{\sqrt{3}} + \epsilon_z - p_2l)} \quad \right| \quad \frac{(V_2'')^y}{t_{e_{2,0}e_{2,6}}^y = t_{e_{2,5}e_{2,7}}^y = (|\epsilon_x - \frac{\delta_e}{\sqrt{3}}| - n_2l)}$$

$$3) V_8'' = (\frac{\delta_e}{\sqrt{3}} + \epsilon_x, \epsilon_y + 3\frac{\delta_e}{\sqrt{3}}, \epsilon_z + \frac{\delta_e}{\sqrt{3}})$$

$$\frac{(V_8'')^z}{t_{e_{8,10}e_{8,11}}^z = t_{e_{8,5}e_{8,12}}^z = (\epsilon_x + \frac{\delta_e}{\sqrt{3}} - m_8l)} \quad \left| \quad \frac{(V_8'')^x}{t_{e_{8,5}e_{8,10}}^x = t_{e_{8,12}e_{8,11}}^x = (\epsilon_z + \frac{\delta_e}{\sqrt{3}} - p_8l)} \quad \right| \quad \frac{(V_8'')^y}{t_{e_{8,11}e_{8,5}}^y = t_{e_{8,10}e_{8,12}}^y = (\frac{\delta_e}{\sqrt{3}} + \epsilon_z - p_8l)}$$

$$5) V_{13}'' = (\epsilon_x, \epsilon_y + 2\frac{\delta_e}{\sqrt{3}}, \epsilon_z - 2\frac{\delta_e}{\sqrt{3}})$$

$$\frac{(V_{13}'')^z}{t_{e_{13,3}e_{13,15}}^z = t_{e_{13,19}e_{13,18}}^z = (\epsilon_x - n_{13}l)} \quad \left| \quad \frac{(V_{13}'')^x}{t_{e_{13,19}e_{13,15}}^x = t_{e_{13,18}e_{13,3}}^x = (|\epsilon_z - 2\frac{\delta_e}{\sqrt{3}}| - p_{13}l)} \quad \right| \quad \frac{(V_{13}'')^y}{t_{e_{13,15}e_{13,18}}^y = t_{e_{13,19}e_{13,3}}^y = (\epsilon_x - n_{13}l)}$$

The upper-half entries of the matrix \sqrt{A}^{-1} are listed in the following table. It should be noted that the lower indices refer to the matrix entries, while the upper ones indicate the edges that we are considering. Therefore $(\sqrt{A}^{-1})_{2,1}^{10,20}$ denotes the matrix entry at row 1 column 2, which is the term $\frac{t_{e_{0,1},e_{0,2}}}{\sqrt{t_{e_{0,1}}t_{e_{0,2}}}}$ corresponding to the edges $e_{0,1}$ and $e_{0,2}$, which join vertex V_0 to V_1 and V_0 to V_2 respectively.

$$\begin{array}{lll} (\sqrt{A}^{-1})_{2,1}^{10,20} = -\frac{1}{2}C_0 & (\sqrt{A}^{-1})_{3,1}^{10,30} = -\frac{1}{2}B_0 & (\sqrt{A}^{-1})_{4,1}^{10,40} = -\frac{1}{2}C_0 \\ (\sqrt{A}^{-1})_{3,2}^{20,30} = -\frac{1}{2}C_0 & (\sqrt{A}^{-1})_{4,2}^{20,40} = -\frac{1}{2}B_0 & (\sqrt{A}^{-1})_{5,2}^{02,72} = -\frac{1}{2}A_2 \\ (\sqrt{A}^{-1})_{6,2}^{02,52} = -\frac{1}{2}C_2 & (\sqrt{A}^{-1})_{7,2}^{02,62} = -\frac{1}{2}A_2 & (\sqrt{A}^{-1})_{4,3}^{30,40} = -\frac{1}{2}C_0 \\ (\sqrt{A}^{-1})_{6,5}^{72,52} = -\frac{1}{2}A_2 & (\sqrt{A}^{-1})_{7,5}^{72,62} = -\frac{1}{2}C_2 & (\sqrt{A}^{-1})_{7,6}^{52,62} = -\frac{1}{2}B_2 \\ (\sqrt{A}^{-1})_{9,8}^{19_{13},18_{13}} = -\frac{1}{2}A_{13} & (\sqrt{A}^{-1})_{10,8}^{19_{13},15_{13}} = -\frac{1}{2}C_{13} & (\sqrt{A}^{-1})_{11,8}^{19_{13},3_{13}} = -\frac{1}{2}A_{13} \\ (\sqrt{A}^{-1})_{10,9}^{18_{13},15_{13}} = -\frac{1}{2}A_{13} & (\sqrt{A}^{-1})_{11,9}^{18_{13},3_{13}} = -\frac{1}{2}C_{13} & (\sqrt{A}^{-1})_{11,10}^{15_{13},3_{13}} = -\frac{1}{2}A_{13} \\ (\sqrt{A}^{-1})_{13,12}^{10_8,11_8} = -\frac{1}{2}A_8 & (\sqrt{A}^{-1})_{14,12}^{10_8,12_8} = -\frac{1}{2}C_8 & (\sqrt{A}^{-1})_{15,12}^{10_8,5_8} = -\frac{1}{2}C_8 \\ (\sqrt{A}^{-1})_{14,13}^{11_8,12_8} = -\frac{1}{2}C_8 & (\sqrt{A}^{-1})_{15,13}^{11_8,5_8} = -\frac{1}{2}C_8 & (\sqrt{A}^{-1})_{15,14}^{12_8,5_8} = -\frac{1}{2}A_8 \end{array}$$

where $A_i = (|x_{V_i}| - n_{il})\frac{1}{\delta\sqrt{3}}$, $B_i = (|y_{V_i}| - m_{il})\frac{1}{\delta\sqrt{3}}$, $C_i = (|z_{V_i}| - p_{il})\frac{1}{\delta\sqrt{3}}$.

In all the above formulae, the term $\frac{1}{\delta_e\sqrt{3}}$ comes from the fact that $t_{e_i} = t_{e_i}^x + t_{e_i}^y + t_{e_i}^z = \delta_e\sqrt{3}$ for all edges e_i

A.2 Edge metric components for the 6-valent graph

In this Section we give the values of the terms $\frac{t_{e_{i,j}e_{i,j}}}{\sqrt{t_{e_{i,j}}t_{e_{i,j}}}}$ that represent the entries of the matrix \sqrt{A}^{-1} for the 6-valent graph. We do this for all non-rotated, rotated and translated cases respectively.

A.2.1 Aligned 6-valent graph

For the 6-valent graph, the periodicity cell contains *nine* vertices. Thus the matrix \sqrt{A}^{-1} is a 46×46 matrix.

We will now give the values for the terms $\frac{t_{e_{k,i}e_{k,j}}}{\sqrt{t_{e_{k,i}}t_{e_{k,j}}}}$ which we denote as Γ_{i_k,j_k} . We will also use the

following short-hand notations

$$\begin{aligned}
\alpha &:= \frac{\frac{\sqrt{2}}{2} - nl}{\delta(1 + \frac{\sqrt{2}}{2})} & \alpha' &:= \frac{\frac{\sqrt{2}}{2} - nl}{\delta\sqrt{\sqrt{2} + 1}} \\
\beta &:= \frac{\frac{1}{2} - n''l}{\delta(1 + \frac{\sqrt{2}}{2})} & \beta' &:= \frac{\frac{1}{2} - n''l}{\delta\sqrt{\sqrt{2} + 1}} \\
A_k &:= \frac{|V_k^x| - n'l}{\delta(1 + \frac{\sqrt{2}}{2})} & A'_k &:= \frac{|V_k^x| - n'l}{\delta\sqrt{\sqrt{2} + 1}}
\end{aligned} \tag{A.7}$$

1) V_0 all terms $\Gamma_{i_k, j_k} = 0$

2) V_2

$$\begin{array}{c}
\Gamma_{0_2, 11_2} = -\frac{\alpha'}{2} \\
\Gamma_{0_2, 9_2} = -\frac{\alpha'}{\sqrt{2}} \\
\Gamma_{12_2, 3_2} = -\frac{\alpha'}{\sqrt{2}} \\
\Gamma_{3_2, 9_2} = -\frac{\alpha'\sqrt{2}}{4}
\end{array}
\left| \begin{array}{c}
\Gamma_{0_2, 3_2} = -\frac{\alpha'}{2} \\
\Gamma_{11_2, 12_2} = -\frac{\alpha'}{\sqrt{2}} \\
\Gamma_{12_2, 10_2} = -\frac{\alpha'\sqrt{2}}{4}
\end{array} \right|
\begin{array}{c}
\Gamma_{0_2, 10_2} = -\frac{\alpha'}{2} \\
\Gamma_{11_2, 10_2} = -\frac{\alpha'\sqrt{2}}{4} \\
\Gamma_{12_2, 9_2} = -\frac{\alpha'\sqrt{2}}{4}
\end{array}$$

3) V_3

$$\begin{array}{c}
\Gamma_{2_3, 17_3} = -\frac{A'_3}{2} \\
\Gamma_{2_3, 16_3} = -\frac{\beta'}{2} \\
\Gamma_{17_3, 15_3} = -\beta' \\
\Gamma_{19_3, 15_3} = -A_3(\frac{1}{\sqrt{2}} - \frac{1}{2})
\end{array}
\left| \begin{array}{c}
\Gamma_{2_3, 13_3} = -\beta(\frac{1}{\sqrt{2}} + \frac{1}{2}) \\
\Gamma_{17_3, 13_3} = -\frac{A'_3}{2} \\
\Gamma_{13_3, 15_3} = -\frac{A_3}{2} \\
\Gamma_{19_3, 16_3} = -\frac{\beta'}{\sqrt{2}}
\end{array} \right|
\begin{array}{c}
\Gamma_{2_3, 19_3} = -\frac{A_3}{2} \\
\Gamma_{17_3, 19_3} = -\frac{A'_3}{2} \\
\Gamma_{16_3, 13_3} = -\frac{\alpha'\sqrt{2}}{2} \\
\Gamma_{16_3, 15_3} = -\frac{A'_3}{\sqrt{2}}
\end{array}$$

4) V_4

$$\begin{array}{c}
\Gamma_{a_4, 18_4} = -\beta(\frac{2}{\sqrt{2}} + 1) \\
\Gamma_{a_4, b_4} = -\frac{\alpha'\sqrt{2}}{2} \\
\Gamma_{18_4, 16_4} = -\frac{\alpha'\sqrt{2}}{2} \\
\Gamma_{b_4, c_4} = -\frac{\alpha'}{\sqrt{2}}
\end{array}
\left| \begin{array}{c}
\Gamma_{a_4, 13_4} = -\alpha' \\
\Gamma_{18_4, 13_4} = -\frac{\beta'}{\sqrt{2}} \\
\Gamma_{13_4, c_4} = -\alpha' \\
\Gamma_{16_4, c_4} = -\beta(\frac{2}{\sqrt{2}} + 1)
\end{array} \right|
\begin{array}{c}
\Gamma_{a_4, c_4} = -\frac{\alpha'\sqrt{2}}{2} \\
\Gamma_{18_4, b_4} = -\beta' \\
\Gamma_{13_4, 16_4} = -\beta' \\
\Gamma_{b_4, 16_4} = -\frac{\beta'}{\sqrt{2}}
\end{array}$$

5) V_5

$$\Gamma_{r_5, 17_5} = -\beta(\frac{2}{\sqrt{2}} + 1) \quad \left| \quad \Gamma_{6_5, q_5} = -\beta(\frac{2}{\sqrt{2}} + 1)
\right.$$

6) V_{13}

$$\begin{array}{c}
\Gamma_{5_{13}, 9_{13}} = -\frac{\alpha'}{2} \\
\Gamma_{5_{13}, 14_{13}} = -\frac{\alpha'}{2} \\
\Gamma_{4_{13}, 21_{13}} = -\frac{\alpha'}{\sqrt{2}} \\
\Gamma_{9_{13}, 14_{13}} = -\frac{2\beta}{\sqrt{2}} - \frac{\alpha'\sqrt{2}}{4}
\end{array}
\left| \begin{array}{c}
\Gamma_{5_{13}, 3_{13}} = -\frac{\alpha'}{2} \\
\Gamma_{4_{13}, 9_{13}} = -\frac{\sqrt{2}\alpha'}{4} \\
\Gamma_{4_{13}, 14_{13}} = -\frac{\alpha'\sqrt{2}}{4} \\
\Gamma_{3_{13}, 21_{13}} = -\beta - \frac{\alpha}{\sqrt{2}}
\end{array} \right|
\begin{array}{c}
\Gamma_{5_{13}, 21_{13}} = -\frac{\alpha'}{2} \\
\Gamma_{4_{13}, 3_{13}} = -\frac{2\beta'}{\sqrt{2}} \\
\Gamma_{3_{13}, 9_{13}} = -\frac{\alpha'\sqrt{2}}{4} \\
\Gamma_{21_{13}, 14_{13}} = -\frac{\alpha'\sqrt{2}}{4}
\end{array}$$

7) V_{18}

$$\begin{array}{c}
\Gamma_{4_{18}, 9_{18}} = -\frac{\alpha'}{2} \\
\Gamma_{4_{18}, e_{18}} = -\frac{\sqrt{2}\alpha'}{4} \\
\Gamma_{e_{18}, 9_{18}} = -\frac{A'_{18}}{2} \\
\Gamma_{d_{18}, f_{18}} = -\frac{\beta'}{2}
\end{array}
\left| \begin{array}{c}
\Gamma_{4_{18}, 12_{18}} = -\beta(\frac{1}{\sqrt{2}} + \frac{1}{2}) \\
\Gamma_{12_{18}, 9_{18}} = -\frac{\beta'}{2} \\
\Gamma_{12_{18}, f_{18}} = -\frac{\alpha'\sqrt{2}}{4} \\
\Gamma_{e_{18}, f_{18}} = -\beta(\frac{1}{\sqrt{2}} - \frac{1}{2})
\end{array} \right|
\begin{array}{c}
\Gamma_{4_{18}, d_{18}} = -\frac{A'_{18}}{\sqrt{2}} \\
\Gamma_{f_{18}, 9_{18}} = -\frac{\beta'}{\sqrt{2}} \\
\Gamma_{d_{18}, 12_{18}} = -\frac{\beta'}{\sqrt{2}} \\
\Gamma_{e_{18}, d_{18}} = -\frac{\alpha'\sqrt{2}}{4}
\end{array}$$

8) V_{15}

$$\begin{array}{l} \Gamma_{3_{15},d'_{15}} = -\frac{A_{15}}{2} \\ \Gamma_{3_{15},a'_{15}} = -\frac{A_{15}}{\sqrt{2}} - \beta \\ \Gamma_{e'_{15},f'_{15}} = -\frac{3\alpha'}{2} \\ \Gamma_{f'_{15},d'_{15}} = -\beta' \end{array} \left| \begin{array}{l} \Gamma_{3_{15},c'_{15}} = -\frac{3\alpha'\sqrt{2}}{4} \\ \Gamma_{e'_{15},d'_{15}} = -\beta\left(\frac{2}{\sqrt{2}} + 1\right) \\ \Gamma_{e'_{15},a'_{15}} = -\frac{A_{15}}{2} \\ \Gamma_{c'_{15},a'_{15}} = -\frac{3\alpha'\sqrt{2}}{4} \end{array} \right| \begin{array}{l} \Gamma_{3_{15},f'_{15}} = -\frac{A'_{15}}{\sqrt{2}} \\ \Gamma_{e'_{15},c'_{15}} = -\frac{A'_{15}}{2} \\ \Gamma_{c'_{15},d'_{15}} = -\frac{A'_{15}}{2} \\ \Gamma_{a'_{15},f'_{15}} = -\frac{A'_{15}}{\sqrt{2}} \end{array}$$

9) V_{14}

$$\begin{array}{l} \Gamma_{13_{14},a_{14}} = -\frac{3\beta'}{\sqrt{2}} \\ \Gamma_{j_{14},l_{14}} = -\beta\left(\frac{3}{\sqrt{2}} + \frac{3}{2}\right) \end{array} \left| \begin{array}{l} \Gamma_{h_{14},a_{14}} = -\frac{A'_{14}}{\sqrt{2}} \\ \Gamma_{j_{14},k_{14}} = -\frac{A'_{14}}{2} \end{array} \right| \begin{array}{l} \Gamma_{13_{14},h_{14}} = -\frac{A_{14}}{\sqrt{2}} - \frac{3\beta}{\sqrt{2}} \\ \Gamma_{l_{14},k_{14}} = -\frac{A_{14}}{2} \end{array}$$

The upper-diagonal entries of the matrix \sqrt{A}^{-1} are listed below. Similarly, as for the 4-valent case, the lower indices represent the matrix entries while the top indices indicate the edges we are considering.

$$\begin{aligned}
(\sqrt{A}^{-1})_{7,2}^{02,112} &= -\frac{\alpha'}{2} & (\sqrt{A}^{-1})_{9,2}^{02,32} &= -\frac{\alpha'}{2} & (\sqrt{A}^{-1})_{10,2}^{02,102} &= -\frac{\alpha'}{2} \\
(\sqrt{A}^{-1})_{11,2}^{02,92} &= -\frac{\alpha'}{\sqrt{2}} & (\sqrt{A}^{-1})_{8,7}^{122,122} &= -\frac{\alpha'}{\sqrt{2}} & (\sqrt{A}^{-1})_{10,7}^{112,102} &= -\frac{\alpha\sqrt{2}}{4} \\
(\sqrt{A}^{-1})_{9,8}^{122,32} &= -\frac{\alpha'}{\sqrt{2}} & (\sqrt{A}^{-1})_{10,8}^{122,102} &= -\frac{\alpha'\sqrt{2}}{4} & (\sqrt{A}^{-1})_{11,8}^{122,92} &= -\frac{\alpha'\sqrt{2}}{4} \\
(\sqrt{A}^{-1})_{11,9}^{32,92} &= -\frac{\alpha\sqrt{2}}{4} & (\sqrt{A}^{-1})_{12,9}^{23,173} &= -\frac{A_3'}{2} & (\sqrt{A}^{-1})_{13,9}^{23,133} &= -\beta\left(\frac{1}{\sqrt{2}} + \frac{1}{2}\right) \\
(\sqrt{A}^{-1})_{14,9}^{23,193} &= -\frac{A_3'}{2} & (\sqrt{A}^{-1})_{16,9}^{23,163} &= -\frac{\beta'}{2} & (\sqrt{A}^{-1})_{13,12}^{173,133} &= -\frac{A_3'}{2} \\
(\sqrt{A}^{-1})_{14,12}^{173,193} &= -\frac{A_3'}{2} & (\sqrt{A}^{-1})_{15,12}^{173,153} &= -\beta' & (\sqrt{A}^{-1})_{15,13}^{133,153} &= -\frac{A_3'}{2} \\
(\sqrt{A}^{-1})_{16,13}^{133,163} &= -\frac{\alpha'\sqrt{2}}{2} & (\sqrt{A}^{-1})_{17,13}^{313,413} &= -\frac{2\beta'}{\sqrt{2}}\rho & (\sqrt{A}^{-1})_{18,13}^{313,513} &= -\frac{\alpha'}{2} \\
(\sqrt{A}^{-1})_{20,13}^{313,913} &= -\frac{\alpha\sqrt{2}}{2} & (\sqrt{A}^{-1})_{21,13}^{313,2113} &= -\frac{\alpha\sqrt{2}}{4} & (\sqrt{A}^{-1})_{15,14}^{193,153} &= -A_3\left(\frac{1}{2} + \frac{1}{\sqrt{2}}\right) \\
(\sqrt{A}^{-1})_{16,14}^{193,163} &= -\frac{\beta'}{\sqrt{2}} & (\sqrt{A}^{-1})_{17,15}^{153,163} &= -\frac{A_3'}{\sqrt{2}} & (\sqrt{A}^{-1})_{38,15}^{315,d'_{15}} &= -\frac{A_{15}}{2} \\
(\sqrt{A}^{-1})_{39,15}^{315,c'_{15}} &= -\frac{3\alpha'\sqrt{2}}{4} & (\sqrt{A}^{-1})_{40,15}^{315,f'_{15}} &= -\frac{A_{15}}{\sqrt{2}} - \beta\rho & (\sqrt{A}^{-1})_{18,17}^{a_4,184} &= -\frac{2\beta}{\sqrt{2}} - \beta \\
(\sqrt{A}^{-1})_{19,17}^{a_4,134} &= -\alpha' & (\sqrt{A}^{-1})_{20,17}^{a_4,c_4} &= -\frac{\alpha\sqrt{2}}{4} & (\sqrt{A}^{-1})_{21,17}^{a_4,b_4} &= -\frac{\alpha'\sqrt{2}}{2} \\
(\sqrt{A}^{-1})_{19,18}^{184,134} &= -\frac{\beta'}{2} & (\sqrt{A}^{-1})_{21,18}^{184,b_4} &= -\beta' & (\sqrt{A}^{-1})_{22,18}^{184,164} &= -\frac{\alpha\sqrt{2}}{2} \\
(\sqrt{A}^{-1})_{32,18}^{418,918} &= -\frac{\alpha'}{2} & (\sqrt{A}^{-1})_{33,18}^{418,1218} &= -\beta\left(\frac{1}{\sqrt{2}} + \frac{1}{2}\right) & (\sqrt{A}^{-1})_{35,18}^{418,d_{18}} &= -\frac{A'_{18}}{\sqrt{2}} \\
(\sqrt{A}^{-1})_{36,18}^{418,e_{18}} &= -\frac{\alpha\sqrt{2}}{4} & (\sqrt{A}^{-1})_{20,19}^{134,c_4} &= -\alpha' & (\sqrt{A}^{-1})_{22,19}^{134,164} &= -\beta' \\
(\sqrt{A}^{-1})_{29,19}^{413,1413} &= -\frac{\alpha'\sqrt{2}}{4}\rho & (\sqrt{A}^{-1})_{30,19}^{413,913} &= -\frac{\alpha'\sqrt{2}}{4} & (\sqrt{A}^{-1})_{31,19}^{413,2113} &= -\frac{\alpha'}{\sqrt{2}} \\
(\sqrt{A}^{-1})_{21,20}^{c_4,b_4} &= -\frac{2\alpha'}{\sqrt{2}} & (\sqrt{A}^{-1})_{22,20}^{c_4,164} &= -\beta\left(\frac{2}{\sqrt{2}} + 1\right) & (\sqrt{A}^{-1})_{22,21}^{b_4,164} &= -\frac{2\beta}{\sqrt{2}} \\
(\sqrt{A}^{-1})_{23,24}^{r_{15},1715} &= -\beta(\sqrt{2} + 1) & (\sqrt{A}^{-1})_{29,25}^{513,1413} &= -\frac{\alpha'}{2} & (\sqrt{A}^{-1})_{30,25}^{513,913} &= -\frac{\alpha'}{2} \\
(\sqrt{A}^{-1})_{31,25}^{513,2113} &= -\frac{\alpha'}{2} & (\sqrt{A}^{-1})_{28,27}^{q_5,6_5} &= -\beta(\sqrt{2} + 1) & (\sqrt{A}^{-1})_{30,29}^{1413,913} &= -\frac{2\beta}{\sqrt{2}} - \frac{\sqrt{2}\alpha}{4} \\
(\sqrt{A}^{-1})_{31,29}^{1413,2113} &= -\frac{\alpha\sqrt{2}}{4} & (\sqrt{A}^{-1})_{43,29}^{1314,a_{14}} &= -\frac{2\beta'}{\sqrt{2}} & (\sqrt{A}^{-1})_{46,29}^{1314,h_{14}} &= -\frac{A_{14}}{\sqrt{2}} - \frac{3\beta}{2} \\
(\sqrt{A}^{-1})_{33,32}^{918,1218} &= -\frac{\beta'}{2} & (\sqrt{A}^{-1})_{34,32}^{918,f_{18}} &= -\frac{\beta'}{2} & (\sqrt{A}^{-1})_{36,33}^{918,e_{18}} &= -\frac{A_{18}}{2}\rho \\
(\sqrt{A}^{-1})_{35,34}^{1218,f_{18}} &= -\frac{\alpha\sqrt{2}}{4} & (\sqrt{A}^{-1})_{36,34}^{1218,d_{18}} &= -\frac{\beta'}{\sqrt{2}} & (\sqrt{A}^{-1})_{36,35}^{f_{18},d_{18}} &= -\frac{\beta'}{2} \\
(\sqrt{A}^{-1})_{37,35}^{f_{18},e_{18}} &= -\beta\left(\frac{1}{\sqrt{2}} + \frac{1}{2}\right) & (\sqrt{A}^{-1})_{37,36}^{d_{18},e_{18}} &= -\frac{\alpha'\sqrt{2}}{4} & (\sqrt{A}^{-1})_{39,38}^{e'_{15},d'_{15}} &= -\beta(\sqrt{2} + 1) \\
(\sqrt{A}^{-1})_{40,38}^{e'_{15},c'_{15}} &= -\frac{A'_{15}}{2} & (\sqrt{A}^{-1})_{41,39}^{e'_{15},f'_{15}} &= -\frac{3\alpha'}{2} & (\sqrt{A}^{-1})_{42,39}^{e'_{15},a'_{15}} &= -\frac{A_{15}}{2} \\
(\sqrt{A}^{-1})_{41,40}^{d'_{15},c'_{15}} &= -\frac{A'_{15}}{2}\rho & (\sqrt{A}^{-1})_{42,40}^{d'_{15},f'_{15}} &= -\beta' & (\sqrt{A}^{-1})_{43,41}^{c'_{15},a'_{15}} &= -\frac{3\alpha'\sqrt{2}}{4} \\
(\sqrt{A}^{-1})_{43,42}^{f'_{15},a'_{15}} &= -\frac{A_{15}}{\sqrt{2}} & (\sqrt{A}^{-1})_{45,43}^{k_{14},l_{14}} &= -\frac{A'_{14}}{2} & (\sqrt{A}^{-1})_{46,43}^{k_{14},j_{14}} &= -\frac{A_{14}}{2} \\
(\sqrt{A}^{-1})_{47,44}^{a_{14},h_{14}} &= -\frac{A'_{14}}{\sqrt{2}} & (\sqrt{A}^{-1})_{46,45}^{l_{14},j_{14}} &= -3\beta\left(\frac{1}{\sqrt{2}} + \frac{1}{2}\right)
\end{aligned}$$

A.2.2 Rotated 6-valent graph

In this Section we give the values of all the terms $\frac{t_{e_i e_j}}{\sqrt{t_{e_i} t_{e_j}}}$ that appear in the matrix \sqrt{A}^{-1} for the rotated 6-valent graph. In order to carry out the calculations we will rotate the graph such that the edges incident at vertex V_0 : $e_{0,1}$, $e_{0,2}$, $e_{0,6}$, $e_{0,7}$, $e_{0,8}$ and $e_{0,17}$ lie in the octants H , D , G , F , A and B respectively. As for the aligned graph, we consider the periodicity cell composed of nine vertices. Therefore \sqrt{A}^{-1} will be a 46×46 matrix.

In what follows the terms ρ_{i_k, j_k} represent the values for $\frac{t_{e_k, i e_k, j}}{\sqrt{t_{e_k, i} t_{e_k, j}}}$ and are defined as for the 4-valent case (see A.1.1)

Given the above, the upper-half elements of the matrix \sqrt{A}^{-1} are:

$$\begin{aligned}
(\sqrt{A})_{20,2}^{-1} &= -\frac{1}{2}\rho_{0_2,9_2} & (\sqrt{A})_{22,2}^{-1} &= -\frac{1}{2}\rho_{0_2,11_2} & (\sqrt{A})_{24,2}^{-1} &= -\frac{1}{2}\rho_{0_2,3_2} \\
(\sqrt{A})_{25,2}^{-1} &= -\frac{1}{2}\rho_{0_2,10_2} & (\sqrt{A})_{8,7}^{-1} &= -\frac{1}{2}\rho_{a_4,18_4} & (\sqrt{A})_{9,7}^{-1} &= -\frac{1}{2}\rho_{a_4,13_4} \\
(\sqrt{A})_{10,7}^{-1} &= -\frac{1}{2}\rho_{a_4,c_4} & (\sqrt{A})_{11,7}^{-1} &= -\frac{1}{2}\rho_{a_4,b_4} & (\sqrt{A})_{9,8}^{-1} &= -\frac{1}{2}\rho_{13_4,18_4} \\
(\sqrt{A})_{11,8}^{-1} &= -\frac{1}{2}\rho_{b_4,18_4} & (\sqrt{A})_{12,8}^{-1} &= -\frac{1}{2}\rho_{16_4,18_4} & (\sqrt{A})_{21,8}^{-1} &= -\frac{1}{2}\rho_{9_{18},4_{18}} \\
(\sqrt{A})_{35,8}^{-1} &= -\frac{1}{2}\rho_{d_{18},4_{18}} & (\sqrt{A})_{36,8}^{-1} &= -\frac{1}{2}\rho_{4_{18},e_{18}} & (\sqrt{A})_{10,9}^{-1} &= -\frac{1}{2}\rho_{c_4,13_4} \\
(\sqrt{A})_{12,9}^{-1} &= -\frac{1}{2}\rho_{16_4,13_4} & (\sqrt{A})_{19,9}^{-1} &= -\frac{1}{2}\rho_{4_{13},9_{13}} & (\sqrt{A})_{27,9}^{-1} &= -\frac{1}{2}\rho_{3_{13},4_{13}} \\
(\sqrt{A})_{31,9}^{-1} &= -\frac{1}{2}\rho_{4_{13},2_{13}} & (\sqrt{A})_{32,9}^{-1} &= -\frac{1}{2}\rho_{4_{13},14_{13}} & (\sqrt{A})_{33,9}^{-1} &= -\frac{1}{2}\rho_{4_{18},12_{18}} \\
(\sqrt{A})_{11,10}^{-1} &= -\frac{1}{2}\rho_{b_4,c_4} & (\sqrt{A})_{12,10}^{-1} &= -\frac{1}{2}\rho_{c_4,16_4} & (\sqrt{A})_{12,11}^{-1} &= -\frac{1}{2}\rho_{b_4,18_4} \\
(\sqrt{A})_{14,13}^{-1} &= -\frac{1}{2}\rho_{r_5,17_5} & (\sqrt{A})_{15,13}^{-1} &= -\frac{1}{2}\rho_{r_5,13_5} & (\sqrt{A})_{16,13}^{-1} &= -\frac{1}{2}\rho_{r_5,p_5} \\
(\sqrt{A})_{17,13}^{-1} &= -\frac{1}{2}\rho_{r_5,q_5} & (\sqrt{A})_{15,14}^{-1} &= -\frac{1}{2}\rho_{13_5,17_5} & (\sqrt{A})_{16,14}^{-1} &= -\frac{1}{2}\rho_{p_5,17_5} \\
(\sqrt{A})_{18,14}^{-1} &= -\frac{1}{2}\rho_{6_5,17_5} & (\sqrt{A})_{17,15}^{-1} &= -\frac{1}{2}\rho_{q_5,13_5} & (\sqrt{A})_{18,15}^{-1} &= -\frac{1}{2}\rho_{6_5,13_5} \\
(\sqrt{A})_{19,15}^{-1} &= -\frac{1}{2}\rho_{9_{13},5_5} & (\sqrt{A})_{27,15}^{-1} &= -\frac{1}{2}\rho_{3_{13},5_{13}} & (\sqrt{A})_{31,15}^{-1} &= -\frac{1}{2}\rho_{2_{13},5_{13}} \\
(\sqrt{A})_{32,15}^{-1} &= -\frac{1}{2}\rho_{14_{13},5_{13}} & (\sqrt{A})_{17,16}^{-1} &= -\frac{1}{2}\rho_{q_5,p_5} & (\sqrt{A})_{18,16}^{-1} &= -\frac{1}{2}\rho_{6_5,p_5} \\
(\sqrt{A})_{18,17}^{-1} &= -\frac{1}{2}\rho_{6_5,9_5} & (\sqrt{A})_{27,19}^{-1} &= -\frac{1}{2}\rho_{3_{13},9_{13}} & (\sqrt{A})_{32,19}^{-1} &= -\frac{1}{2}\rho_{14_{13},9_{13}} \\
(\sqrt{A})_{26,20}^{-1} &= -\frac{1}{2}\rho_{12_2,9_2} & (\sqrt{A})_{27,20}^{-1} &= -\frac{1}{2}\rho_{3_2,9_2} & (\sqrt{A})_{28,20}^{-1} &= -\frac{1}{2}\rho_{10_2,9_2} \\
(\sqrt{A})_{33,21}^{-1} &= -\frac{1}{2}\rho_{12_{18},9_{18}} & (\sqrt{A})_{34,21}^{-1} &= -\frac{1}{2}\rho_{f_{18},9_{18}} & (\sqrt{A})_{36,21}^{-1} &= -\frac{1}{2}\rho_{e_{18},9_{18}} \\
(\sqrt{A})_{23,22}^{-1} &= -\frac{1}{2}\rho_{12_2,11_2} & (\sqrt{A})_{24,22}^{-1} &= -\frac{1}{2}\rho_{3_2,11_2} & (\sqrt{A})_{25,22}^{-1} &= -\frac{1}{2}\rho_{10_2,11_2} \\
(\sqrt{A})_{24,23}^{-1} &= -\frac{1}{2}\rho_{3_2,12_2} & (\sqrt{A})_{25,23}^{-1} &= -\frac{1}{2}\rho_{10_2,12_2} & (\sqrt{A})_{26,24}^{-1} &= -\frac{1}{2}\rho_{17_3,2_3} \\
(\sqrt{A})_{27,24}^{-1} &= -\frac{1}{2}\rho_{13_3,2_3} & (\sqrt{A})_{28,24}^{-1} &= -\frac{1}{2}\rho_{19_3,2_3} & (\sqrt{A})_{30,24}^{-1} &= -\frac{1}{2}\rho_{16_3,2_3} \\
(\sqrt{A})_{27,26}^{-1} &= -\frac{1}{2}\rho_{13_3,17_3} & (\sqrt{A})_{28,26}^{-1} &= -\frac{1}{2}\rho_{19_3,17_3} & (\sqrt{A})_{29,26}^{-1} &= -\frac{1}{2}\rho_{15_3,17_3} \\
(\sqrt{A})_{29,27}^{-1} &= -\frac{1}{2}\rho_{15_3,13_3} & (\sqrt{A})_{30,27}^{-1} &= -\frac{1}{2}\rho_{16_3,13_3} & (\sqrt{A})_{31,27}^{-1} &= -\frac{1}{2}\rho_{2_{13},3_{13}} \\
(\sqrt{A})_{29,28}^{-1} &= -\frac{1}{2}\rho_{15_3,19_3} & (\sqrt{A})_{30,28}^{-1} &= -\frac{1}{2}\rho_{16_3,19_3} & (\sqrt{A})_{30,29}^{-1} &= -\frac{1}{2}\rho_{16_3,15_3} \\
(\sqrt{A})_{38,29}^{-1} &= -\frac{1}{2}\rho_{d'_{15},3_{15}} & (\sqrt{A})_{39,29}^{-1} &= -\frac{1}{2}\rho_{c'_{15},3_{15}} & (\sqrt{A})_{40,29}^{-1} &= -\frac{1}{2}\rho_{f'_{15},3_{15}} \\
(\sqrt{A})_{41,29}^{-1} &= -\frac{1}{2}\rho_{a'_{15},3_{15}} & (\sqrt{A})_{32,31}^{-1} &= -\frac{1}{2}\rho_{14_{13},2_{13}} & (\sqrt{A})_{42,32}^{-1} &= -\frac{1}{2}\rho_{a_{14},13_{14}} \\
(\sqrt{A})_{43,32}^{-1} &= -\frac{1}{2}\rho_{h_{14},13_{14}} & (\sqrt{A})_{45,32}^{-1} &= -\frac{1}{2}\rho_{k_{14},13_{14}} & (\sqrt{A})_{46,32}^{-1} &= -\frac{1}{2}\rho_{l_{14},13_{14}} \\
(\sqrt{A})_{34,33}^{-1} &= -\frac{1}{2}\rho_{f_{18},12_{18}} & (\sqrt{A})_{35,33}^{-1} &= -\frac{1}{2}\rho_{d_{18},12_{18}} & (\sqrt{A})_{35,34}^{-1} &= -\frac{1}{2}\rho_{d_{18},f_{18}} \\
(\sqrt{A})_{36,34}^{-1} &= -\frac{1}{2}\rho_{e_{18},f_{18}} & (\sqrt{A})_{36,35}^{-1} &= -\frac{1}{2}\rho_{e_{18},d_{18}} & (\sqrt{A})_{38,37}^{-1} &= -\frac{1}{2}\rho_{d'_{15},e'_{15}} \\
(\sqrt{A})_{39,37}^{-1} &= -\frac{1}{2}\rho_{c'_{15},e'_{15}} & (\sqrt{A})_{40,37}^{-1} &= -\frac{1}{2}\rho_{f'_{15},e'_{15}} & (\sqrt{A})_{41,37}^{-1} &= -\frac{1}{2}\rho_{a'_{15},e'_{15}} \\
(\sqrt{A})_{39,38}^{-1} &= -\frac{1}{2}\rho_{c'_{15},d'_{15}} & (\sqrt{A})_{40,38}^{-1} &= -\frac{1}{2}\rho_{f'_{15},d'_{15}} & (\sqrt{A})_{41,39}^{-1} &= -\frac{1}{2}\rho_{a'_{15},c'_{15}} \\
(\sqrt{A})_{41,40}^{-1} &= -\frac{1}{2}\rho_{a'_{15},f'_{15}} & (\sqrt{A})_{45,42}^{-1} &= -\frac{1}{2}\rho_{h_{14},a_{14}} & (\sqrt{A})_{46,42}^{-1} &= -\frac{1}{2}\rho_{j_{15},a_{15}} \\
(\sqrt{A})_{47,42}^{-1} &= -\frac{1}{2}\rho_{l_{14},a_{14}} & (\sqrt{A})_{44,43}^{-1} &= -\frac{1}{2}\rho_{j_{14},h_{14}} & (\sqrt{A})_{45,43}^{-1} &= -\frac{1}{2}\rho_{j_{15},k_{15}} \\
(\sqrt{A})_{45,44}^{-1} &= -\frac{1}{2}\rho_{k_{14},j_{14}} & (\sqrt{A})_{46,44}^{-1} &= -\frac{1}{2}\rho_{l_{14},j_{14}} & (\sqrt{A})_{46,45}^{-1} &= -\frac{1}{2}\rho_{l_{15},k_{15}}
\end{aligned}$$

A.2.3 Translated 6-valent graph

We will now give the values for the terms $t_{e_i e_j} = t_{e_i e_j}^x + t_{e_i e_j}^y + t_{e_i e_j}^z$ as computed for each of the nine vertices comprising the periodicity cell for the 6-valent graph. The (Gauss brackets) terms $n_i = [\frac{V_i^x}{t}]$, $m_i = [\frac{V_i^y}{t}]$ and $p_i = [\frac{V_i^z}{t}]$ represent the number of stacks which each edge e_i intersects in the x -, y - and z -direction respectively (see Section 3.1).

1) $V_0'' = (\epsilon_x, \epsilon_y, \epsilon_z)$ with $\epsilon_x > \epsilon_y > \epsilon_z$

$(V''_0)^z$	$(V''_0)^x$	$(V''_0)^y$
$t_{e_0,1e_0,6}^z = (\epsilon_y - m_0l)Z_6^y$	$t_{e_0,1e_0,6}^x = (\epsilon_z - p_0l)T_1^x$	$t_{e_0,1e_0,8}^y = (\epsilon_z - p_0l)T_1^y$
$t_{e_0,6e_0,7}^z = (\epsilon_y - m_0l)Z_6^y$	$t_{e_0,2e_0,6}^x = (\epsilon_z - p_0l)T_6^x$	$t_{e_0,6e_0,17}^y = (\epsilon_z - p_0l)T_6^y$
$t_{e_0,1e_0,7}^z = (\epsilon_x - n_0l)Z_7^x$	$t_{e_0,2e_0,1}^x = (\epsilon_z - p_0l)T_1^x$	
$t_{e_0,2e_0,8}^z = (\epsilon_x - n_0l)Z_8^x$	$t_{e_0,8e_0,7}^x = (\epsilon_z - p_0l)T_7^x$	
$t_{e_0,2e_0,17}^z = (\epsilon_y - m_0l)Z_{17}^y$	$t_{e_0,8e_0,17}^x = (\epsilon_y - m_0l)F_{17}^x$	
$t_{e_0,8e_0,17}^z = (\epsilon_y - m_0l)Z_{17}^y$	$t_{e_0,7e_0,17}^x = (\epsilon_z - p_0l)T_7^x$	

2) $V_2'' = (\frac{\delta_e\sqrt{2}}{2} + \epsilon_x, \epsilon_y, \frac{\delta_e\sqrt{2}}{2} + \epsilon_z)$

$(V_2'')^z$	$(V_2'')^x$	$(V_2'')^y$
$t_{e_2,0e_2,10}^z = (\epsilon_x + \frac{\delta_e\sqrt{2}}{2} - n_2l)Z_0^x$	$t_{e_2,12e_2,10}^x = (\frac{\delta_e\sqrt{2}}{2} + \epsilon_z - p_2l)T_{10}^x$	$t_{e_2,10e_2,11}^y = (\frac{\delta_e\sqrt{2}}{2} + \epsilon_z - p_2l)T_{10}^y$
$t_{e_2,9e_2,0}^z = (\epsilon_y - m_2l)Z_9^y$	$t_{e_2,9e_2,12}^x = (\epsilon_y - m_2p)F_9^x$	$t_{e_2,9e_2,3}^y = (\frac{\delta_e\sqrt{2}}{2} + \epsilon_z - p_2l)T_9^y$
$t_{e_2,9e_2,10}^z = (\epsilon_y - m_2l)Z_9^y$	$t_{e_2,9e_2,10}^x = (\epsilon_y - m_2p)F_9^x$	
$t_{e_2,11e_2,12}^z = (\epsilon_x + \frac{\delta_e\sqrt{2}}{2} - n_2l)Z_{11}^x$	$t_{e_2,11e_2,0}^x = (\frac{\delta_e\sqrt{2}}{2} + \epsilon_z - p_2l)T_0^x$	
$t_{e_2,3e_2,12}^z = (\epsilon_y - m_2l)Z_3^y$	$t_{e_2,11e_2,3}^x = (\epsilon_y - m_2l)F_3^x$	
$t_{e_2,11e_2,3}^z = (\epsilon_x + \frac{\delta_e\sqrt{2}}{2} - n_2l)Z_3^x$	$t_{e_2,3e_2,0}^x = (\epsilon_y - m_2p)F_3^x$	

3) $V_3'' = (\epsilon_x + \delta_e(\frac{\sqrt{2}}{2} - \frac{1}{2}), \epsilon_y - \frac{\delta_e}{2}, 2\frac{\delta_e\sqrt{2}}{2} + \epsilon_z)$

$(V_3'')^z$	$(V_3'')^x$	$(V_3'')^y$
$t_{e_3,2e_3,13}^z = (\epsilon_y - \frac{\delta_e}{2} - m_3l)Z_2^y$	$t_{e_3,16e_3,2}^x = (\epsilon_y + \frac{\delta_e}{2} - m_3l)F_2^x$	$t_{e_3,19e_3,2}^y = (\epsilon_x + \delta_e(\frac{\sqrt{2}}{2} - \frac{1}{2}) - n_3l)F_{19}^x$
$t_{e_3,17e_3,2}^z = (\epsilon_y - \frac{\delta_e}{2} - m_3l)Z_2^y$	$t_{e_3,16e_3,13}^x = (\epsilon_z + 2\frac{\delta_e\sqrt{2}}{2} - p_3l)T_{13}^x$	$t_{e_3,15e_3,13}^y = (\epsilon_x + \delta_e(\frac{\sqrt{2}}{2} - \frac{1}{2}) - n_3l)F_{15}^x$
$t_{e_3,17e_3,13}^z = (\epsilon_x + \delta_e(\frac{\sqrt{2}}{2} - \frac{1}{2}) - n_3l)Z_{17}^x$	$t_{e_3,13e_3,2}^x = (\epsilon_y + \frac{\delta_e}{2} - m_3l)F_2^x$	
$t_{e_3,16e_3,15}^z = (\epsilon_x + \delta_e(\frac{\sqrt{2}}{2} - \frac{1}{2}) - n_3l)Z_{15}^x$	$t_{e_3,15e_3,17}^x = (\epsilon_z + 2\frac{\delta_e\sqrt{2}}{2} - p_3l)T_{17}^x$	
$t_{e_3,16e_3,19}^z = (\epsilon_y - \frac{\delta_e}{2} - m_3l)Z_{19}^y$	$t_{e_3,15e_3,19}^x = (\epsilon_y - \frac{\delta_e}{2} - m_3l)F_{19}^x$	
$t_{e_3,19e_3,15}^z = (\epsilon_y - \frac{\delta_e}{2} - m_3l)Z_{19}^y$	$t_{e_3,19e_3,17}^x = (\epsilon_y - \frac{\delta_e}{2} - m_3l)F_{19}^x$	

4) $V_4'' = (2\frac{\delta_e\sqrt{2}}{2} + \epsilon_x, \epsilon_y - 2\frac{\delta_e}{2}, 2\frac{\delta_e\sqrt{2}}{2} + \epsilon_z)$

$(V_4'')^z$	$(V_4'')^x$	$(V_4'')^y$
$t_{e_4,a e_4,18}^z = (\epsilon_y - \delta_e - m_4l)Z_{18}^y$	$t_{e_4,a e_4,18}^x = (\epsilon_y - \delta_e - m_4l)F_{18}^x$	$t_{e_4,16e_4,18}^y = (\epsilon_z + 2\frac{\delta_e\sqrt{2}}{2} - p_4l)T_{18}^y$
$t_{e_4,13e_4,a}^z = (\epsilon_x + 2\frac{\delta_e\sqrt{2}}{2} - m_4l)Z_{13}^x$	$t_{e_4,b e_4,a}^x = (\epsilon_z + 2\frac{\delta_e\sqrt{2}}{2} - p_4l)T_a^x$	$t_{e_4,a e_4,c}^y = (\epsilon_z + 2\frac{\delta_e\sqrt{2}}{2} - p_4l)T_a^y$
$t_{e_4,13e_4,18}^z = (\epsilon_y - \delta_e - m_4l)Z_{18}^y$	$t_{e_4,18e_4,b}^x = (\epsilon_y - \delta_e - m_4l)F_{18}^x$	
$t_{e_4,b e_4,16}^z = (\epsilon_y - \delta_e - m_4l)Z_{16}^y$	$t_{e_4,16e_4,13}^x = (\epsilon_y - \delta_e - m_4l)F_{16}^x$	
$t_{e_4,c e_4,16}^z = (\epsilon_y - \delta_e - m_4l)Z_{16}^y$	$t_{e_4,16e_4,c}^x = (\epsilon_y - \delta_e - m_4l)F_{16}^x$	
$t_{e_4,c e_4,b}^z = (\epsilon_x + 2\frac{\delta_e\sqrt{2}}{2} - n_4l)Z_c^x$	$t_{e_4,13e_4,c}^x = (\epsilon_z + 2\frac{\delta_e\sqrt{2}}{2} - p_4l)T_{13}^x$	

5) $V_5'' = (\epsilon_x, \epsilon_y - \delta_e, \epsilon_z)$

$(V_5'')^z$	$(V_5'')^x$	$(V_5'')^y$
$t_{e_5,q e_5,6}^z = (\epsilon_y - \delta_e - m_5l)Z_6^y$	$t_{e_5,q e_5,6}^x = (\epsilon_z - p_5l)T_6^x$	$t_{e_5,17e_5,6}^y = (\epsilon_z - p_5l)T_6^y$
$t_{e_5,q e_5,p}^z = (\epsilon_x - n_5l)Z_p^x$	$t_{e_5,q e_5,13}^x = (\epsilon_z - p_5l)T_q^x$	$t_{e_5,r e_5,q}^y = (\epsilon_z - p_5l)T_q^y$
$t_{e_5,6e_5,p}^z = (\epsilon_x - n_5l)Z_p^x$	$t_{e_5,6e_5,13}^x = (\epsilon_z - p_5l)T_6^x$	
$t_{e_5,13e_5,17}^z = (\epsilon_x - n_5l)Z_{17}^x$	$t_{e_5,p e_5,17}^x = (\epsilon_z - p_5l)T_p^x$	
$t_{e_5,r e_5,17}^z = (\epsilon_x - n_5l)Z_r^x$	$t_{e_5,r e_5,17}^x = (\epsilon_y - \delta_e - m_5l)F_r^x$	
$t_{e_5,r e_5,13}^z = (\epsilon_x - n_5l)Z_r^x$	$t_{e_5,r e_5,p}^x = (\epsilon_z - p_5l)T_p^x$	

$$6) V''_{13} = (\epsilon_x + \frac{\delta_e \sqrt{2}}{2}, \epsilon_y - \delta_e, \epsilon_z + \frac{\delta_e \sqrt{2}}{2})$$

$(V''_{13})^z$	$(V''_{13})^x$	$(V''_{13})^y$
$t_{e_{13,14}e_{13,9}}^z = (\epsilon_y - \delta_e - m_{13}l)Z_9^y$	$t_{e_{13,9}e_{13,14}}^x = (\epsilon_y - \delta_e - m_{13}l)F_9^x$	$t_{e_{13,3}e_{13,9}}^y = (\epsilon_z + \frac{\delta_e \sqrt{2}}{2} - p_{13}l)T_9^y$
$t_{e_{13,5}e_{13,14}}^z = (\epsilon_- n_{13}l)Z_5^x$	$t_{e_{13,4}e_{13,14}}^x = (\epsilon_z + \frac{\delta_e \sqrt{2}}{2} - p_{13}l)T_{14}^x$	$t_{e_{13,14}e_{13,21}}^y = (\epsilon_z + \frac{\delta_e \sqrt{2}}{2} p_{13}l)T_{14}^y$
$t_{e_{13,5}e_{13,9}}^z = (\epsilon_y - \delta_e - m_{13}l)Z_9^y$	$t_{e_{13,4}e_{13,9}}^x = (\epsilon_y - \delta_e - m_{13}l)F_9^x$	
$t_{e_{13,3}e_{13,4}}^z = (\epsilon_y - \delta_e - m_{13}l)Z_3^y$	$t_{e_{13,3}e_{13,5}}^x = (\epsilon_y - \delta_e - m_{13}l)F_3^x$	
$t_{e_{13,3}e_{13,21}}^z = (\epsilon_y - \delta_e - m_{13}l)Z_3^y$	$t_{e_{13,3}e_{13,21}}^x = (\epsilon_y - \delta_e - m_{13}l)F_3^x$	
$t_{e_{13,4}e_{13,21}}^z = (\epsilon_x - n_{13}l)Z_{21}^x$	$t_{e_{13,5}e_{13,21}}^x = (\epsilon_z + \frac{\delta_e \sqrt{2}}{2} - p_{13}l)T_5^x$	

$$7) V''_{18} = (\epsilon_x + \delta_e(2\frac{\sqrt{2}}{2} + \frac{1}{2}), \epsilon_y - \frac{\delta_e}{2}, \epsilon_z + \frac{\delta_e \sqrt{2}}{2})$$

$(V''_{18})^z$	$(V''_{18})^x$	$(V''_{18})^y$
$t_{e_{18,f}e_{18,e}}^z = (\epsilon_y - \frac{\delta_e}{2} - m_{18}l)Z_f^y$	$t_{e_{18,f}e_{18,e}}^x = (\epsilon_y - \frac{\delta_e}{2} - m_{18}l)F_f^x$	$t_{e_{18,12}e_{18,f}}^y = (\epsilon_z + \frac{\delta_e \sqrt{2}}{2} - p_{18}l)T_f^y$
$t_{e_{18,e}e_{18,9}}^z = (\epsilon_x + \delta_e(2\frac{\sqrt{2}}{2} + \frac{1}{2} - n_{18}l)Z_9^x$	$t_{e_{18,d}e_{18,e}}^x = (\epsilon_z + \frac{\delta_e \sqrt{2}}{2} - p_{18}l)T_e^x$	$t_{e_{18,e}e_{18,4}}^y = (\epsilon_z + \frac{\delta_e \sqrt{2}}{2} - p_{18}l)T_e^y$
$t_{e_{18,f}e_{18,9}}^z = (\epsilon_y - \frac{\delta_e}{2} - m_{18}l)Z_f^y$	$t_{e_{18,f}e_{18,d}}^x = (\epsilon_y - \frac{\delta_e}{2} - m_{18}l)F_f^x$	
$t_{e_{18,12}e_{18,d}}^z = (\epsilon_y - \frac{\delta_e}{2} - m_{18}l)Z_{12}^y$	$t_{e_{18,12}e_{18,9}}^x = (\epsilon_y - \frac{\delta_e}{2} - m_{18}l)F_{12}^x$	
$t_{e_{18,12}e_{18,4}}^z = (\epsilon_y - \frac{\delta_e}{2} - m_{18}l)Z_{12}^y$	$t_{e_{18,12}e_{18,4}}^x = (\epsilon_y - \frac{\delta_e}{2} - m_{18}l)F_{12}^x$	
$t_{e_{18,d}e_{18,4}}^z = (\epsilon_x + \delta_e(2\frac{\sqrt{2}}{2} + \frac{1}{2} - n_{18}l)Z_4^x$	$t_{e_{18,9}e_{18,4}}^x = (\epsilon_z + \frac{\delta_e \sqrt{2}}{2} - p_{18}l)T_9^y$	

$$8) V''_{15} = (\epsilon_x + \delta_e(\frac{\sqrt{2}}{2} - 1), \epsilon_y - \delta_e, \epsilon_z + 3\frac{\delta_e \sqrt{2}}{2})$$

$(V''_{15})^z$	$(V''_{15})^x$	$(V''_{15})^y$
$t_{e_{15,3}e_{15,a'}}^z = (\epsilon_x + \delta_e(\frac{\sqrt{2}}{2} - 1) - n_{15}l)Z_3^x$	$t_{e_{15,a'}e_{15,3}}^x = (\epsilon_y - \delta_e - m_{15}l)F_3^x$	$t_{e_{15,d'}e_{15,3}}^y = (\epsilon_x + \delta_e(\frac{\sqrt{2}}{2} - 1) - n_{15}l)F_3^y$
$t_{e_{15,f'}e_{15,a'}}^z = (\epsilon_x + \delta_e(\frac{\sqrt{2}}{2} - 1) - n_{15}l)Z_{a'}^x$	$t_{e_{15,a'}e_{15,c'}}^x = (\epsilon_z + 3\frac{\delta_e \sqrt{2}}{2} - p_{15}l)T_{a'}^x$	$t_{e_{15,a'}e_{15,e'}}^y = (\epsilon_x + \delta_e(\frac{\sqrt{2}}{2} - 1) - n_{15}l)F_{a'}^y$
$t_{e_{15,f'}e_{15,3}}^z = (\epsilon_x + \delta_e(\frac{\sqrt{2}}{2} - 1) - n_{15}l)Z_3^x$	$t_{e_{15,3}e_{15,c'}}^x = (\epsilon_y - \delta_e - m_{15}l)F_3^x$	
$t_{e_{15,d'}e_{15,c'}}^z = (\epsilon_x + \delta_e(\frac{\sqrt{2}}{2} - 1) - n_{15}l)Z_{c'}^x$	$t_{e_{15,d'}e_{15,f'}}^x = (\epsilon_y - \delta_e - m_{15}l)F_{d'}^x$	
$t_{e_{15,d'}e_{15,e'}}^z = (\epsilon_y - \delta_e - m_{15}l)Z_{d'}^y$	$t_{e_{15,d'}e_{15,e'}}^x = (\epsilon_y - \delta_e - m_{15}l)F_{d'}^x$	
$t_{e_{15,c'}e_{15,e'}}^z = (\epsilon_x + \delta_e(\frac{\sqrt{2}}{2} - 1) - n_{15}l)Z_{c'}^x$	$t_{e_{15,f'}e_{15,e'}}^x = (\epsilon_z + 3\frac{\delta_e \sqrt{2}}{2} - p_{15}l)T_{f'}^x$	

$$9) V''_{14} = (\epsilon_x + \delta_e(\frac{\delta_e \sqrt{2}}{2} + \frac{1}{2}), \epsilon_y - 3\frac{\delta_e}{2}, \epsilon_z)$$

$(V''_{14})^z$	$(V''_{14})^x$	$(V''_{14})^y$
$t_{e_{14,j}e_{9,l}}^z = (\epsilon_y - 3\frac{\sqrt{2}}{2} - m_{14}l)Z_l^y$	$t_{e_{14,j}e_{14,l}}^x = (\epsilon_z - p_{14}l)T_l^x$	$t_{e_{14,13}e_{14,l}}^y = (\epsilon_z - p_{14}l)T_l^y$
$t_{e_{14,k}e_{14,j}}^z = (\epsilon_x + \delta_e(\frac{\delta_e \sqrt{2}}{2} + \frac{1}{2}) - n_{14}l)Z_k^x$	$t_{e_{14,a}e_{14,j}}^x = (\epsilon_z - p_{14}l)T_j^x$	$t_{e_{14,h}e_{14,j}}^y = (\epsilon_z - p_{14}l)T_j^y$
$t_{e_{14,k}e_{14,l}}^z = (\epsilon_y - 3\frac{\sqrt{2}}{2} - m_{14}l)Z_l^y$	$t_{e_{14,l}e_{14,a}}^x = (\epsilon_z - p_{14}l)T_l^x$	
$t_{e_{14,a}e_{14,13}}^z = (\epsilon_y - 3\frac{\sqrt{2}}{2} - m_{14}l)Z_{13}^y$	$t_{e_{14,13}e_{14,k}}^x = (\epsilon_z - p_{14}l)T_k^x$	
$t_{e_{14,h}e_{14,13}}^z = (\epsilon_y - 3\frac{\sqrt{2}}{2} - m_{14}l)Z_{13}^y$	$t_{e_{14,13}e_{14,h}}^x = (\epsilon_y - 3\frac{\delta_e}{2} - m_{14}l)F_{13}^x$	
$t_{e_{14,h}e_{14,a}}^z = (\epsilon_x + \delta_e(\frac{\delta_e \sqrt{2}}{2} + \frac{1}{2}) - n_{14}l)Z_h^x$	$t_{e_{14,k}e_{14,h}}^x = (\epsilon_z - p_{14}l)T_k^x$	

We now need to define the off-diagonal elements of the matrix \sqrt{A}^{-1} given by $\frac{t_{e_i, e_j}}{\sqrt{t_{e_i} t_{e_j}}}$. The terms $t_{e_i} = t_{e_i}^z + t_{e_i}^x + t_{e_i}^y$ represent the total number of stacks intersected by the edge e_i in the z -, x - and y -direction

respectively. Therefore we obtain

$$t_{e_i} = \delta(\sin(\phi_{e_i}) \cos(\theta_{e_i}) + \sin(\phi_{e_i}) \sin(\theta_{e_i}) + \sin(\phi_{e_i})) = \begin{cases} \delta_e(1 + \frac{\sqrt{2}}{2}) & \text{for all edges } e_i \text{ such that } \theta_{e_i} \neq 0 \\ \delta(\sqrt{2} + 1) & \text{for those edges such that } \theta_{e_i} = 0 \end{cases} \quad (\text{A.8})$$

Throughout we will use the following short-hand notation

$$\begin{aligned} A'_i &= \frac{|x_{V_i}| - n_i}{\delta(\sqrt{\sqrt{2} + 1})} & A_i &= \frac{(|x_{V_i}| - n_i)l}{\delta_e(1 + \frac{\sqrt{2}}{2})} \\ B'_i &= \frac{(|y_{V_i}| - m_i)l}{\delta(\sqrt{\sqrt{2} + 1})} & B_i &= \frac{(|y_{V_i}| - m_i)l}{\delta_e(1 + \frac{\sqrt{2}}{2})} \\ C'_i &= \frac{(|z_{V_i}| - p_i)l}{\delta(\sqrt{\sqrt{2} + 1})} & C_i &= \frac{(|z_{V_i}| - p_i)l}{\delta_e(1 + \frac{\sqrt{2}}{2})} \end{aligned}$$

Here, $e_{k,i}$ denotes the edge starting at vertex V_i and ending at vertex V_j

We will now give the values of the upper-diagonal entries of the matrix \sqrt{A}^{-1} .

$$\begin{aligned}
(\sqrt{A}^{-1})_{2,1}^{10,20} &= \frac{-C'_0\sqrt{2}}{4} \\
(\sqrt{A}^{-1})_{6,1}^{10,70} &= \frac{-A'_0}{2} \\
(\sqrt{A}^{-1})_{5,2}^{20,50} &= \frac{-C'_0\sqrt{2}}{4} \\
(\sqrt{A}^{-1})_{9,2}^{02,32} &= \frac{-B'_2}{\sqrt{2}} \\
(\sqrt{A}^{-1})_{6,3}^{80,70} &= \frac{-C'_0}{2} \\
(\sqrt{A}^{-1})_{7,5}^{60,70} &= \frac{-B'_0}{\sqrt{2}} \\
(\sqrt{A}^{-1})_{11,7}^{102,112} &= \frac{-C_2\sqrt{2}}{4} \\
(\sqrt{A}^{-1})_{10,9}^{32,122} &= \frac{-B_2}{\sqrt{2}} \\
(\sqrt{A}^{-1})_{14,9}^{23,193} &= \frac{-A_3}{2} \\
(\sqrt{A}^{-1})_{11,10}^{122,112} &= \frac{-A'_2}{\sqrt{2}} \\
(\sqrt{A}^{-1})_{15,12}^{153,173} &= \frac{-C_3}{2} \\
(\sqrt{A}^{-1})_{39,12}^{315,c15} &= \frac{-C'_{15}\sqrt{2}}{4} \\
(\sqrt{A}^{-1})_{14,13}^{163,193} &= \frac{-B_3}{\sqrt{2}} \\
(\sqrt{A}^{-1})_{16,15}^{173,133} &= \frac{-A_3}{2} \\
(\sqrt{A}^{-1})_{29,16}^{313,913} &= \frac{-C_{13}\sqrt{2}}{4} \\
(\sqrt{A}^{-1})_{19,17}^{a4,134} &= \frac{-A'_4}{2} \\
(\sqrt{A}^{-1})_{19,18}^{184,134} &= \frac{-B'_4}{\sqrt{2}} \\
(\sqrt{A}^{-1})_{32,18}^{418,e18} &= \frac{-C_{18}\sqrt{2}}{4} \\
(\sqrt{A}^{-1})_{36,18}^{418,d18} &= \frac{-A'_4}{\sqrt{2}} \\
(\sqrt{A}^{-1})_{29,19}^{413,913} &= \frac{-B'_{13}}{2} \\
(\sqrt{A}^{-1})_{21,20}^{c4,b4} &= \frac{-A'_4}{\sqrt{2}} \\
(\sqrt{A}^{-1})_{24,23}^{65,p5} &= \frac{-A'_5}{2} \\
(\sqrt{A}^{-1})_{27,23}^{65,135} &= \frac{-C'_5\sqrt{2}}{4} \\
(\sqrt{A}^{-1})_{28,24}^{p5,r5} &= \frac{-C'_5}{2} \\
(\sqrt{A}^{-1})_{27,26}^{175,135} &= \frac{-A'_5}{\sqrt{2}} \\
(\sqrt{A}^{-1})_{29,27}^{513,913} &= \frac{-B'_{13}}{\sqrt{2}} \\
(\sqrt{A}^{-1})_{30,29}^{913,1413} &= \frac{-B_{13}}{2} \left(\frac{2}{\sqrt{2}} + 1 \right) \\
(\sqrt{A}^{-1})_{43,30}^{1314,a14} &= \frac{-B'_{14}}{\sqrt{2}} \\
(\sqrt{A}^{-1})_{34,32}^{e18,f18} &= \frac{-B_{18}}{2} \left(\frac{2}{\sqrt{2}} + 1 \right) \\
(\sqrt{A}^{-1})_{34,33}^{1218,f18} &= \frac{-C_{18}\sqrt{2}}{4} \\
(\sqrt{A}^{-1})_{35,34}^{f18,918} &= \frac{-B'_{18}}{\sqrt{2}} \\
(\sqrt{A}^{-1})_{39,37}^{e'_{15},c'_{15}} &= \frac{-A'_{15}}{2} \\
(\sqrt{A}^{-1})_{39,38}^{d'_{15},c'_{15}} &= \frac{-A'_{15}}{2} \\
(\sqrt{A}^{-1})_{41,40}^{f'_{15},a'_{15}} &= \frac{-A'_{15}}{\sqrt{2}} \\
(\sqrt{A}^{-1})_{46,42}^{k14,h14} &= \frac{-C'_{14}}{2} \\
(\sqrt{A}^{-1})_{a14,h14} &= \frac{-A'_{14}}{2}
\end{aligned}$$

$$\begin{aligned}
(\sqrt{A}^{-1})_{3,1}^{10,80} &= \frac{-C_0\sqrt{2}}{4} \\
(\sqrt{A}^{-1})_{3,2}^{20,30} &= \frac{-A'_0}{\sqrt{2}} \\
(\sqrt{A}^{-1})_{7,2}^{02,102} &= \frac{A'_2}{2} \\
(\sqrt{A}^{-1})_{11,2}^{02,112} &= \frac{-C'_2}{2} \\
(\sqrt{A}^{-1})_{5,4}^{170,60} &= \frac{-C_0\sqrt{2}}{4} \\
(\sqrt{A}^{-1})_{8,7}^{102,92} &= \frac{-B_2}{2} \left(1 + \frac{2}{\sqrt{2}} \right) \\
(\sqrt{A}^{-1})_{9,8}^{92,32} &= \frac{-C_2\sqrt{2}}{4} \\
(\sqrt{A}^{-1})_{11,9}^{32,112} &= \frac{-B_2}{2} \left(1 + \frac{2}{\sqrt{2}} \right) \\
(\sqrt{A}^{-1})_{15,9}^{23,173} &= \frac{-B_3}{\sqrt{2}} \\
(\sqrt{A}^{-1})_{13,12}^{153,163} &= \frac{-A_3}{\sqrt{2}} \\
(\sqrt{A}^{-1})_{16,12}^{153,133} &= \frac{-A_3}{2} \\
(\sqrt{A}^{-1})_{40,12}^{315,f15} &= \frac{-A'_{15}}{\sqrt{2}} \\
(\sqrt{A}^{-1})_{16,13}^{163,133} &= \frac{-C_3\sqrt{2}}{4} \\
(\sqrt{A}^{-1})_{19,16}^{313,413} &= \frac{-B'_{13}}{\sqrt{2}} \\
(\sqrt{A}^{-1})_{31,16}^{313,2113} &= \frac{-B_{13}}{2} \left(\frac{2}{\sqrt{2}} + 1 \right) \\
(\sqrt{A}^{-1})_{20,17}^{a4,c4} &= \frac{-C_4\sqrt{2}}{4} \\
(\sqrt{A}^{-1})_{21,18}^{184,b4} &= \frac{-B'_4}{2} \\
(\sqrt{A}^{-1})_{33,18}^{418,1218} &= \frac{-B_{18}}{2} \left(\frac{2}{\sqrt{2}} + 1 \right) \\
(\sqrt{A}^{-1})_{20,19}^{134,c4} &= \frac{-C'_4}{2} \\
(\sqrt{A}^{-1})_{30,19}^{413,1413} &= \frac{-C'_{13}\sqrt{2}}{2} \\
(\sqrt{A}^{-1})_{22,20}^{c4,164} &= \frac{-B_4}{2} \left(\frac{2}{\sqrt{2}} + 1 \right) \\
(\sqrt{A}^{-1})_{25,23}^{65,q5} &= \frac{-B_5}{2} - \frac{C_5\sqrt{2}}{4} \\
(\sqrt{A}^{-1})_{25,24}^{p5,q5} &= \frac{-A'_5}{2} \\
(\sqrt{A}^{-1})_{27,25}^{q5,135} &= \frac{-C'_5\sqrt{2}}{4} \\
(\sqrt{A}^{-1})_{28,26}^{175,r5} &= -\frac{A_5}{\sqrt{2}} - \frac{B_5}{2} \\
(\sqrt{A}^{-1})_{30,27}^{513,1413} &= \frac{-C'_{13}\sqrt{2}}{4} \\
(\sqrt{A}^{-1})_{31,30}^{1413,2113} &= \frac{-C_{13}\sqrt{2}}{4} \\
(\sqrt{A}^{-1})_{44,30}^{1314,l14} &= \frac{-C_{14}\sqrt{2}}{4} \\
(\sqrt{A}^{-1})_{35,32}^{e18,918} &= \frac{-A'_{18}}{2} \\
(\sqrt{A}^{-1})_{35,33}^{1218,918} &= \frac{-B'_{18}}{2} \\
(\sqrt{A}^{-1})_{36,34}^{f18,d18} &= \frac{-B'_{18}}{2} \\
(\sqrt{A}^{-1})_{40,37}^{e'_{15},f'_{15}} &= \frac{-C'_{15}}{2} \\
(\sqrt{A}^{-1})_{40,38}^{d'_{15},f'_{15}} &= \frac{-B'_{15}}{2} \\
(\sqrt{A}^{-1})_{44,42}^{k14,l14} &= \frac{-B'_{14}}{\sqrt{2}} \\
(\sqrt{A}^{-1})_{44,43}^{a14,l14} &= \frac{-C_{14}\sqrt{2}}{4} \\
(\sqrt{A}^{-1})_{l14,j14} &= \frac{C_{14}\sqrt{2}}{2} B_{14}
\end{aligned}$$

$$\begin{aligned}
(\sqrt{A}^{-1})_{5,1}^{10,60} &= \frac{-C_0\sqrt{2}}{4} - \frac{B_0}{\sqrt{2}} \\
(\sqrt{A}^{-1})_{4,2}^{20,40} &= \frac{-B'_0}{\sqrt{2}} \\
(\sqrt{A}^{-1})_{8,2}^{02,92} &= \frac{-B'_2}{\sqrt{2}} \\
(\sqrt{A}^{-1})_{4,3}^{80,170} &= \frac{-B_0}{2} \left(1 + \frac{2}{\sqrt{2}} \right) \\
(\sqrt{A}^{-1})_{6,4}^{170,70} &= \frac{-C'_0}{2} \\
(\sqrt{A}^{-1})_{10,7}^{102,122} &= \frac{-C'_2\sqrt{2}}{4} \\
(\sqrt{A}^{-1})_{10,8}^{92,122} &= \frac{-B'_2}{2} \\
(\sqrt{A}^{-1})_{13,9}^{23,163} &= \frac{-B_3}{2} \\
(\sqrt{A}^{-1})_{16,9}^{23,133} &= \frac{-B_3}{2} \left(\frac{2}{\sqrt{2}} + 1 \right) \\
(\sqrt{A}^{-1})_{14,12}^{153,193} &= \frac{-B_3}{2} \left(\frac{2}{\sqrt{2}} + 1 \right) \\
(\sqrt{A}^{-1})_{38,12}^{315,d15} &= \frac{-A_{15}}{2} \\
(\sqrt{A}^{-1})_{41,12}^{315,a15} &= -\frac{B_{15}}{2} - \frac{A_{15}}{\sqrt{2}} \\
(\sqrt{A}^{-1})_{15,14}^{193,173} &= \frac{-B_3}{2} \\
(\sqrt{A}^{-1})_{27,16}^{313,513} &= \frac{-B'_{13}}{2} \\
(\sqrt{A}^{-1})_{18,17}^{a4,184} &= \frac{-B_4}{2} \left(\frac{2}{\sqrt{2}} + 1 \right) \\
(\sqrt{A}^{-1})_{21,17}^{a4,b4} &= \frac{-C'_4\sqrt{2}}{4} \\
(\sqrt{A}^{-1})_{22,18}^{184,164} &= \frac{-A_4}{2} \\
(\sqrt{A}^{-1})_{35,18}^{418,918} &= \frac{-C'_{18}}{2} \\
(\sqrt{A}^{-1})_{22,19}^{134,164} &= \frac{-B'_4}{4} \\
(\sqrt{A}^{-1})_{31,19}^{413,2113} &= \frac{-B_{13}}{2} \left(\frac{2}{\sqrt{2}} + 1 \right) \\
(\sqrt{A}^{-1})_{22,21}^{b4,164} &= \frac{-B'_4}{\sqrt{2}} \\
(\sqrt{A}^{-1})_{26,23}^{65,175} &= \frac{-C_5\sqrt{2}}{4} \\
(\sqrt{A}^{-1})_{26,24}^{p5,175} &= \frac{-C'_5}{2} \\
(\sqrt{A}^{-1})_{28,25}^{q5,r5} &= \frac{-C_5\sqrt{2}}{4} \\
(\sqrt{A}^{-1})_{28,27}^{135,r5} &= \frac{-A'_5}{\sqrt{2}} \\
(\sqrt{A}^{-1})_{31,27}^{513,2113} &= \frac{-C'_{13}}{2} \\
(\sqrt{A}^{-1})_{42,30}^{1314,k14} &= \frac{-C'_{14}}{2} \\
(\sqrt{A}^{-1})_{46,30}^{1314,l14} &= \frac{-B_{14}}{2} \left(\frac{2}{\sqrt{2}} + 1 \right) \\
(\sqrt{A}^{-1})_{36,32}^{e18,d18} &= \frac{-C'_{18}\sqrt{2}}{4} \\
(\sqrt{A}^{-1})_{36,33}^{1218,d18} &= \frac{-B'_{18}}{\sqrt{2}} \\
(\sqrt{A}^{-1})_{38,37}^{e'_{15},d'_{15}} &= \frac{-B_{15}}{2} \left(\frac{2}{\sqrt{2}} + 1 \right) \\
(\sqrt{A}^{-1})_{41,37}^{e'_{15},a'_{15}} &= \frac{-A_{15}}{2} \\
(\sqrt{A}^{-1})_{41,39}^{c'_{15},a'_{15}} &= \frac{-C'_{15}\sqrt{2}}{2} \\
(\sqrt{A}^{-1})_{45,42}^{k14,j14} &= \frac{-A'_{14}}{2} \\
(\sqrt{A}^{-1})_{45,43}^{a14,j14} &= \frac{-C'_{14}\sqrt{2}}{4} \\
(\sqrt{A}^{-1})_{j14,h14} &= -C_{14}\sqrt{2}
\end{aligned}$$

A.3 Edge-metric components for the 8-valent graph

In this Section we give the values for the terms $\frac{t_{e_i,j}e_{i,j}}{\sqrt{t_{e_i,j}t_{e_i,j}}}$ for the 8-valent graph as computed for aligned, rotated, and translated graphs respectively.

A.3.1 Aligned 8-valent graph

For the case of an 8-valent graph, the periodicity cell contains five vertices, therefore \sqrt{A}^{-1} is a 36×36 matrix. Below we give the non-zero upper-diagonal elements of the matrix \sqrt{A}^{-1} . The lower indices refer to the matrix elements while, the upper indices, indicate which edges we are taking into consideration.

$$\begin{aligned}
(\sqrt{A}^{-1})_{10,1}^{01,131} &= -\beta & (\sqrt{A}^{-1})_{11,1}^{01,121} &= -\frac{1}{2}\beta & (\sqrt{A}^{-1})_{12,1}^{01,111} &= -\beta \\
(\sqrt{A}^{-1})_{13,1}^{01,91} &= -\frac{1}{2}\beta & (\sqrt{A}^{-1})_{14,1}^{01,151} &= -\beta & (\sqrt{A}^{-1})_{15,1}^{01,101} &= -\frac{1}{2}\beta \\
(\sqrt{A}^{-1})_{10,9}^{141,131} &= -\frac{1}{2}\beta & (\sqrt{A}^{-1})_{11,9}^{141,121} &= -\beta & (\sqrt{A}^{-1})_{12,9}^{141,111} &= -\frac{1}{2}\beta \\
(\sqrt{A}^{-1})_{13,9}^{141,91} &= -\beta & (\sqrt{A}^{-1})_{14,9}^{141,151} &= -\beta & (\sqrt{A}^{-1})_{15,9}^{141,101} &= -\beta \\
(\sqrt{A}^{-1})_{11,10}^{131,121} &= -\frac{1}{2}\beta & (\sqrt{A}^{-1})_{12,10}^{131,111} &= -\beta & (\sqrt{A}^{-1})_{14,10}^{131,151} &= -\beta \\
(\sqrt{A}^{-1})_{15,10}^{131,101} &= -\frac{1}{2}\beta & (\sqrt{A}^{-1})_{12,11}^{121,111} &= -\frac{1}{2}\beta & (\sqrt{A}^{-1})_{13,11}^{-1} &= -\beta \\
(\sqrt{A}^{-1})_{14,11}^{121,91} &= -\beta & (\sqrt{A}^{-1})_{16,11}^{101,91} &= -\beta & (\sqrt{A}^{-1})_{23,11}^{112,m12} &= -\beta \\
(\sqrt{A}^{-1})_{24,11}^{112,a12} &= -2\beta & (\sqrt{A}^{-1})_{28,11}^{112,e12} &= -2\beta & (\sqrt{A}^{-1})_{13,12}^{111,91} &= -\frac{1}{2}\beta \\
(\sqrt{A}^{-1})_{14,12}^{111,151} &= -\beta & (\sqrt{A}^{-1})_{14,13}^{91,151} &= -\frac{1}{2}\beta & (\sqrt{A}^{-1})_{15,13}^{91,101} &= -\beta \\
(\sqrt{A}^{-1})_{16,13}^{19,a9} &= -\beta & (\sqrt{A}^{-1})_{15,14}^{151,101} &= -\frac{1}{2}\beta & (\sqrt{A}^{-1})_{18,17}^{49,b9} &= -\beta \\
(\sqrt{A}^{-1})_{20,19}^{59,c9} &= -\beta & (\sqrt{A}^{-1})_{22,21}^{69,d9} &= -\beta & (\sqrt{A}^{-1})_{24,23}^{m12,a12} &= -2\beta \\
(\sqrt{A}^{-1})_{28,23}^{m12,e12} &= -2\beta & (\sqrt{A}^{-1})_{28,24}^{a12,e12} &= -\beta & (\sqrt{A}^{-1})_{26,25}^{b12,412} &= -2\beta \\
(\sqrt{A}^{-1})_{27,25}^{b12,h12} &= -\beta & (\sqrt{A}^{-1})_{29,25}^{b12,k12} &= -2\beta & (\sqrt{A}^{-1})_{27,26}^{412,h12} &= -2\beta \\
(\sqrt{A}^{-1})_{29,26}^{412,k12} &= -\beta & (\sqrt{A}^{-1})_{29,27}^{h12,k12} &= -2\beta & (\sqrt{A}^{-1})_{31,30}^{11e,12e} &= -\beta \\
(\sqrt{A}^{-1})_{32,30}^{11e,14e} &= -\frac{1}{2}\beta & (\sqrt{A}^{-1})_{33,30}^{11e,pe} &= -2\beta & (\sqrt{A}^{-1})_{34,30}^{11e,qe} &= -\frac{1}{2}\beta \\
(\sqrt{A}^{-1})_{36,30}^{11e,ge} &= -\frac{1}{2}\beta & (\sqrt{A}^{-1})_{32,31}^{13e,14e} &= -\beta & (\sqrt{A}^{-1})_{33,31}^{13e,pe} &= -\frac{1}{2}\beta \\
(\sqrt{A}^{-1})_{34,31}^{13e,qe} &= -\beta & (\sqrt{A}^{-1})_{35,31}^{13e,re} &= -\frac{1}{2}\beta & (\sqrt{A}^{-1})_{34,32}^{14e,qe} &= -\frac{1}{2}\beta \\
(\sqrt{A}^{-1})_{35,32}^{14e,re} &= -2\beta & (\sqrt{A}^{-1})_{36,32}^{14e,ge} &= -\frac{1}{2}\beta & (\sqrt{A}^{-1})_{34,33}^{pe,qe} &= -\beta \\
(\sqrt{A}^{-1})_{35,33}^{pe,re} &= -\frac{1}{2}\beta & (\sqrt{A}^{-1})_{36,33}^{pe,ge} &= -\beta & (\sqrt{A}^{-1})_{35,34}^{qe,re} &= -\beta \\
(\sqrt{A}^{-1})_{36,34}^{qe,ge} &= -\frac{1}{2}\beta & (\sqrt{A}^{-1})_{36,35}^{re,ge} &= -\beta & &
\end{aligned}$$

where $\beta = \frac{(\frac{\delta}{\sqrt{3}}-nl)}{\delta\sqrt{3}}$.

A.3.2 Rotated 8-Valent graph

In this Section we give the values of all the terms $\frac{t_{e_{k,i}}e_{k,j}}{\sqrt{t_{e_{k,i}}t_{e_{k,j}}}}$ that appear in the matrix \sqrt{A}^{-1} for the rotated 8-valent graph. As in the aligned case, the matrix \sqrt{A}^{-1} is a 36×36 matrix labelled by the edges of the five vertices that comprise the periodicity cell. The following short-hand notation is used: $\mu_{k_i,k_j} = \frac{t_{e_{k,i}}e_{k,j}}{\sqrt{t_{e_{k,i}}t_{e_{k,j}}}}$ which is defined in a similar manner as that done for the 4, and 6-valent graphs.

The elements of the upper-half of the matrix \sqrt{A}^{-1} are:

$$\begin{aligned}
(\sqrt{A})_{11,1}^{-1} &= -\frac{1}{2}\mu_{12,0_1} & (\sqrt{A})_{12,1}^{-1} &= -\frac{1}{2}\mu_{11,0_1} & (\sqrt{A})_{10,1}^{-1} &= -\frac{1}{2}\mu_{13,0_1} \\
(\sqrt{A})_{13,1}^{-1} &= -\frac{1}{2}\mu_{9_1,0_1} & (\sqrt{A})_{15,1}^{-1} &= -\frac{1}{2}\mu_{10,0_1} & (\sqrt{A})_{15,1}^{-1} &= -\frac{1}{2}\mu_{15,0_1} \\
(\sqrt{A})_{12,11}^{-1} &= -\frac{1}{2}\mu_{11_1,12_1} & (\sqrt{A})_{10,9}^{-1} &= -\frac{1}{2}\mu_{13,14_1} & (\sqrt{A})_{11,9}^{-1} &= -\frac{1}{2}\mu_{14,12_1} \\
(\sqrt{A})_{13,11}^{-1} &= -\frac{1}{2}\mu_{9_1,12_1} & (\sqrt{A})_{15,11}^{-1} &= -\frac{1}{2}\mu_{10_1,12_1} & (\sqrt{A})_{27,11}^{-1} &= -\frac{1}{2}\mu_{4_{12},1_{12}} \\
(\sqrt{A})_{24,11}^{-1} &= -\frac{1}{2}\mu_{a_{12},1_{12}} & (\sqrt{A})_{25,11}^{-1} &= -\frac{1}{2}\mu_{b_{12},1_{12}} & (\sqrt{A})_{28,11}^{-1} &= -\frac{1}{2}\mu_{e_{12},1_{12}} \\
(\sqrt{A})_{27,11}^{-1} &= -\frac{1}{2}\mu_{h_{12},1_{12}} & (\sqrt{A})_{23,11}^{-1} &= -\frac{1}{2}\mu_{m_{12},1_{12}} & (\sqrt{A})_{12,10}^{-1} &= -\frac{1}{2}\mu_{13_1,11_1} \\
(\sqrt{A})_{9,12}^{-1} &= -\frac{1}{2}\mu_{14_1,11_1} & (\sqrt{A})_{13,12}^{-1} &= -\frac{1}{2}\mu_{9_1,11_1} & (\sqrt{A})_{14,12}^{-1} &= -\frac{1}{2}\mu_{15_1,11_1} \\
(\sqrt{A})_{36,32}^{-1} &= -\frac{1}{2}\mu_{14_e,g_e} & (\sqrt{A})_{10,9}^{-1} &= -\frac{1}{2}\mu_{14_1,13_1} & (\sqrt{A})_{15,10}^{-1} &= -\frac{1}{2}\mu_{10_1,13_1} \\
(\sqrt{A})_{14,10}^{-1} &= -\frac{1}{2}\mu_{15_1,13_1} & (\sqrt{A})_{13,9}^{-1} &= -\frac{1}{2}\mu_{9_1,14_1} & (\sqrt{A})_{15,9}^{-1} &= -\frac{1}{2}\mu_{10_1,14_1} \\
(\sqrt{A})_{14,9}^{-1} &= -\frac{1}{2}\mu_{15_1,14_1} & (\sqrt{A})_{15,13}^{-1} &= -\frac{1}{2}\mu_{10_1,9_1} & (\sqrt{A})_{14,15}^{-1} &= -\frac{1}{2}\mu_{15_1,9_1} \\
(\sqrt{A})_{17,13}^{-1} &= -\frac{1}{2}\mu_{4_9,1_9} & (\sqrt{A})_{16,13}^{-1} &= -\frac{1}{2}\mu_{a_9,1_9} & (\sqrt{A})_{18,13}^{-1} &= -\frac{1}{2}\mu_{b_9,1_9} \\
(\sqrt{A})_{21,13}^{-1} &= -\frac{1}{2}\mu_{6_9,1_9} & (\sqrt{A})_{19,13}^{-1} &= -\frac{1}{2}\mu_{5_9,1_9} & (\sqrt{A})_{22,13}^{-1} &= -\frac{1}{2}\mu_{d_9,1_9} \\
(\sqrt{A})_{15,14}^{-1} &= -\frac{1}{2}\mu_{15_1,10_1} & (\sqrt{A})_{17,16}^{-1} &= -\frac{1}{2}\mu_{a_9,4_9} & (\sqrt{A})_{18,17}^{-1} &= -\frac{1}{2}\mu_{b_9,4_9} \\
(\sqrt{A})_{21,17}^{-1} &= -\frac{1}{2}\mu_{6_9,4_9} & (\sqrt{A})_{19,17}^{-1} &= -\frac{1}{2}\mu_{5_9,4_9} & (\sqrt{A})_{20,17}^{-1} &= -\frac{1}{2}\mu_{c_9,4_9} \\
(\sqrt{A})_{18,16}^{-1} &= -\frac{1}{2}\mu_{b_9,a_9} & (\sqrt{A})_{21,16}^{-1} &= -\frac{1}{2}\mu_{6_9,a_9} & (\sqrt{A})_{22,16}^{-1} &= -\frac{1}{2}\mu_{d_9,a_9} \\
(\sqrt{A})_{20,16}^{-1} &= -\frac{1}{2}\mu_{c_9,a_9} & (\sqrt{A})_{19,18}^{-1} &= -\frac{1}{2}\mu_{5_9,b_9} & (\sqrt{A})_{22,18}^{-1} &= -\frac{1}{2}\mu_{d_9,b_9} \\
(\sqrt{A})_{20,18}^{-1} &= -\frac{1}{2}\mu_{c_9,b_9} & (\sqrt{A})_{21,19}^{-1} &= -\frac{1}{2}\mu_{5_9,6_9} & (\sqrt{A})_{22,21}^{-1} &= -\frac{1}{2}\mu_{d_9,6_9} \\
(\sqrt{A})_{21,22}^{-1} &= -\frac{1}{2}\mu_{c_9,6_9} & (\sqrt{A})_{22,19}^{-1} &= -\frac{1}{2}\mu_{d_9,5_9} & (\sqrt{A})_{20,19}^{-1} &= -\frac{1}{2}\mu_{c_9,5_9} \\
(\sqrt{A})_{22,20}^{-1} &= -\frac{1}{2}\mu_{c_9,d_9} & (\sqrt{A})_{32,31}^{-1} &= -\frac{1}{2}\mu_{13_e,14_e} & (\sqrt{A})_{30,28}^{-1} &= -\frac{1}{2}\mu_{12_e,11_e} \\
(\sqrt{A})_{33,30}^{-1} &= -\frac{1}{2}\mu_{p_e,11_e} & (\sqrt{A})_{34,30}^{-1} &= -\frac{1}{2}\mu_{q_e,11_e} & (\sqrt{A})_{36,30}^{-1} &= -\frac{1}{2}\mu_{g_e,11_e} \\
(\sqrt{A})_{32,30}^{-1} &= -\frac{1}{2}\mu_{14_e,11_e} & (\sqrt{A})_{31,30}^{-1} &= -\frac{1}{2}\mu_{13_e,11_e} & (\sqrt{A})_{26,24}^{-1} &= -\frac{1}{2}\mu_{a_{12},4_{12}} \\
(\sqrt{A})_{26,25}^{-1} &= -\frac{1}{2}\mu_{b_{12},4_{12}} & (\sqrt{A})_{28,26}^{-1} &= -\frac{1}{2}\mu_{e_{12},4_{12}} & (\sqrt{A})_{27,26}^{-1} &= -\frac{1}{2}\mu_{h_{12},4_{12}} \\
(\sqrt{A})_{29,26}^{-1} &= -\frac{1}{2}\mu_{k_{12},4_{12}} & (\sqrt{A})_{25,24}^{-1} &= -\frac{1}{2}\mu_{b_{12},a_{12}} & (\sqrt{A})_{28,24}^{-1} &= -\frac{1}{2}\mu_{e_{12},a_{12}} \\
(\sqrt{A})_{29,33}^{-1} &= -\frac{1}{2}\mu_{m_{12},a_{12}} & (\sqrt{A})_{29,24}^{-1} &= -\frac{1}{2}\mu_{k_{12},a_{12}} & (\sqrt{A})_{27,25}^{-1} &= -\frac{1}{2}\mu_{h_{12},b_{12}} \\
(\sqrt{A})_{25,23}^{-1} &= -\frac{1}{2}\mu_{m_{12},b_{12}} & (\sqrt{A})_{29,25}^{-1} &= -\frac{1}{2}\mu_{b_{12},k_{12}} & (\sqrt{A})_{28,27}^{-1} &= -\frac{1}{2}\mu_{h_{12},e_{12}} \\
(\sqrt{A})_{28,23}^{-1} &= -\frac{1}{2}\mu_{m_{12},e_{12}} & (\sqrt{A})_{29,28}^{-1} &= -\frac{1}{2}\mu_{k_{12},e_{12}} & (\sqrt{A})_{35,28}^{-1} &= -\frac{1}{2}\mu_{r_e,12_e} \\
(\sqrt{A})_{33,28}^{-1} &= -\frac{1}{2}\mu_{p_e,12_e} & (\sqrt{A})_{36,23}^{-1} &= -\frac{1}{2}\mu_{g_e,12_e} & (\sqrt{A})_{32,28}^{-1} &= -\frac{1}{2}\mu_{14_e,12_e} \\
(\sqrt{A})_{31,28}^{-1} &= -\frac{1}{2}\mu_{13_e,12_e} & (\sqrt{A})_{27,23}^{-1} &= -\frac{1}{2}\mu_{m_{12},h_{12}} & (\sqrt{A})_{29,27}^{-1} &= -\frac{1}{2}\mu_{k_{12},h_{12}} \\
(\sqrt{A})_{29,23}^{-1} &= -\frac{1}{2}\mu_{k_{12},m_{12}} & (\sqrt{A})_{35,33}^{-1} &= -\frac{1}{2}\mu_{p_e,r_e} & (\sqrt{A})_{35,34}^{-1} &= -\frac{1}{2}\mu_{q_e,r_e} \\
(\sqrt{A})_{36,35}^{-1} &= -\frac{1}{2}\mu_{g_e,r_e} & (\sqrt{A})_{35,32}^{-1} &= -\frac{1}{2}\mu_{14_e,r_e} & (\sqrt{A})_{35,31}^{-1} &= -\frac{1}{2}\mu_{13_e,r_e} \\
(\sqrt{A})_{34,33}^{-1} &= -\frac{1}{2}\mu_{q_e,p_e} & (\sqrt{A})_{36,33}^{-1} &= -\frac{1}{2}\mu_{g_e,p_e} & (\sqrt{A})_{33,31}^{-1} &= -\frac{1}{2}\mu_{13_e,p_e} \\
(\sqrt{A})_{36,33}^{-1} &= -\frac{1}{2}\mu_{g_e,q_e} & (\sqrt{A})_{34,32}^{-1} &= -\frac{1}{2}\mu_{14_e,q_e} & (\sqrt{A})_{34,31}^{-1} &= -\frac{1}{2}\mu_{13_e,q_e}
\end{aligned}$$

A.3.3 Translated 8-valent graph

In this Section we will first give the values of all the terms $t_{e_i e_j} = t_{e_i e_j}^x + t_{e_i e_j}^y + t_{e_i e_j}^z$ as computed for all the five vertices comprising the periodicity cell for the 8-valent graph. We then give the values for the terms $\frac{t_{e_i, k} e_{j, k}}{\sqrt{t_{e_i, k} t_{e_j, k}}}$ that appear in the matrix \sqrt{A}^{-1} . As for the aligned case, the matrix \sqrt{A}^{-1} is a 36×36 matrix labelled by the edges of the five vertices that comprise the periodicity cell.

The values for $t_{e_i e_j}$ are listed below. The (Gauss brackets) terms $n_i = [\frac{V_i^x}{t}]$, $m_i = [\frac{V_i^y}{t}]$ and $p_i = [\frac{V_i^z}{t}]$ are the number of stacks that each edge e_i intersects in the x -, y - and z -direction respectively (see Section 3.1)

1) $V_0'' = (\epsilon_x, \epsilon_y, \epsilon_z)$

$(V_0'')^z$	$(V_0'')^x$	$(V_0'')^y$
$t_{e_0,5e_0,6}^z = t_{e_0,5e_0,7}^z =$	$t_{e_0,5e_0,7}^x = t_{e_0,5e_0,4}^x$	$t_{e_0,5e_0,6}^y = t_{e_0,5e_0,4}^y =$
$t_{e_0,8e_0,6}^z = t_{e_0,5e_0,8}^z =$	$t_{e_0,5e_0,3}^x = t_{e_0,4e_0,7}^x$	$t_{e_0,4e_0,6}^y = t_{e_0,5e_0,1}^y =$
$t_{e_0,3e_0,1}^z = t_{e_0,7e_0,6}^z =$	$t_{e_0,7e_0,3}^x = t_{e_0,6e_0,8}^x$	$t_{e_0,6e_0,1}^y = t_{e_0,8e_0,7}^y =$
$t_{e_0,4e_0,3}^z = t_{e_0,4e_0,2}^z =$	$t_{e_0,6e_0,1}^x = t_{e_0,6e_0,2}^x$	$t_{e_0,8e_0,3}^y = t_{e_0,8e_0,2}^y =$
$t_{e_0,2e_0,1}^z = t_{e_0,1e_0,4}^z = (\epsilon_y - m_0 l)$	$t_{e_0,8e_0,1}^x = t_{e_0,8e_0,2}^x = (\epsilon_z - p_0 l)$	$t_{e_0,7e_0,3}^y = t_{e_0,7e_0,2}^y = (\epsilon_z - p_0 l)$
$t_{e_0,3e_0,2}^z = t_{e_0,7e_0,8}^z = (\epsilon_x - n_0 l)$	$t_{e_0,1e_0,2}^x = t_{e_0,4e_0,3}^x = (\epsilon_y - m_0 l)$	$t_{e_0,2e_0,3}^y = t_{e_0,4e_0,1}^y = (\epsilon_x - n_0 l)$

$$2) V_1'' = (\epsilon_x - \frac{\delta_e \sqrt{2}}{2}, \epsilon_y - \frac{\delta_e \sqrt{2}}{2}, \epsilon_z + \frac{\delta_e \sqrt{2}}{2})$$

$(V_1'')^z$	$(V_1'')^x$	$(V_1'')^y$
$t_{e_1,11e_1,13}^z = t_{e_1,9e_1,0}^z =$	$t_{e_1,9e_1,0}^x = t_{e_1,14e_1,13}^x$	$t_{e_1,9e_1,10}^y = t_{e_1,9e_1,12}^y =$
$t_{e_1,15e_1,10}^z = t_{e_1,9e_1,15}^z =$	$t_{e_1,9e_1,11}^x = t_{e_1,12e_1,0}^x$	$t_{e_1,12e_1,10}^y = t_{e_1,9e_1,14}^y =$
$t_{e_1,11e_1,14}^z = t_{e_1,0e_1,10}^z =$	$t_{e_1,0e_1,11}^x = t_{e_1,10e_1,15}^x$	$t_{e_1,12e_1,14}^y = t_{e_1,15e_1,0}^y =$
$t_{e_1,12e_1,11}^z = t_{e_1,12e_1,13}^z =$	$t_{e_1,12e_1,11}^x = t_{e_1,10e_1,13}^x$	$t_{e_1,15e_1,11}^y = t_{e_1,13e_1,11}^y =$
$t_{e_1,13e_1,14}^z = t_{e_1,0e_1,15}^z = (\epsilon_y - \frac{\delta}{\sqrt{3}} - m_1 l)$	$t_{e_1,15e_1,14}^x = t_{e_1,15e_1,13}^x = (\epsilon_y - \frac{\delta}{\sqrt{3}} - m_1 l)$	$t_{e_1,0e_1,11}^y = t_{e_1,0e_1,13}^y =$
$t_{e_1,9e_1,10}^z = t_{e_1,14e_1,12}^z = (\epsilon_x - \frac{\delta}{\sqrt{3}} - n_1 l)$	$t_{e_1,9e_1,12}^x = t_{e_1,10e_1,14}^x = (\epsilon_x - \frac{\delta}{\sqrt{3}} - n_1 l)$	$= (\epsilon_x - \frac{\delta}{\sqrt{3}} - n_1 l)$
		$t_{e_1,15e_1,13}^y = t_{e_1,10e_1,14}^y =$
		$= (\epsilon_z + \frac{\delta}{\sqrt{3}} - m_1 l)$

$$3) V_9'' = (\epsilon_x, \epsilon_y - 2\frac{\delta_e \sqrt{2}}{2}, \epsilon_z + \frac{\delta_e \sqrt{2}}{2})$$

$(V_9'')^z$	$(V_9'')^x$	$(V_9'')^y$
$t_{e_9,4e_9,1}^z = t_{e_9,ce_9,5}^z =$	$t_{e_9,ce_9,5}^x = t_{e_9,ae_9,1}^x$	$t_{e_9,ce_9,d}^y = t_{e_9,ce_9,b}^y =$
$t_{e_9,6e_9,d}^z = t_{e_9,ce_9,6}^z =$	$t_{e_9,ce_9,4}^x = t_{e_9,be_9,5}^x$	$t_{e_9,be_9,d}^y = t_{e_9,ce_9,a}^y =$
$t_{e_9,4e_9,a}^z = t_{e_9,5e_9,d}^z =$	$t_{e_9,5e_9,4}^x = t_{e_9,de_9,6}^x$	$t_{e_9,be_9,a}^y = t_{e_9,6e_9,5}^y =$
$t_{e_9,6e_9,4}^z = t_{e_9,be_9,1}^z =$	$t_{e_9,6e_9,4}^x = t_{e_9,de_9,1}^x$	$t_{e_9,6e_9,4}^y = t_{e_9,6e_9,1}^y =$
$t_{e_9,1e_9,a}^z = t_{e_9,5e_9,6}^z = (\epsilon_y - 2\frac{\delta}{\sqrt{3}} - m_9 l)$	$t_{e_9,6e_9,a}^x = t_{e_9,6e_9,1}^x = (\epsilon_y - 2\frac{\delta}{\sqrt{3}} - m_9 l)$	$t_{e_9,5e_9,4}^y = t_{e_9,5e_9,1}^y = (\epsilon_z - p_9 l)$
$t_{e_9,ce_9,d}^z = t_{e_9,ae_9,b}^z = (\epsilon_x - n_9 l)$	$t_{e_9,ce_9,b}^x = t_{e_9,de_9,a}^x = (\epsilon_z - p_9 l)$	$t_{e_9,de_9,a}^y = t_{e_9,1e_9,4}^y = (\epsilon_x - n_9 l)$

$$4) V_{12}'' = (\epsilon_x, \epsilon_y - \frac{\delta_e \sqrt{2}}{2}, \epsilon_z + 2\frac{\delta_e \sqrt{2}}{2})$$

$(V_{12}'')^z$	$(V_{12}'')^x$	$(V_{12}'')^y$
$t_{e_{12},be_{12},a}^z = t_{e_{12},4e_{12},1}^z =$	$t_{e_{12},be_{12},4}^x = t_{e_{12},me_{12},e}^x$	$t_{e_{12},be_{12},a}^y = t_{e_{12},e_{12},h}^y =$
$t_{e_{12},1e_{12},a}^z = t_{e_{12},be_{12},1}^z =$	$t_{e_{12},b_{12},h}^x = t_{e_{12},ke_{12},4}^x$	$t_{e_{12},ke_{12},a}^y = t_{e_{12},be_{12},m}^y =$
$t_{e_{12},he_{12},m}^z = t_{e_{12},4e_{12},a}^z =$	$t_{e_{12},4e_{12},h}^x = t_{e_{12},ae_{12},1}^x$	$t_{e_{12},ae_{12},m}^y = t_{e_{12},1e_{12},4}^y =$
$t_{e_{12},he_{12},e}^z = t_{e_{12},ke_{12},e}^z =$	$t_{e_{12},ke_{12},h}^x = t_{e_{12},ae_{12},e}^x$	$t_{e_{12},1e_{12},h}^y = t_{e_{12},1e_{12},e}^y =$
$t_{e_{12},e_{12},m}^z = t_{e_{12},me_{12},k}^z = (\epsilon_x - n_1 2l)$	$t_{e_{12},1e_{12},m}^x = t_{e_{12},1e_{12},e}^x = (\epsilon_y - 2\frac{\delta}{\sqrt{3}} - m_1 2l)$	$t_{e_{12},ke_{12},m}^y = t_{e_{12},4e_{12},e}^y =$
$t_{e_{12},ke_{12},h}^z = t_{e_{12},be_{12},4}^z = (\epsilon_y - 2\frac{\delta}{\sqrt{3}} - m_1 2l)$	$t_{e_{12},be_{12},k}^x = t_{e_{12},ae_{12},m}^x = (\epsilon_z + 2\frac{\delta}{\sqrt{3}} - p_1 2l)$	$= (\epsilon_x - n_1 2l)$
		$t_{e_{12},be_{12},k}^y = t_{e_{12},4e_{12},h}^y =$
		$(\epsilon_z + 2\frac{\delta}{\sqrt{3}} - p_1 2l)$

$$5) V_e'' = (\epsilon_x - \frac{\delta_e \sqrt{2}}{2}, \epsilon_y - \frac{\delta_e \sqrt{2}}{2}, \epsilon_z + 3\frac{\delta_e \sqrt{2}}{2})$$

$(V_e'')^z$	$(V_e'')^x$	$(V_e'')^y$
$t_{e_e,p e_e,q}^z = t_{e_e,12 e_e,11}^z =$	$t_{e_e,12 e_e,11}^x = t_{e_e,r e_e,q}^x$	$t_{e_e,12 e_e,14}^y = t_{e_e,12 e_e,g}^y =$
$t_{e_e,13 e_e,14}^z = t_{e_e,12 e_e,13}^z =$	$t_{e_e,12 e_e,p}^x = t_{e_e,g e_e,11}^x$	$t_{e_e,g e_e,14}^y = t_{e_e,12 e_e,r}^y =$
$t_{e_e,p e_e,r}^z = t_{e_e,11 e_e,14}^z$	$t_{e_e,11 e_e,p}^x = t_{e_e,14 e_e,13}^x$	$t_{e_e,g e_e,r}^y = t_{e_e,13 e_e,11}^y =$
$t_{e_e,g e_e,p}^z = t_{e_e,g e_e,q}^z =$	$t_{e_e,g e_e,p}^x = t_{e_e,14 e_e,q}^x$	$t_{e_e,13 e_e,p}^y = t_{e_e,q e_e,p}^y =$
$t_{e_e,q e_e,r}^z = t_{e_e,11 e_e,13}^z = (\epsilon_y - \frac{\delta}{\sqrt{3}} - m_e l)$	$t_{e_e,13 e_e,r}^x = t_{e_e,13 e_e,q}^x = (\epsilon_y - \frac{\delta}{\sqrt{3}} - m_e l)$	$t_{e_e,11 e_e,p}^y = t_{e_e,11 e_e,q}^y =$
$t_{e_e,12 e_e,14}^z = t_{e_e,r e_e,g}^z = (\epsilon_x - \frac{\delta}{\sqrt{3}} - n_e l)$	$t_{e_e,12 e_e,g}^x = t_{e_e,14 e_e,r}^x = (\epsilon_z + 3\frac{\delta}{\sqrt{3}} - p_e l)$	$= (\epsilon_x - \frac{\delta}{\sqrt{3}} - n_e l)$
		$t_{e_e,13 e_e,q}^y = t_{e_e,14 e_e,r}^y =$
		$= (\epsilon_z + 3\frac{\delta}{\sqrt{3}} - p_e l)$

The values for the upper-half of the matrix \sqrt{A}^{-1} are given in the following table. As for the 4- and 6-valent graphs, the lower indices represent the matrix entries while the upper indices indicate the edges under consideration.

$$\begin{aligned}
(\sqrt{A}^{-1})_{2,1}^{50,60} &= -\frac{1}{2}D_0 & (\sqrt{A}^{-1})_{3,1}^{50,70} &= -\frac{1}{2}D_0 & (\sqrt{A}^{-1})_{4,1}^{50,80} &= -\frac{1}{2}B_0 \\
(\sqrt{A}^{-1})_{5,1}^{50,40} &= -C_0 & (\sqrt{A}^{-1})_{6,1}^{50,30} &= -\frac{1}{2}C_0 & (\sqrt{A}^{-1})_{8,1}^{50,10} &= -\frac{1}{2}C_0 \\
(\sqrt{A}^{-1})_{3,2}^{60,70} &= -\frac{1}{2}B_0 & (\sqrt{A}^{-1})_{4,2}^{60,80} &= -\frac{1}{2}D_0 & (\sqrt{A}^{-1})_{5,2}^{60,40} &= -\frac{1}{2}C_0 \\
(\sqrt{A}^{-1})_{7,2}^{60,20} &= -\frac{1}{2}C_0 & (\sqrt{A}^{-1})_{8,2}^{60,10} &= -2C_0 & (\sqrt{A}^{-1})_{4,3}^{70,80} &= -\frac{1}{2}E_0 \\
(\sqrt{A}^{-1})_{5,3}^{70,40} &= -\frac{1}{2}C_0 & (\sqrt{A}^{-1})_{6,3}^{70,30} &= -C_0 & (\sqrt{A}^{-1})_{7,3}^{70,20} &= -C_0 \\
(\sqrt{A}^{-1})_{6,4}^{80,30} &= -\frac{1}{2}C_0 & (\sqrt{A}^{-1})_{7,4}^{80,20} &= -C_0 & (\sqrt{A}^{-1})_{8,4}^{80,10} &= -\frac{1}{2}C_0 \\
(\sqrt{A}^{-1})_{6,5}^{40,30} &= -B_0 & (\sqrt{A}^{-1})_{7,5}^{40,20} &= -\frac{1}{2}B_0 & (\sqrt{A}^{-1})_{8,5}^{40,10} &= -\frac{1}{2}F_0 \\
(\sqrt{A}^{-1})_{7,6}^{30,20} &= -A_0 & (\sqrt{A}^{-1})_{8,6}^{30,10} &= -\frac{1}{2}B_0 & (\sqrt{A}^{-1})_{8,7}^{20,10} &= -B_0 \\
(\sqrt{A}^{-1})_{9,8}^{01,91} &= -B_1 & (\sqrt{A}^{-1})_{10,8}^{01,101} &= -\frac{1}{2}B_1 & (\sqrt{A}^{-1})_{11,8}^{01,151} &= -F_1 \\
(\sqrt{A}^{-1})_{13,8}^{01,121} &= -\frac{1}{2}B_1 & (\sqrt{A}^{-1})_{14,8}^{01,111} &= -\frac{1}{2}F_1 & (\sqrt{A}^{-1})_{15,8}^{01,131} &= -\frac{1}{2}A_1 \\
(\sqrt{A}^{-1})_{10,9}^{91,101} &= -A_1 & (\sqrt{A}^{-1})_{11,9}^{91,151} &= -\frac{1}{2}B_1 & (\sqrt{A}^{-1})_{12,9}^{91,141} &= -\frac{1}{2}A_1 \\
(\sqrt{A}^{-1})_{13,9}^{91,121} &= -A_1 & (\sqrt{A}^{-1})_{14,9}^{91,111} &= -\frac{1}{2}B_1 & (\sqrt{A}^{-1})_{16,9}^{19,d_9} &= -\frac{1}{2}B_9 \\
(\sqrt{A}^{-1})_{18,9}^{19,59} &= -\frac{1}{2}C_9 & (\sqrt{A}^{-1})_{19,9}^{19,69} &= -\frac{1}{2}D_9 & (\sqrt{A}^{-1})_{19,9}^{19,49} &= -\frac{1}{2}F_9 \\
(\sqrt{A}^{-1})_{20,9}^{19,b_9} &= -\frac{1}{2}B_9 & (\sqrt{A}^{-1})_{21,9}^{19,a_9} &= -B_9 & (\sqrt{A}^{-1})_{11,10}^{101,151} &= -B_1 \\
(\sqrt{A}^{-1})_{12,10}^{101,141} &= -\frac{1}{2}E_1 & (\sqrt{A}^{-1})_{13,10}^{101,121} &= -\frac{1}{2}A_1 & (\sqrt{A}^{-1})_{15,10}^{101,131} &= -\frac{1}{2}B_1 \\
(\sqrt{A}^{-1})_{12,11}^{151,141} &= -\frac{1}{2}B_1 & (\sqrt{A}^{-1})_{14,11}^{151,111} &= -\frac{1}{2}A_1 & (\sqrt{A}^{-1})_{15,11}^{151,131} &= -\frac{1}{2}D_1 \\
(\sqrt{A}^{-1})_{13,12}^{141,121} &= -A_1 & (\sqrt{A}^{-1})_{14,12}^{141,111} &= -\frac{1}{2}B_1 & (\sqrt{A}^{-1})_{15,12}^{141,131} &= -B_1 \\
(\sqrt{A}^{-1})_{14,13}^{121,111} &= -B_1 & (\sqrt{A}^{-1})_{15,13}^{121,131} &= -\frac{1}{2}B_1 & (\sqrt{A}^{-1})_{23,13}^{112,a_{12}} &= -\frac{1}{2}F_{12} \\
(\sqrt{A}^{-1})_{24,13}^{112,b_{12}} &= -\frac{1}{2}A_{12} & (\sqrt{A}^{-1})_{25,13}^{112,4_{12}} &= -A_{12} & (\sqrt{A}^{-1})_{26,13}^{112,m_{12}} &= -\frac{1}{2}B_{12} \\
(\sqrt{A}^{-1})_{28,13}^{112,h_{12}} &= -\frac{1}{2}A_{12} & (\sqrt{A}^{-1})_{29,13}^{112,e_{12}} &= -\frac{1}{2}F_{12} & (\sqrt{A}^{-1})_{15,14}^{111,131} &= -\frac{1}{2}F_1 \\
(\sqrt{A}^{-1})_{15,16}^{d_9,c_9} &= -\frac{1}{2}E_9 & (\sqrt{A}^{-1})_{18,16}^{d_9,5_9} &= -\frac{1}{2}B_9 & (\sqrt{A}^{-1})_{19,16}^{d_9,6_9} &= -B_9 \\
(\sqrt{A}^{-1})_{21,16}^{d_9,b_9} &= -\frac{1}{2}C_9 & (\sqrt{A}^{-1})_{22,16}^{d_9,a_9} &= -\frac{1}{2}E_9 & (\sqrt{A}^{-1})_{18,17}^{c_9,5_9} &= -B_9 \\
(\sqrt{A}^{-1})_{19,17}^{c_9,6_9} &= -\frac{1}{2}B_9 & (\sqrt{A}^{-1})_{20,17}^{c_9,4_9} &= -\frac{1}{2}B_9 & (\sqrt{A}^{-1})_{21,17}^{c_9,b_9} &= -C_9 \\
(\sqrt{A}^{-1})_{22,17}^{c_9,a_9} &= -\frac{1}{2}C_9 & (\sqrt{A}^{-1})_{19,18}^{5_9,6_9} &= -\frac{1}{2}D_9 & (\sqrt{A}^{-1})_{20,18}^{5_9,4_9} &= -\frac{1}{2}D_9 \\
(\sqrt{A}^{-1})_{21,18}^{5_9,b_9} &= -\frac{1}{2}B_9 & (\sqrt{A}^{-1})_{20,19}^{6_9,4_9} &= -\frac{1}{2}C_9 & (\sqrt{A}^{-1})_{22,19}^{6_9,a_9} &= -\frac{1}{2}B_9 \\
(\sqrt{A}^{-1})_{21,20}^{4_9,b_9} &= -B_9 & (\sqrt{A}^{-1})_{22,20}^{4_9,a_9} &= -\frac{1}{2}B_9 & (\sqrt{A}^{-1})_{22,21}^{b_9,a_9} &= -\frac{1}{2}E_9 \\
(\sqrt{A}^{-1})_{24,23}^{a_{12},b_{12}} &= -A_{12} & (\sqrt{A}^{-1})_{25,23}^{a_{12},4_{12}} &= -\frac{1}{2}A_{12} & (\sqrt{A}^{-1})_{26,23}^{a_{12},m_{12}} &= -\frac{1}{2}E_{12} \\
(\sqrt{A}^{-1})_{27,23}^{a_{12},k_{12}} &= -\frac{1}{2}A_{12} & (\sqrt{A}^{-1})_{29,23}^{a_{12},e_{12}} &= -\frac{1}{2}B_{12} & (\sqrt{A}^{-1})_{25,24}^{b_{12},14_{12}} &= -B_{12} \\
(\sqrt{A}^{-1})_{26,24}^{b_{12},m_{12}} &= -\frac{1}{2}A_{12} & (\sqrt{A}^{-1})_{27,24}^{b_{12},k_{12}} &= -C_{12} & (\sqrt{A}^{-1})_{28,24}^{b_{12},h_{12}} &= -\frac{1}{2}B_{12} \\
(\sqrt{A}^{-1})_{27,25}^{14_{12},k_{12}} &= -\frac{1}{2}B_{12} & (\sqrt{A}^{-1})_{28,25}^{14_{12},h_{12}} &= -\frac{1}{2}D_{12} & (\sqrt{A}^{-1})_{29,25}^{14_{12},e_{12}} &= -\frac{1}{2}A_{12} \\
(\sqrt{A}^{-1})_{27,26}^{m_{12},k_{12}} &= -A_{12} & (\sqrt{A}^{-1})_{28,26}^{m_{12},h_{12}} &= -\frac{1}{2}A_{12} & (\sqrt{A}^{-1})_{29,26}^{m_{12},e_{12}} &= -\frac{1}{2}F_{12} \\
(\sqrt{A}^{-1})_{28,27}^{k_{12},h_{12}} &= -B_{12} & (\sqrt{A}^{-1})_{29,27}^{k_{12},e_{12}} &= -\frac{1}{2}A_{12} & (\sqrt{A}^{-1})_{29,28}^{h_{12},e_{12}} &= -A_{12} \\
(\sqrt{A}^{-1})_{30,29}^{12_e,11_e} &= -B_e & (\sqrt{A}^{-1})_{31,29}^{12_e,14_e} &= -A_e & (\sqrt{A}^{-1})_{32,29}^{12_e,13_e} &= -\frac{1}{2}B_e \\
(\sqrt{A}^{-1})_{33,29}^{12_e,g_e} &= -\frac{1}{2}E_e & (\sqrt{A}^{-1})_{34,29}^{12_e,p_e} &= -\frac{1}{2}B_e & (\sqrt{A}^{-1})_{36,29}^{12_e,r_e} &= -\frac{1}{2}A_e \\
(\sqrt{A}^{-1})_{31,30}^{11_e,14_e} &= -\frac{1}{2}B_e & (\sqrt{A}^{-1})_{32,30}^{11_e,13_e} &= -\frac{1}{2}F_e & (\sqrt{A}^{-1})_{33,30}^{11_e,g_e} &= -\frac{1}{2}B_e \\
(\sqrt{A}^{-1})_{34,30}^{11_e,p_e} &= -\frac{1}{2}F_e & (\sqrt{A}^{-1})_{35,30}^{11_e,q_e} &= -\frac{1}{2}A_e & (\sqrt{A}^{-1})_{32,31}^{14_e,13_e} &= -B_e \\
(\sqrt{A}^{-1})_{33,31}^{14_e,g_e} &= -\frac{1}{2}A_e & (\sqrt{A}^{-1})_{35,31}^{14_e,q_e} &= -\frac{1}{2}B_e & (\sqrt{A}^{-1})_{36,31}^{14_e,r_e} &= -C_e \\
(\sqrt{A}^{-1})_{34,32}^{13_e,p_e} &= -\frac{1}{2}A_e & (\sqrt{A}^{-1})_{35,32}^{13_e,q_e} &= -\frac{1}{2}D_e & (\sqrt{A}^{-1})_{36,32}^{13_e,r_e} &= -\frac{1}{2}B_e \\
(\sqrt{A}^{-1})_{34,33}^{g_e,p_e} &= -B_e & (\sqrt{A}^{-1})_{35,33}^{g_e,q_e} &= -\frac{1}{2}B_e & (\sqrt{A}^{-1})_{36,33}^{g_e,r_e} &= -A_e \\
(\sqrt{A}^{-1})_{35,34}^{p_e,q_e} &= -\frac{1}{2}F_e & (\sqrt{A}^{-1})_{36,34}^{p_e,r_e} &= -\frac{1}{2}B_e & (\sqrt{A}^{-1})_{36,35}^{q_e,r_e} &= -B_e
\end{aligned}$$

where $A_i = (x_{V_i} - n_i l) \frac{1}{\delta\sqrt{3}}$, $B_i = (y_{V_i} - m_i l) \frac{1}{\delta\sqrt{3}}$, $C_i = (z_{V_i} - p_i l) \frac{1}{\delta\sqrt{3}}$, $D_i = B_i + C_i$, $E_i = A_i + C_i$, $F_i = B_i + A_i$, and the quantities x_{V_i} , y_{V_i} , z_{V_i} are the x -, y -, z -coordinates of the vertex V_i . In all the above formulae the term $\frac{1}{\delta_e\sqrt{3}}$ comes from the fact that $t_{e_i} = t_{e_i}^x + t_{e_i}^y + t_{e_i}^z = \delta_e\sqrt{3}$ for all edges e_i .

References

- [1] C. Rovelli. *Quantum Gravity*. (Cambridge University Press, Cambridge, 2004).
- [2] T. Thiemann. *Modern Canonical Quantum General Relativity*. (Cambridge University Press, Cambridge, 2007).
- [3] C. Rovelli. Loop quantum gravity, *Living Rev. Rel.* **1** (1998), 1. [gr-qc/9710008]
 A. Ashtekar and J. Lewandowski. Background independent quantum gravity: a status report. *Class. Quant. Grav.* **21** (2004), R53. [gr-qc/0404018]
 T. Thiemann. Lectures on loop quantum gravity. *Lect. Notes Phys.* **631** (2003), 41-135. [gr-qc/0210094]
- [4] T. Thiemann. Anomaly-free formulation of non-perturbative, four-dimensional Lorentzian quantum gravity. *Physics Letters* **B380** (1996), 257-264. [gr-qc/9606088]
 T. Thiemann. Quantum Spin Dynamics (QSD). *Class. Quantum Grav.* **15** (1998), 839-73. [gr-qc/9606089]
 T. Thiemann. Quantum Spin Dynamics (QSD): II. The kernel of the Wheeler-DeWitt constraint operator. *Class. Quantum Grav.* **15** (1998), 875-905. [gr-qc/9606090]
 T. Thiemann. Quantum Spin Dynamics (QSD): III. Quantum constraint algebra and physical scalar product in quantum general relativity. *Class. Quantum Grav.* **15** (1998), 1207-1247. [gr-qc/9705017]
 T. Thiemann. Quantum Spin Dynamics (QSD): IV. 2+1 Euclidean quantum gravity as a model to test 3+1 Lorentzian quantum gravity. *Class. Quantum Grav.* **15** (1998), 1249-1280. [gr-qc/9705018]
 T. Thiemann. Quantum Spin Dynamics (QSD): V. Quantum gravity as the natural regulator of the Hamiltonian constraint of matter quantum field theories. *Class. Quantum Grav.* **15** (1998), 1281-1314. [gr-qc/9705019]
 T. Thiemann. Quantum Spin Dynamics (QSD): VI. Quantum Poincaré algebra and a quantum positivity of energy theorem for canonical quantum gravity. *Class. Quantum Grav.* **15** (1998), 1463-1485. [gr-qc/9705020]
 T. Thiemann. Kinematical Hilbert spaces for fermionic and Higgs quantum field theories. *Class. Quantum Grav.* **15** (1998), 1487-1512. [gr-qc/9705021]
- [5] T. Thiemann. The phoenix project: master constraint programme for loop quantum gravity. *Class. Quant. Grav.* **23** (2006), 2211-2248. [gr-qc/0305080]
 T. Thiemann. Quantum spin dynamics (QSD): VIII. The master constraint. *Class. Quant. Grav.* **23** (2006), 2249-2266. [gr-qc/0510011]
- [6] K. Giesel and T. Thiemann. Algebraic quantum gravity (AQG). IV. Reduced phase space quantisation of loop quantum gravity. [arXiv:0711.0119 [gr-qc]]
- [7] M. Bojowald. Loop quantum cosmology. *Living Rev. Rel.* **8** (2005), 11. [gr-qc/0601085]
- [8] C. Rovelli and L. Smolin. Discreteness of volume and area in quantum gravity. *Nucl. Phys.* **B442** (1995), 593-622. Erratum: *Nucl. Phys.* **B456** (1995), 753. [gr-qc/9411005]
- [9] A. Ashtekar and J. Lewandowski. Quantum theory of geometry II: Volume operators. *Adv. Theo. Math. Phys.* **1** (1997), 388-429. [gr-qc/9711031]
- [10] K. Giesel and T. Thiemann. Consistency check on volume and triad operator quantisation in loop quantum gravity. I. *Class. Quant. Grav.* **23** (2006), 5667-5691. [gr-qc/0507036]
 K. Giesel and T. Thiemann. Consistency check on volume and triad operator quantisation in loop quantum gravity. II. *Class. Quant. Grav.* **23** (2006), 5693-5771. [gr-qc/0507037]
- [11] T. Thiemann and O. Winkler. Gauge field theory coherent states (GCS): II. Peakedness properties. *Class. Quant. Grav.* **18** (2001), 2561-2636. [hep-th/0005237]
 T. Thiemann and O. Winkler. Gauge field theory coherent states (GCS): III. Ehrenfest theorems. *Class. Quant. Grav.* **18** (2001), 4629-4681. [hep-th/0005234]
 T. Thiemann and O. Winkler. Gauge field theory coherent states (GCS): IV. Infinite tensor product

- and thermodynamic limit. *Class. Quant. Grav.* **18** (2001), 4997-5033. [hep-th/0005235]
- H. Sahlmann, T. Thiemann and O. Winkler. Coherent states for canonical quantum general relativity and the infinite tensor product extension. *Nucl. Phys.* **B606** (2001), 401-440. [gr-qc/0102038]
- [12] T. Thiemann. Closed formula for the matrix elements of the volume operator in canonical quantum gravity. *Journ. Math. Phys.* **39** (1998), 3347-3371. [gr-qc/9606091]
- [13] C. Rovelli and L. Smolin. Spin networks and quantum gravity. *Phys. Rev.* **D53** (1995), 5743-5759. [gr-qc/9505006]
- [14] A. Ashtekar and C.J. Isham. Representations of the holonomy algebras of gravity and non-Abelian gauge theories. *Class. Quant. Grav.* **9** (1992), 1433. [hep-th/9202053]
- A. Ashtekar and J. Lewandowski. Representation theory of analytic holonomy C^* algebras. In *Knots and Quantum Gravity*, J. Baez (ed.), (Oxford University Press, Oxford 1994). [gr-qc/9311010]
- [15] J. Lewandowski, A. Okolow, H. Sahlmann and T. Thiemann. Uniqueness of diffeomorphism invariant states on holonomy – flux algebras. *Commun. Math. Phys.* **267** (2006), 703-733. [gr-qc/0504147]
- C. Fleischhack. Representations of the Weyl algebra in quantum geometry. [math-ph/0407006]
- [16] J. Brunnemann and T. Thiemann. Simplification of the spectral analysis of the volume operator in loop quantum gravity. *Class. Quant. Grav.* **23** (2006), 1289-1346. [gr-qc/0405060]
- [17] A. R. Edmonds. *Angular Momentum in Quantum Mechanics*, (Princeton University Press, Princeton, 1974).
- [18] J. Brunnemann and D. Rideout. Spectral Analysis of the Volume Operator in Loop Quantum Gravity. [gr-qc/0612147]
- J. Brunnemann and D. Rideout. Properties of the volume operator in loop quantum gravity. I. Results. *Class. Quant. Grav.* **25** (2008), 065001. [arXiv:0706.0469 [gr-qc]]
- J. Brunnemann and D. Rideout. Properties of the Volume Operator in Loop Quantum Gravity II: Detailed Presentation. [arXiv:0706.0382]
- [19] K. Giesel and T. Thiemann. Algebraic quantum gravity (AQG) III. Semiclassical perturbation theory. *Class. Quant. Grav.* **24** (2007), 2499-2564. [gr-qc/0607101]
- [20] H. Sahlmann and T. Thiemann. Towards the QFT on curved spacetime limit of QGR. 1. A general scheme. *Class. Quant. Grav.* **23** (2006), 867-908. [gr-qc/0207030]
- H. Sahlmann and T. Thiemann. Towards the QFT on curved spacetime limit of QGR. 2. A concrete implementation. *Class. Quant. Grav.* **23** (2006), 909-954. [gr-qc/0207031]
- [21] K. Giesel and T. Thiemann. Algebraic Quantum Gravity (AQG). I. Conceptual Setup. *Class. Quant. Grav.* **24** (2007), 2465-2498. [gr-qc/0607099]
- K. Giesel and T. Thiemann. Algebraic Quantum Gravity (AQG). II. Semiclassical Analysis. *Class. Quant. Grav.* **24** (2007), 2499-2564. [gr-qc/0607100]
- [22] T. Thiemann. Complexifier coherent states for canonical quantum general relativity. *Class. Quant. Grav.* **23** (2006), 2063-2118. [gr-qc/0206037]
- [23] C. Flori and T. Thiemann. Semiclassical analysis of the Loop Quantum Gravity volume operator: Flux Coherent States. [arXiv:0812.1537v1 gr-qc]
- [24] B. C. Hall. The Segal-Bargmann coherent state transform for compact Lie groups. *Journ. Funct. Analysis.* **122** (1994), 103-151.
- [25] M. Varadarajan. Fock representations from $U(1)$ holonomy algebras. *Phys. Rev.* **D61** (2000), 104001. [gr-qc/0001050]
- M. Varadarajan. Photons from quantised electric flux representations. *Phys. Rev.* **D64** (2001), 104003. [gr-qc/0104051]
- M. Varadarajan. Gravitons from a loop representation of linearised gravity. *Phys. Rev.* **D66** (2002), 024017. [gr-qc/0204067]
- M. Varadarajan. The graviton vacuum as a distributional state in kinematic loop quantum gravity. *Class. Quant. Grav.* **22** (2005), 1207-1238. [gr-qc/0410120]
- [26] A. Ashtekar and J. Lewandowski. Relation between polymer and Fock excitations. *Class. Quant. Grav.* **18** (2001), L117-L128. [gr-qc/0107043]
- [27] A. Perez. Spin foam models for quantum gravity. *Class. Quant. Grav.* **20** (2003), R43. [gr-qc/0301113]

- [28] E. Livine and S. Speziale. A New spinfoam vertex for quantum gravity. *Phys. Rev.* **D76** (2007), 084028. [arXiv:0705.0674 [gr-qc]]
 J. Engle, R. Pereira and C. Rovelli. The Loop-quantum-gravity vertex-amplitude. *Phys. Rev. Lett.* **99** (2007), 161301. [arXiv:0705.2388 [gr-qc]]
 E. Livine and S. Speziale. Consistently Solving the Simplicity Constraints for Spinfoam Quantum Gravity. [arXiv:0708.1915 [gr-qc]]
 J. Engle, R. Pereira and C. Rovelli. Flipped spinfoam vertex and loop gravity. *Nucl. Phys.* **B798** (2008), 251-290. [arXiv:0708.1236 [gr-qc]]
 L. Freidel and K. Krasnov. A New Spin Foam Model for 4d Gravity. [e-Print: arXiv:0708.1595 [gr-qc]]
 J. Engle, E. Livine, R. Pereira and C. Rovelli. LQG vertex with finite Immirzi parameter. *Nucl. Phys.* **B799** (2008), 136-149. [arXiv:0711.0146 [gr-qc]]
- [29] J. W. Barrett and L. Crane. Relativistic spin networks and quantum gravity. *J. Math. Phys.* **39** (1998), 3296-3302. [gr-qc/9709028]
 J. W. Barrett and L. Crane. A Lorentzian signature model for quantum general relativity. *Class. Quant. Grav.* **17** (2000), 3101-3118. [gr-qc/9904025]
- [30] S. Alexandrov. Simplicity and closure constraints in spin foam models of gravity. [arXiv:0802.3389 [gr-qc]]
- [31] H. Sahlmann and T. Thiemann. Irreducibility of the Ashtekar – Isham – Lewandowski representation. *Class. Quant. Grav.* **23** (2006), 4453-4472. [gr-qc/0303074]
 C. Fleischhack. Irreducibility of the Weyl algebra in loop quantum gravity. *Phys. Rev. Lett.* **97** (2006), 061302.
- [32] E. Alesci and C. Rovelli. The Complete LQG propagator. I. Difficulties with the Barrett-Crane vertex. *Phys. Rev.* **D76** (2007), 104012. [arXiv:0708.0883 [gr-qc]]
 E. Alesci and C. Rovelli. The Complete LQG propagator. II. Asymptotic behavior of the vertex. *Phys. Rev.* **D77** (2008), 044024. [arXiv:0711.1284 [gr-qc]]
 V. Bonzom, E. Livine, M. Smerlak and S. Speziale
 Towards the graviton from spinfoams: The Complete perturbative expansion of the 3d toy model. [arXiv:0802.3983 [gr-qc]]
- [33] Joao Faria Martins, Aleksandar Mikovic. Spin Foam Perturbation Theory for Three-Dimensional Quantum Gravity. [arXiv:0804.2811 [gr-qc]]
- [34] A. Baratin, C. Flori and T. Thiemann. The Holst Spin Foam Model on Cubulations. [arXiv:0812.4055v2 [gr-qc]].
- [35] J. Klauder and B.-S. Skagerstam. *Coherent States*, (World Scientific, Singapore, 1985).
- [36] T. Thiemann. Reality conditions inducing transforms for quantum gauge field theories and quantum gravity. *Class. Quant. Grav.* **13** (1996), 1383-1403. [gr-qc/9511057]
- [37] A. Ashtekar, J. Lewandowski, D. Marolf, J. Mourão and T. Thiemann. Quantisation of diffeomorphism invariant theories of connections with local degrees of freedom. *Journ. Math. Phys.* **36** (1995), 6456-6493. [gr-qc/9504018]
- [38] A. Ashtekar, J. Lewandowski, D. Marolf, J. Mourão and T. Thiemann. Coherent state transforms for spaces of connections. *Journ. Funct. Analysis.* **135** (1996), 519-551. [gr-qc/9412014]
- [39] O. Bratteli and D. W. Robinson. *Operator algebras and quantum statistical mechanics*, vol. 1,2, (Springer Verlag, Berlin, 1997).
- [40] A. Ashtekar and J. Lewandowski. Projective techniques and functional integration for gauge theories. *J. Math. Phys.* **36** (1995), 2170-2191. [gr-qc/9411046]
- [41] A. Ashtekar and J. Lewandowski. Quantum theory of geometry I: Area Operators. *Class. Quant. Grav.* **14** (1997), A55-A82. [gr-qc/9602046]
- [42] B. Bahr and T. Thiemann. Gauge-invariant coherent states for Loop Quantum Gravity. I. Abelian gauge groups. [arXiv:0709.4619 [gr-qc]]
 B. Bahr and T. Thiemann. Gauge-invariant coherent states for loop quantum gravity. II. Non-Abelian gauge groups. [arXiv:0709.4636 [gr-qc]]

- [43] J. Velhinho. A groupoid approach to spaces of generalised connections. *J. Geom. Phys.* **41** (2002), 166-180. [hep-th/0011200]
J. Velhinho. On the structure of the space of generalised connections. *Int. J. Geom. Meth. Mod. Phys.* **1** (2004), 311-334. [math-ph/0402060]
B. Bahr and T. Thiemann, Automorphisms in loop quantum gravity. [arXiv:0711.0373 [gr-qc]]
- [44] C. Itzykson, J. M. Drouffe *Statistical Field Theory*, vol. 2, (Cambridge University Press, Cambridge, 1997).

